



Pacific Northwest
NATIONAL LABORATORY

Proudly Operated by Battelle Since 1965

Isotope Enrichment Using Microchannel Distillation Technology

FINAL REPORT

November 2018

W TeGrotenhuis
D Bottenus
E Hoppe

P Humble
R Lucke
M Powell

DISCLAIMER

This report was prepared as an account of work sponsored by an agency of the United States Government. Neither the United States Government nor any agency thereof, nor Battelle Memorial Institute, nor any of their employees, makes **any warranty, express or implied, or assumes any legal liability or responsibility for the accuracy, completeness, or usefulness of any information, apparatus, product, or process disclosed, or represents that its use would not infringe privately owned rights.** Reference herein to any specific commercial product, process, or service by trade name, trademark, manufacturer, or otherwise does not necessarily constitute or imply its endorsement, recommendation, or favoring by the United States Government or any agency thereof, or Battelle Memorial Institute. The views and opinions of authors expressed herein do not necessarily state or reflect those of the United States Government or any agency thereof.

PACIFIC NORTHWEST NATIONAL LABORATORY
operated by
BATTELLE
for the
UNITED STATES DEPARTMENT OF ENERGY
under Contract DE-AC05-76RL01830

Printed in the United States of America

Available to DOE and DOE contractors from the
Office of Scientific and Technical Information,
P.O. Box 62, Oak Ridge, TN 37831-0062;
ph: (865) 576-8401
fax: (865) 576-5728
email: reports@adonis.osti.gov

Available to the public from the National Technical Information Service
5301 Shawnee Rd., Alexandria, VA 22312
ph: (800) 553-NTIS (6847)
email: orders@ntis.gov <<http://www.ntis.gov/about/form.aspx>>
Online ordering: <http://www.ntis.gov>



This document was printed on recycled paper.

(8/2010)

Isotope Enrichment Using Microchannel Distillation Technology

Final Report

W TeGrotenhuis¹
D Bottenus
E Hoppe

P Humble
R Lucke
M Powell

November 2018

Prepared for
the U.S. Department of Energy
under Contract DE-AC05-76RL01830

Pacific Northwest National Laboratory
Richland, Washington 99352

¹ Contact: Dr. Ward TeGrotenhuis, (509)372-4049, ward.tegrotenhuis@pnnl.gov

Summary

The Pacific Northwest National Laboratory has successfully demonstrated isotopic enrichment with microchannel distillation (MCD) technology, a capability for process intensification of chemical boiling point separations (CBPS). Here the goal of process intensification is to reduce the CBPS column length that is required for a given isotopic separation through enhanced mass transfer. Total column length is equal to the height required for a single separation stage times the number of separation stages required. Therefore, reducing separation stage length dramatically shortens the total column length, which is particularly important for isotopic enrichment that typically requires thousands of stages. For example, enriching ^{13}C to 99% from natural carbon monoxide (CO) requires 2000-3000 stages and traditional CBPS columns that are 400-600 meters tall. Reducing the stage length from 0.2 m to 0.005 m with MCD can shorten the column to 10-15 meters. Here, MCD technology has been demonstrated on short devices, 10.2 cm and 25.4 cm long, so the number of stages and overall separation factors are relatively small. However, results are directly scalable to longer devices for increased separation.

Sixty separation stages were achieved in a single device, a new record for process intensification technologies. The minimum length of a separation stage was 0.41 cm, a factor of 5 smaller than the best commercial advanced structured packing. A key advantage of MCD technology is scalability, which was demonstrated by increasing the length of the test device by a factor of 2.5 and doubling the number of channels while improving performance. Previous efforts at PNNL with MCD have included chemical separations of a military diesel fuel, JP-8, and high purity polishing of n-octane as a surrogate for electronic materials. This work produced results for two new separations, propane from propylene and isotopic enrichment of methane, which demonstrate the versatility and utility of MCD for difficult separations, both chemical separations and isotopic enrichment. By employing capillary forces, MCD devices can be operated in a horizontal configuration that facilitates a lower equipment profile and compact systems. Compact systems are easier and cheaper to insulate and operate at cryogenic temperatures that are typical for isotopic enrichment. MCD devices have been operated as low as the normal boiling point of methane, -162°C , and as high as the boiling point of diesel fuel, $\sim 300^{\circ}\text{C}$.

There remains significant opportunity for further improvement of the technology based on dimensional analysis and computational fluid dynamics (CFD) modeling. CFD modeling predicates the potential for reducing HETP to 0.1 cm, representing a further 4-5X reduction in column length. Further investments in improving performance could pay substantial dividends in deploying the technology for isotopic enrichment.

The goal of demonstrating isotopic enrichment of germane to support sizing of a system capable of supplying 86% enriched ^{76}Ge for future neutrinoless double beta decay experiments was confounded by difficulties in measuring relative volatilities of germane isotopes. Nevertheless, scoping calculations were performed using germane isotope relative volatilities surmised from similar compounds including silane and methane. The hypothesized volatilities were used to project 14,423 and 904 as the number of stages and reflux ratio, respectively, which are large even for isotopic enrichment. The number of stages translates to a total active length of 59.1 meters based on measured MCD performance, compared to 289 meters with the best available structured packing. The MCD total active length would shrink to 14.4 m, if theoretical potential was realized. A system capable of producing 1 tonne of 86% $^{76}\text{GeH}_4$ in 4 years was envisioned consisting of 470 parallel cascades of MCD devices each having 118 devices in series for a total of 55,575 MCD devices. Theoretical performance would reduce the number of devices per cascade to 24 and the total number of devices to 11,115. Multiple cascades mitigates the risk of a single point of failure. Configuring the cascades into a compact arrangement would allow the system to fit within a two-story structure.

Additional advances in MCD performance toward theoretical predictions is warranted for further reducing equipment size and cost. Other development steps include further scale-up of devices to increase the number of separation stages and throughput of a single device. Demonstration of a cascade of devices is also a step toward eventual deployment of the technology for isotopic enrichment. Overall, MCD technology holds promise for making isotopic enrichment of stable isotopes cheaper and more readily accessible.

Contents

Summary	iii
1.0 Project Overview	1.1
1.1 Objectives.....	1.1
1.2 Technical Approach	1.1
1.3 Background	1.4
2.0 Experimental Set-Up	2.1
2.1 Test Devices	2.1
2.1.1 Four-inch Test Device	2.1
2.1.2 Ten-inch Test Device	2.4
2.2 Device Functional Testing	2.5
2.2.1 Hermeticity.....	2.5
2.2.2 Static Liquid Holdup	2.5
2.2.3 Liquid Flowrate Measurements.....	2.6
2.3 Experimental Apparatus.....	2.7
2.3.1 Control System.....	2.12
2.3.2 Condenser.....	2.14
2.3.3 Evaporator	2.15
2.3.4 Helium Flow.....	2.15
3.0 Data Analysis.....	3.1
3.1 Height of an Equivalent Theoretical Plate (HETP).....	3.1
3.2 Liquid Flow Rate.....	3.1
3.3 Comparison with Conventional Equipment	3.2
3.4 Dimensional Analysis	3.2
4.0 Experimental Procedure and Results	4.1
4.1 Experimental Procedure and Start-up.....	4.1
4.2 Flow Rate	4.3
4.3 Approach to Steady-State Operation.....	4.4
4.4 Propane/Propylene Chemical Separation	4.6
4.4.1 Propane Propylene Concentrations by GC/MS	4.6
4.4.2 Propane Propylene Results.....	4.7
4.4.3 Effect of Box Temperature.....	4.8
4.4.4 Effect of Helium Flow.....	4.10
4.5 Methane Isotopic Enrichment	4.10
4.5.1 Methane Isotopic Analysis by GC/IRMS.....	4.10
4.5.2 Methane Isotopic Separation.....	4.10
4.6 Analysis of Results.....	4.12

5.0	Modeling.....	5.1
5.1	Model Description.....	5.1
6.0	Germane Isotopic Enrichment.....	6.1
6.1	Relative Volatility.....	6.1
6.2	Column Height.....	6.5
6.3	Projected System Size.....	6.6
7.0	Conclusions.....	7.1
8.0	References.....	8.1
	Appendix A – Detailed Information on the Condenser and Evaporator.....	Error! Bookmark not defined.

Figures

Figure 1.1. Schematic of the microwick concept for enhanced mass transfer.	1.2
Figure 1.2. Interleaved microwick device.	1.2
Figure 1.3. Schematic of a conventional distillation unit operation.	1.3
Figure 1.4. GC-SCD chromatograms showing sulfur distribution of full JP-8 (red), heavy bottom product (green) and light distillate fraction (blue).	1.5
Figure 1.5. Boiling point ranges of the raw JP-8 feed (red), heavy bottom product (brown), and light distillate fraction (green).	1.6
Figure 1.6. Predicted height of a theoretical plate (HETP) as a function of feed flow rate using microwick distillation technology to purify a proprietary specialty chemical; the data shown are for 15 wicks with a reboil ratio of 15.	1.7
Figure 1.7. HETPs achieved at varying liquid feed rates for separation of 1% 3-methylheptane in n-octane; labels indicate reboil ratio (R_b) at each condition.	1.8
Figure 1.8. HETP and HETP scaled by the liquid phase diffusivity for the three impurity compounds. ..	1.8
Figure 2.1. Photograph of the assembled 5-inch active length MCD device. The inlets and outlets along with the ports for Platinum Resistance Temperature Detectors (PRTD) are labeled.	2.2
Figure 2.2. PCM structure used as the middle layer of the wicks in the 5-inch device; dimensions are in inches.	2.3
Figure 2.3. Alternative ‘angled-wire’ vapor channel layer; dimensions are in inches.	2.3
Figure 2.4. Photograph of the assembled 10-inch active length MCD devices. The different inlets and outlets along with the Platinum Resistance Temperature Detectors (PRTD) ports are labeled. ..	2.4
Figure 2.5. PCM structure used as the middle layer of the wicks in the 5-inch device; dimensions are in inches.	2.4
Figure 2.6. Alternative ‘angled-wire’ vapor channel layer; dimensions are in inches.	2.5
Figure 2.7. Grams of iso-octane contained in the microchannel distillation device as a function of the applied suction head. The curves end at the breakthrough pressure which was 13 cm and 8 cm of iso-octane head for the 5-inch (◆) and 10-inch (■) MCD devices, respectively.	2.6
Figure 2.8. Comparison of liquid flux through liquid wicks as a function of iso-octane suction head (ΔP_{Flow}) in both the 5-inch (■) and 10-inch (◆) MCD devices in the working siphon range.	2.7
Figure 2.9. Schematic of MCD operation.	2.8
Figure 2.10. Solidworks assembly (from to left to right) of evaporator, MCD device, and condenser.	2.9
Figure 2.11. (a) The MCD system installed in a cryogenic cold box before insulating system components, (b) after insulating system components, and (c) with the front cover in-place ready for MCD operation.	2.10
Figure 2.12. Process & instrumentation (P&ID) diagram for the MCD device test-stand.	2.11
Figure 2.13. Graphical user interface of MCD control system.	2.13
Figure 2.14. (a) CAD assembly of SLM fabricated condenser (blue) with Swagelok fittings and SS tubing showing flow inlets and outlets, (b) blow-up CAD view of condenser showing extended surface area fins, and (c) photograph of the additively manufactured condenser.	2.14
Figure 2.15. CAD assembly of evaporator indicating important components.	2.15

Figure 4.1.	Box temperature versus time for a sample distillation experiment of methane isotopic enrichment in the 10-inch device.	4.2
Figure 4.2.	Pressure difference through the 10-inch MCD device, measured between the condenser vent line and the evaporator sample line, for a sample distillation experiment of methane isotopic enrichment.	4.3
Figure 4.3.	Capacitance reading from the liquid level sensor in the evaporator versus time for a sample distillation experiment of methane isotopic enrichment in the 10-inch device.	4.3
Figure 4.4.	(a) Calibration curve of liquid mass flux (blue diamonds (◆) and fit) and evaporator cartridge heater output (red triangles (▲) and fit) vs. condenser setpoint temperature for propane propylene in the 5-inch device. Both curves intersect at the zero flow condition (green square (■)) at a condenser temperature of $\sim -51.35^{\circ}\text{C}$	4.4
Figure 4.5.	Calculated HETP vs time for a propane/propylene experiment in the 5-inch device at 1 mL/min liquid flow; the results (●) are fit to an exponential function (—) to obtain the characteristic time, $-1/\beta$, and 95% prediction intervals are also shown (- -). The calculated flowrate for the experimental data was.	4.5
Figure 4.6.	Calculated HETP from consecutive measurements of the bottoms (evaporator) composition as a function of time with all other operating conditions equal after 21 (◆) and 30 (■) hours of stable operation for a propane/propylene experiment in the 5-inch device at 1 mL/min liquid flow.	4.6
Figure 4.7.	Comparison of gas chromatographs for a feed gas sample (—) and an evaporator sample obtained after 20 hours of operation of the 5-inch device at 1 mL/min liquid flow (—).....	4.7
Figure 4.8.	Number of separation stages (■) and HETP (◆) as a function of liquid flux through the wicks in the 5-inch MCD device after 20 hours of stable operation.....	4.8
Figure 4.9.	Txy diagram for propane in propylene at an operating pressure of 4 in.H ₂ O taken from ChemCad.	4.9
Figure 4.10.	Effect of box temperature on performance after > 20 hours of stable operation. The trend lines follow the same path after ~ 5 hours of operation for box temperatures of -47.0°C (◆) and -45.5°C (■), respectively, and the final HETP for both cases was ~ 1 cm.	4.9
Figure 4.11.	Number of separation stages (◆) and resulting HETP (■) in the 5-inch device and the number of separation stages (▲) and resulting HETP (X) in the 10-inch device as a function of liquid flux for methane isotopic enrichment.	4.11
Figure 4.12.	Vapor channels showing the vapor path flow lines. Part of the inlet and the outlet flow of the vapor headers are not fully counter-current. As the device length increases, this end effect is reduced.	4.12
Figure 4.13.	Compilation of HETP results from MCD testing with 1% propane in propylene in the 5-inch device (◆), for methane IE in the 5-inch device (▲), and for methane IE in the 5-inch device (X), along with CFD results for 1% propane in propylene in a 5-inch model device (■).	4.13
Figure 4.14.	Compilation of Stages versus dimensionless residence time, $Tau^* = \tau D_L / h_m^2$, from MCD testing with 1% propane in propylene in the 5-inch device (◆), for methane IE in the 5-inch device (▲), and for methane IE in the 5-inch device (X), along with CFD results for 1% propane in propylene in a 5-inch model device (■).	4.14
Figure 4.15.	Compilation of C_{eff} versus dimensionless residence time, $Tau^* = \tau D_L / h_m^2$, from MCD testing with 1% propane in propylene in the 5-inch device (◆), for methane IE in the 5-inch device (▲), and for methane IE in the 5-inch device (X), along with CFD results for 1% propane in propylene in a 5-inch model device (■).	4.15

Figure 4.16.	Compilation of C_{eff} versus Pe_g , from MCD testing with 1% propane in propylene in the 5-inch device (◆), for methane IE in the 5-inch device (▲), and for methane IE in the 5-inch device (X), along with CFD results for 1% propane in propylene in a 5-inch model device (■).....	4.15
Figure 4.17.	Compilation of HETP versus F factor from MCD testing with 1% propane in propylene in the 5-inch device (◆), for methane IE in the 5-inch device (▲), and for methane IE in the 5-inch device (X), along with CFD results for 1% propane in propylene in a 5-inch model device (■)....	4.16
Figure 4.18.	Compilation of HETP versus F factor from MCD testing with 1% propane in propylene in the 5-inch device (◆), for methane IE in the 5-inch device (▲), and for methane IE in the 5-inch device (X), along with CFD results for 1% propane in propylene in a 5-inch model device (■) at $\frac{1}{2}$ vapor channel thickness.....	4.16
Figure 4.19.	Comparison of HETP versus F factor between Sulzer laboratory packing [20] and MCD results with 1% propane in propylene in the 5-inch device (◆), for methane IE in the 5-inch device (▲), and for methane IE in the 5-inch device (X), along with CFD results for 1% propane in propylene in a 5-inch model device (■).	4.17
Figure 5.1.	2D geometry for simulating the distillation process in MCD devices.....	5.1
Figure 5.2.	Predicted effect of flow rate on HETP for propane/propylene separation in the 5-inch MCD device.....	5.3
Figure 5.3.	Predicted effect of gas diffusivity on HETP for propane/propylene separation in the 5-inch MCD device.....	5.3
Figure 5.4.	Predicted effect of relative volatility on HETP for propane/propylene separation in the 5-inch MCD device.....	5.4
Figure 6.1.	Chromatographic separation of ^{12}C methane enriched with ^{13}C methane on a 100 m x 0.25 mm ID stainless steel column at -80°C with a helium carrier gas at 25 cm/sec flow velocity.	6.2
Figure 6.2.	Relative volatilities in the form of $ 1-\alpha $ for various compounds containing carbon and silicon.....	6.4
Figure 6.3.	Illustration of cascading of MCD devices to increase the number of separation stages.....	6.7
Figure 6.4.	Illustration of scaling up a cascade of MCD devices.	6.7

Tables

Table 1.1. Feed mixture used for distillation experiments.....	1.6
Table 2.1. 5-inch and 10-inch MCD device geometrical properties.	2.1
Table 4.1. Summary of results separating 1% propane in propylene using the 5-inch MCD device.	4.8
Table 4.2. Summary of results separating methane isotopes using the 5-inch and 10-inch MCD devices.	4.11
Table 4.3. Diffusion coefficients and densities at the boiling points of the fluids used in MCD testing.	4.12
Table 6.1. VLE data for selected isotopic compound pairs, including relative volatility (α) and absolute value of $1-\alpha$ [38, 48].	6.4
Table 6.2. Germanium natural isotope abundances and mass as GeH_4 versus $^{76}\text{GeH}_4$	6.5
Table 6.3. Size of MCD systems for producing 1 tonne of 86% ^{76}Ge in 4 years.	6.8

1.0 Project Overview

1.1 Objectives

The objective of this project was to advance microchannel distillation technology as a tool for isotopic enrichment that could become a national capability for supplying primarily enriched stable isotopes but also longer lived radioisotopes [1]. Unique microchannel distillation (MCD) technology is a broad tool capable of chemical boiling point separations (CBPS) of many isotopes in the range up to ~ 100 amu. The principal advantage of the MCD approach is process intensification that reduces the size of the equipment needed to perform the desired separations, which is particularly important for reducing the cost of enriched isotopes that require separation of close boiling compounds.

The target separation for the project was enrichment of ^{76}Ge that is needed within the low-background physics community for use in high-purity germanium (HPGe) detectors. For Ge-based neutrinoless double beta decay experiments, such as the current MAJORANA DEMONSTRATOR [2] and GERDA [3], germanium material enriched to $\sim 86\%$ ^{76}Ge is required with aspirations for a future experiment using 1 tonne of material. Enrichment by CBPS relies on separating isotopes using differences in relative volatility, so isotopic separation requires use of a volatile compound of germanium. Germane (GeH_4) or germanium tetrafluoride (GeF_4) are two possibilities, but germane is pyrophoric and GeF_4 is toxic and reacts with water to produce HF. Therefore, demonstrating isotopic enrichment was first demonstrated using a surrogate compound, methane, before proceeding to a demonstration of germanium enrichment with germane. The end goal was to produce 0.5 g of germane enriched to 86% ^{76}Ge as a demonstration of feasibility.

Another objective was to obtain measurements of the relative volatilities of germane isotopes, which were not available in the literature. Relative volatilities are needed for vapor-liquid equilibrium concentrations that are necessary for process design and distillation equipment sizing.

The project was partially successful in achieving objectives. Isotopic enrichment of methane as a surrogate for germane was demonstrated in two MCD devices in a cryogenic test stand, which is described in Sections 2.0 and 3.0. Testing of Germane with MCD technology and measuring relative volatilities of germane are left for future efforts. Nevertheless, scoping calculations are presented in Section 6.0 for producing 86% ^{76}Ge using MCD technology, including projected size of equipment.

1.2 Technical Approach

Microwick technology [4-9] is the core concept of MCD isotope distillation. Depicted schematically in Figure 1.1, the concept involves thin porous materials that are inserted into a microchannel and have adjacent flow channels for gas or vapor flow. The ends of the microwicks are hydraulically connected to flow headers at the ends of the device. Liquid flows from right to left through the wick in Figure 1.1, while vapor flows counter-current through the adjacent vapor plenum. Flooding of the vapor plenum is controlled by applying a siphon to the wicks relative to the vapor phase pressure (ΔP_{Cap}), so that liquid flows only through the wicks. Capillary forces prevent vapor intrusion into the wicks. A pressure difference applied along the wick length (ΔP_{Flow}) induces liquid flow through the wick. Mass transfer can occur between the liquid flowing through the wick and gas flowing counter-current through the vapor plenum. In general, mass transfer resistance is dominated by the liquid phase, and the wick thickness is the characteristic length-scale for mass transfer. Reducing the wick thickness to around 100 μm causes rapid mass transfer, short residence times, and dramatic reduction in the size of equipment.

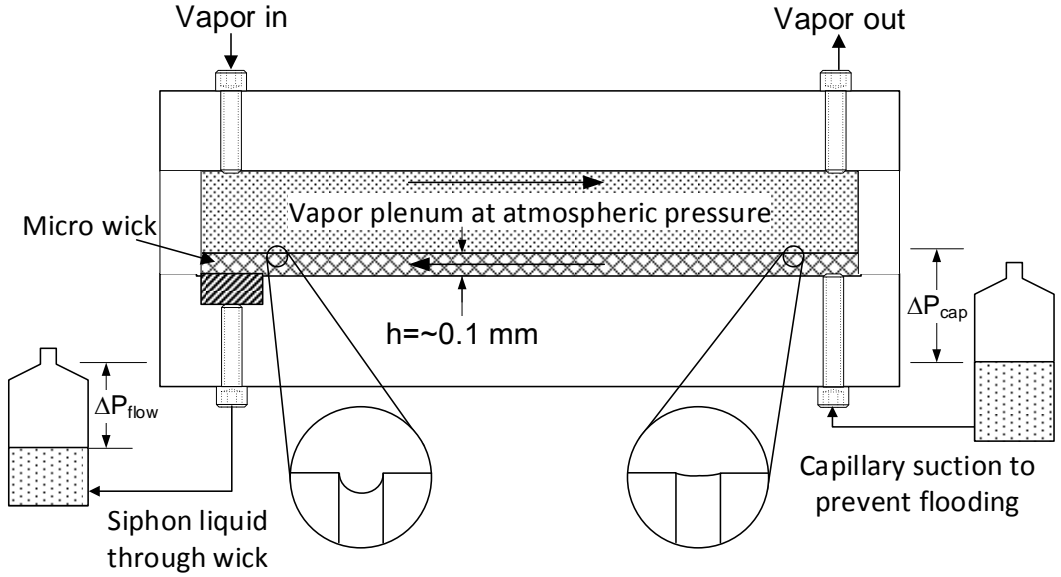


Figure 1.1. Schematic of the microwick concept for enhanced mass transfer.

The characteristic time for diffusion of components through the thickness of the wick is given by:

$$\tau_{diff,wick} = \frac{h^2}{D_{AB,liq}} \quad (1.1)$$

where h is the wick thickness, and $D_{AB,liq}$ is the liquid-phase diffusion coefficient of component A in component B. For example, a thickness of $h=0.01$ cm and a diffusivity of 5×10^{-5} cm²/s gives a characteristic time of only 2 seconds. In contrast, a characteristic length scale of 1 mm has a characteristic mass transfer time of 200 seconds.

Scaling up microwick technologies involves interleaving layers to form a stacked-plate architecture. For adiabatic MCD, wicks and vapor channels are alternately stacked as shown in Figure 1.2 with end-plates on top and bottom. With vapor channels on both sides of the wicks, mass transfer occurs on both sides of the wicks, effectively reducing the mass transfer length-scale by half and reducing the characteristic time by $\frac{1}{4}$ in Equation 1.1. More information is provided on the structures of the liquid and vapor channels in Section 2.

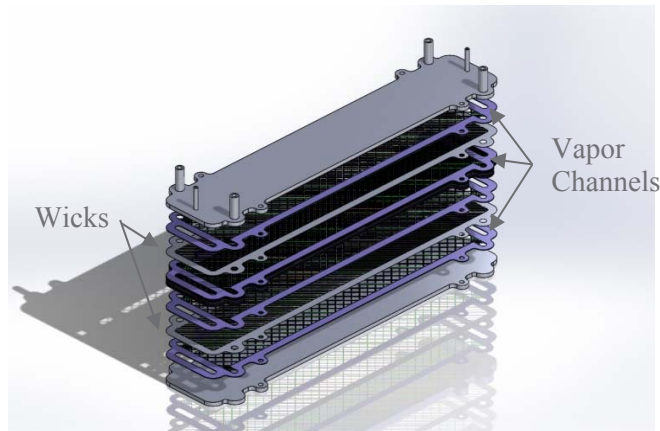


Figure 1.2. Interleaved microwick device.

A typical distillation unit operation is illustrated in Figure 1.3. A feed stream enters the column in the middle with an enriching or rectifying section above and a stripping section below. Vapor flowing from the top of the column is condensed and a fraction is returned to the column as reflux. Similarly, liquid flowing out the bottom of the column is reboiled and returned as vapor. Reflux ratio is the reflux stream flowrate divided by the distillate flowrate. To simplify the MCD demonstration, our approach was to operate only the lower half or stripping section of the column by feeding the condenser and operating in total reboil—no bottoms flow rate so all liquid from the column was evaporated and returned. In this mode, concentrations at one end of the column were effectively fixed to the feed concentration, which for isotopic enrichment is natural abundances. Operating in total reboil gave the maximum number of separation stages, and samples were periodically removed from the reboiler to be analyzed for isotopic concentrations. Distillation columns are operated at the boiling point of the liquid. At atmospheric pressure, germane boils at -88.0°C and methane boils at -161.5°C , so cryogenic operation is required to isotopically enrich these compounds.

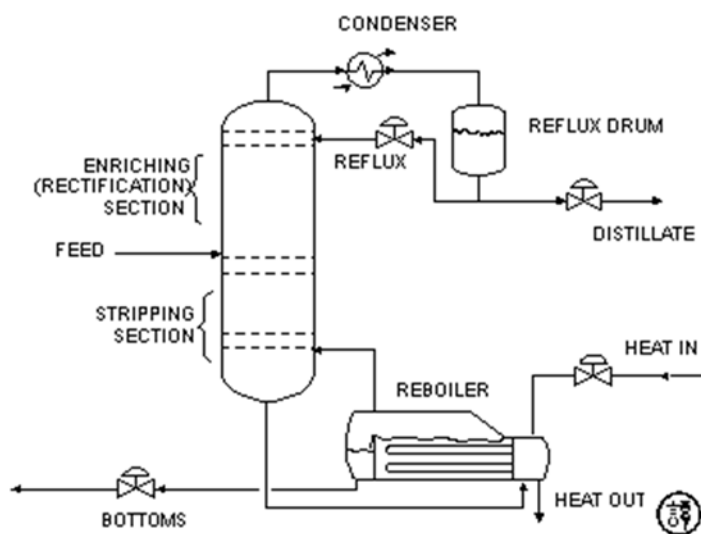


Figure 1.3. Schematic of a conventional distillation unit operation.

Calculating the number of separation stages from concentration data requires knowledge of vapor-liquid equilibrium (VLE) concentrations of the chemical mixture. VLE curves are also needed to design and size distillation systems, including computing the number of theoretical stages required for a specific separation. While VLE curves are readily available for chemical mixtures, they are not easily obtained for isotopic mixtures and could not be found for germane isotopes. Part of the project scope included attempting to obtain VLE data for germane isotopes using gas chromatography mass spectrometry (GC/MS) and a standardized ASTM method [10] widely employed in the refinery industry as a simulated distillation method. This ambitious effort pursued multiple columns and cryogenic configurations, but was unsuccessful at achieving the requisite peak separation between methane isotopes. Alternatively, comparing separation results from MCD testing of germane with results from the surrogate methane would provide a means for estimating relative volatilities of germane isotopes. However, as already mentioned, testing of germane with MCD technology and measuring relative volatilities of germane are left for future efforts.

1.3 Background

Private sector companies in the U.S. engaged in isotope separations use distillation, chemical exchange, and thermal diffusion. CBPS using distillation has been arguably the most successful method of isotope separation of lighter elements [11]. In the past, columns at Los Alamos National Laboratory have produced large quantities of isotopes of carbon, nitrogen, and oxygen [12]. Distillation has also been investigated for tritium separation by water distillation [13]. However, distillation columns for isotopic enrichment are extraordinarily tall, such as the massive 350 m column being built in a mineshaft in Sardinia, Italy as part of the Aria project to enrich argon isotopes [14]. Applying process intensification to reduce column heights [15] will have a major impact on the practicality and capital and operating costs of isotopic enrichment by CBPS, and possibly extend applicability to heavier elements.

Separation of chemicals based on boiling point differences relies on VLE where components with higher volatility—having lower boiling points referred to as lighter components—have higher equilibrium concentrations in the vapor phase than in the liquid phase. This enables processes to use multiple stages of evaporation and condensation to gradually concentrate lighter components in a ‘distillate’ fluid stream and heavier components in a ‘bottoms’ fluid stream. Distillation processes are ubiquitous in the petrochemical industry. The thermodynamics underlying this separation method are VLE curves that relate vapor concentration to liquid concentration at a given temperature and pressure. To separate isotopes using CBPS, a molecule must be chosen that incorporates the isotopes in a form that has VLE isotope effects (IE) great enough to facilitate a separation in a practical number of stages. Boiling point temperature and relative volatility are two metrics that are typically used to indicate the difficulty of a CBPS. Relative volatility, also referred to as the single-stage separation factor, is defined as

$$\alpha_{ij} = \frac{(y_i/x_i)}{(y_j/x_j)} \quad (1.2)$$

where y and x are the equilibrium concentrations of component i and j in the vapor and liquid phases, respectively. As relative volatility approaches 1.0, each CBPS stage provides smaller incremental enrichment and more and more stages are required to accomplish separation of isotopes. Boiling point differences of a fraction of a degree Celsius or relative volatilities very close to 1.0 are typical for isotope separations [16], requiring many stages of separation. One of the largest boiling point differences is between hydrogen isotopes in water. The normal boiling points of HDO and D₂O are 100.7°C and 101.4°C, respectively, compared to 100°C for H₂O [17]. The relative volatility of ¹²CH₄/¹³CH₄ and ¹²CO/¹³CO are 1.0035–1.0054 and 1.007–1.01, respectively [18].

The low relative volatility of isotopic compounds translates into a large number of CBPS stages needed to perform isotopic enrichment. For example, separating ¹³CO from ¹²CO requires 2000-3000 stages to get 99% ¹³C from the natural abundance of 1.11% [18]. Each stage requires a length of column referred to as the height of a theoretical plate (HETP)¹. A given column packing can be characterized by its HETP. An advanced commercial structured packing is typically 0.3-0.5 m [19, 20]. Extensive efforts by others to develop structured packings have achieved HETPs of 0.2 m with SuperCarb[®] 4D packing [21], which results in impractically tall columns of 400 m to 600 m for the ¹²C/¹³C separation. Li et al. [18] demonstrated a special high-performance packing that reduced the HETP to 3-5 cm in achieving 20-30 stages per meter in 18 meters of column. The best available commercial packing is the Sulzer Laboratory

¹ The term HETP originates from conventional distillation equipment constructed of plates or trays where each theoretical plate represented one separation stage. HETP represents a section of a packed column where the vapor and liquid leaving that section are in mass transfer equilibrium, as determined by the vapor-liquid equilibrium curve.

packing [20] reported to have an HETP as low as 2 cm but is available only in diameters of 2 to 8 cm. Considered the best available technology (BAT) for low HETP, the Sulzer laboratory packing still requires columns that are 40 to 60 meters tall of limited diameter for the $^{12}\text{C}/^{13}\text{C}$ separation.

Process intensification offers approaches for reducing the size of conventional process equipment by accelerating heat and mass transfer processes. Sundberg, et al. [22] provide an overview of concepts and methods that have been pursued for process intensification of distillation, including falling films [23], rotating spiral [24], and membrane [25] configurations. Sundberg, Uusi-Kyyny, and Alopaeus used capillary flow in a horizontal configuration very similar to the microwick approach [26]. These efforts resulted in demonstrations of HETP from a few centimeters to lengths approaching 1 cm in a single-channel device and typically accomplished less than 10 separation stages.

The theory of CBPS for isotopic enrichment is identical to that for chemical separations, and technology that is capable of the latter is potentially applicable to the former. A brief review of previous efforts at PNNL to apply MCD for chemical separations is included as relevant background information. The two projects described are distillation of a military diesel fuel, JP-8 [27] and high purity polishing of n-octane as a surrogate for electronic materials [28]. The goal of distilling JP-8 fuel was to separate a distillate fraction free of heavy sulfur compounds that could be readily desulfurized. Hydrodesulfurization (HDS) of the distillate to very low concentration was a prerequisite for steam reforming to make hydrogen for fuel cells. Figure 1.4 and Figure 1.5 show sulfur distribution and boiling curves for the feed, distillate cut, and remaining heavy bottoms. Distillation of JP-8 was the first successful continuous operation of a microchannel distillation device that produced a useful product. The HETP for this separation has been estimated at 1.8 cm [22].

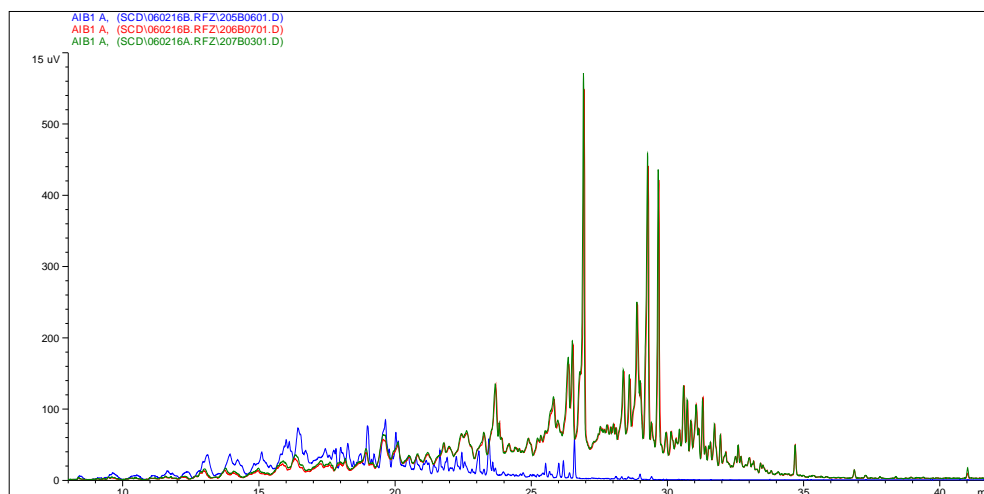


Figure 1.4. GC-SCD chromatograms showing sulfur distribution of full JP-8 (red), heavy bottom product (green) and light distillate fraction (blue).

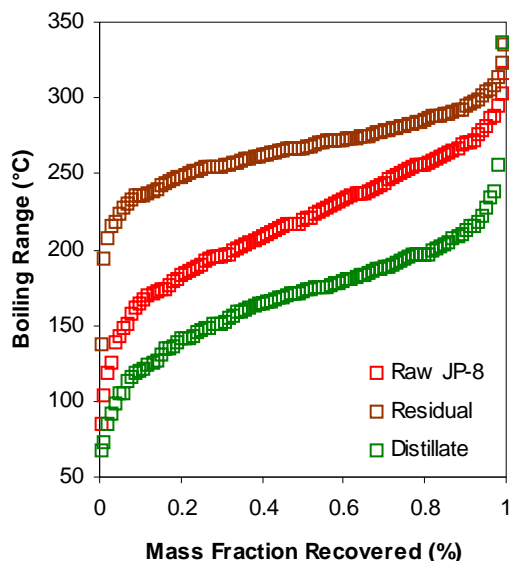


Figure 1.5. Boiling point ranges of the raw JP-8 feed (red), heavy bottom product (brown), and light distillate fraction (green).

In a separate effort with a private industrial client, production of high purity products was successfully demonstrated. Removing impurities having boiling points very close to the desired product makes this prior work highly applicable to isotopic enrichment. Since the desired specialty chemical was pyrophoric, the initial development and demonstration work was done with a surrogate chemical. The chemical system adopted for initial demonstration used n-octane and three other hydrocarbons as impurities having relative volatility ranging from 1.03 to almost 1.5 and in concentrations of 0.1-1 wt% in the feed, as shown in Table 1.1.

Table 1.1. Feed mixture used for distillation experiments

Compound	Boiling point (°C)	Relative volatility to N-octane	Feed conc. (ppm)
N-Octane	125-127	N/A	N/A
Toluene	111	1.49	1000
3-methylheptane	115-118	1.24	10,000
1,4-dimethylcyclohexane	124-125	1.03	1000

A computational fluid dynamics (CFD) model was developed to predict HETP as a function of geometry and operating conditions. Liquid flow through the wicking structure and vapor flow between the wicks is laminar because of the small dimensions of the flow channels. Laminar flow, unlike turbulent flow, can be accurately modeled by Navier-Stokes equations, the momentum balance equations for Newtonian fluids. The laminar flow equations were solved simultaneously with convective-diffusion differential equations for mass transfer in and between flowing fluids. The model produces first-principles solutions to transport between the counter-flowing vapor and liquid phases that yield predictions of HETP.

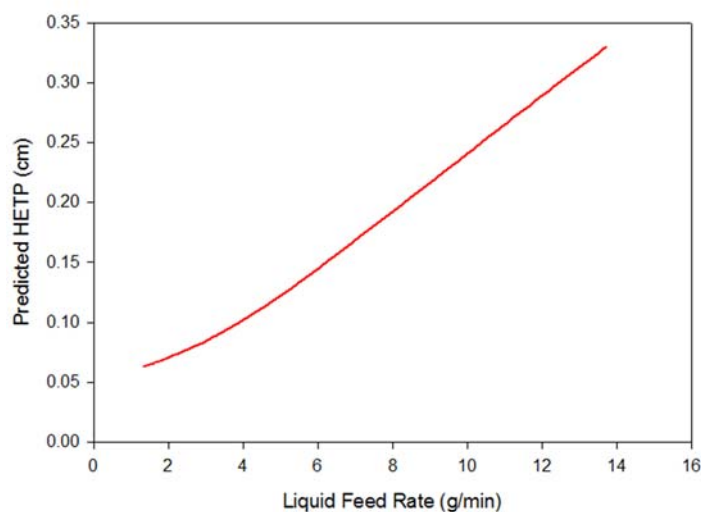


Figure 1.6. Predicted height of a theoretical plate (HETP) as a function of feed flow rate using microwick distillation technology to purify a proprietary specialty chemical; the data shown are for 15 wicks with a reboil ratio of 15.

The model results show that the number of theoretical stages in MCD devices varies inversely with the liquid feed rate, consistent with other packed columns. This inverse relationship allows the number of theoretical separation stages to be increased substantially by simply decreasing the liquid feed rate to the device. Thus, with a single microchannel-based distillation device, a wide range of separations are possible. Results from simulations predict an HETP as low as 0.05 cm at low processing rates, as shown in Figure 1.6. If an HETP of 0.05 cm were achieved, 3000 separation stages could be accomplished in 1.5 m.

Results from a 5-inch MCD device containing 11 wick layers interleaved with 12 vapor channels are presented in Figure 1.7 for the separation of the 3-methylheptane from n-octane. A maximum of 30 stages were achieved in the 5-inch device, representing a record for a single micro-distillation device [22]. Furthermore, an HETP of 0.33 cm would enable 100 stages of separation in 3.3 m. Another important result from the demonstration is the insensitivity of HETP to relative volatility and concentration in the feed. If the separation is controlled by mass transfer in the liquid phase, as described above, then the HETP scaled by diffusivity of the impurity in n-octane should be constant, which is confirmed in Figure 1.8. Furthermore, extrapolating to even lower relative volatilities that are typical for isotopic separations is promising.

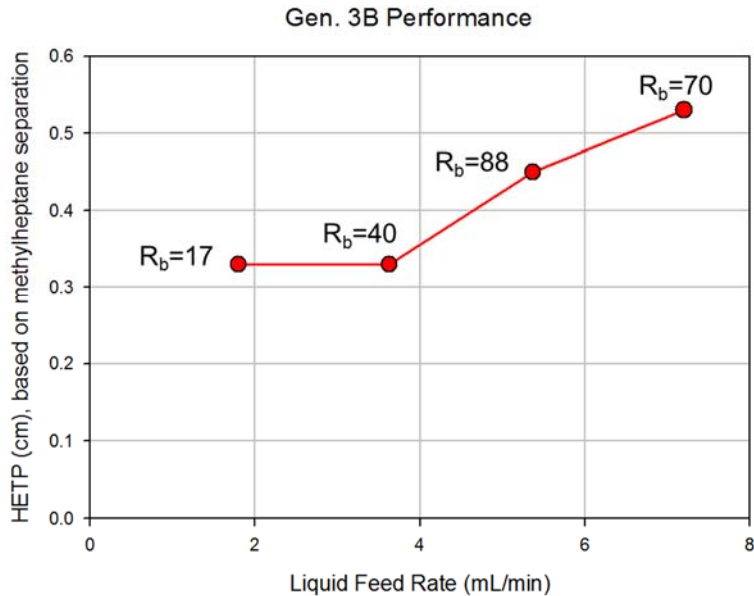


Figure 1.7. HETPs achieved at varying liquid feed rates for separation of 1% 3-methylheptane in n-octane; labels indicate reboil ratio (R_b) at each condition.

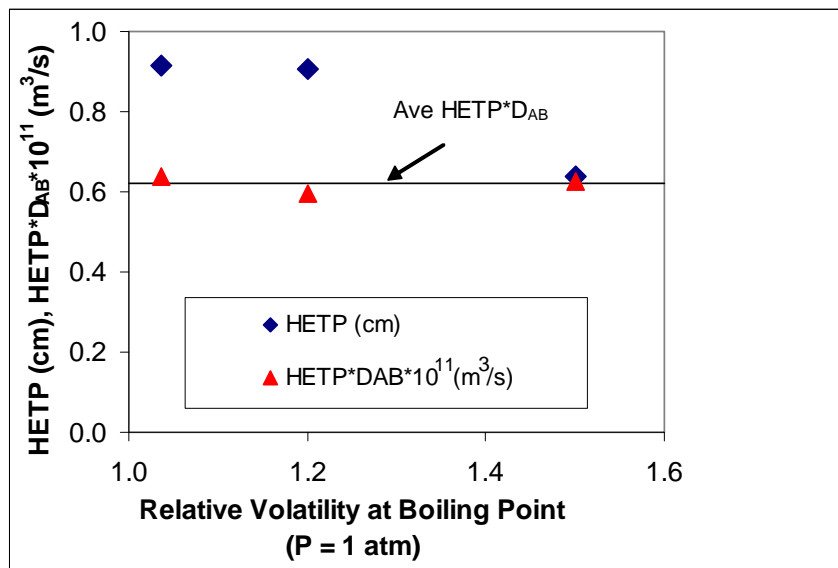


Figure 1.8. HETP and HETP scaled by the liquid phase diffusivity for the three impurity compounds.

Advancing MCD technology for germane isotopic enrichment involves operating MCD devices at cryogenic temperatures at -88°C and at -162°C for methane. Previous testing has been performed above 100°C . Cryogenic operation offers unique challenges for thermal management. Maintaining steady-state operation for long periods required developing unique condenser and reboiler components that could be controlled remotely. In addition, scaling-up the technology to accomplish more separation stages in a single device was a necessary challenge on the pathway to meaningful isotopic separations. In addition to testing a 5-inch device, a 10-inch device containing 20 wick layers was developed in an attempt to achieve greater than 100 stages in a single MCD device. Progress toward achieving these objectives is presented in subsequent sections of this report.

2.0 Experimental Set-Up

2.1 Test Devices

Two test devices were used in performing distillation experiments. The 5-inch device was developed in a prior project, while the 10-inch device was constructed and tested in this project. The dimension refers to the active length for mass transfer; 12.4 cm (4.9 inches) in the shorter device, and 25.4 cm (10 inches) in the second device. Both devices have the same active area width of 4 cm. The 5-inch device has 11 wicks and 12 vapor channels, while the 10-inch device has 20 wicks and 21 vapor channels.

Table 2.1. 5-inch and 10-inch MCD device geometrical properties.

Property	5-inch Device	10-inch Device
Number of Liquid Wicks	11	20
Number of Vapor Channels	12	21
Liquid/Vapor Channel Width (cm)	4.0	4.0
Vapor Channel Thickness (cm)	0.051	0.051*
Liquid Wick Thickness (cm)	0.011	0.011
Total Liquid Wick Thickness (cm)	0.017	0.017
Total Liquid Wick Flow Cross Sectional Area (cm ²)	0.48	0.88
Total Vapor Flow Cross Sectional Area (cm ²)	2.45	4.22
Channel Active Length (cm) [†]	12.45	25.40

*The top and bottom vapor channels have a vapor channel thickness of 0.043 cm compared to the other 19 channels that have a vapor channel thickness of 0.051 cm.

[†]The active length is defined as the available length that the vapor and liquid phases are in direct contact.

2.1.1 Four-inch Test Device

The 5-inch test device was constructed of stainless steel as a layered device with 11 wicks and 12 vapor layers interleaved in a stack. The extra vapor channel provides for vapor channels on both sides of each wick which better balances liquid phase mass transfer. The stack is brazed to seal the device with inlets and outlets for the liquid and vapor streams. The completed device is shown in Figure 2.1. Extra ports along the length of the device are thermocouple wells for measuring temperature profiles, which were not used since isotopic enrichment is nearly isothermal.

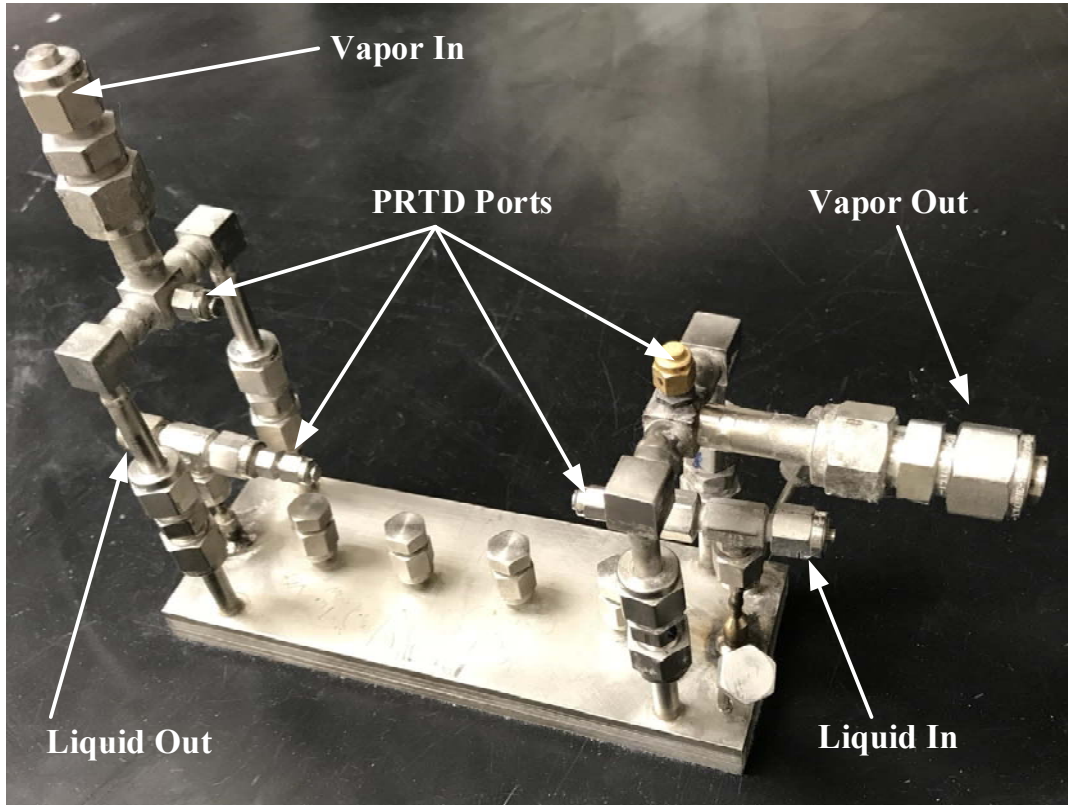


Figure 2.1. Photograph of the assembled 5-inch active length MCD device. The inlets and outlets along with the ports for Platinum Resistance Temperature Detectors (PRTD) are labeled.

The wick layers are pre-assembled by bonding a 0.0015” thick Bopp woven screen to both sides of a middle layer that was fabricated using photochemical machining (PCM). Dimensions of the middle layer are shown in Figure 2.2. The device was assembled by alternating the pre-assembled wicks with vapor shims. A drawing of the vapor shim is shown in Figure 2.3, which was also fabricated using PCM. The cross-hatched pattern consists of ‘wires’ that are etched to half-depth on one side going in one direction and on the other side going in the other direction. This design provides flow paths for the vapor from one end of the shim to the other while providing structural support for the wicks. The stack is sandwiched by 0.125” thick steel plates and brazed together to form a hermetic device. Tubes are subsequently welded onto holes in the top plate above the headers for liquid and vapor flow in and out of the device.

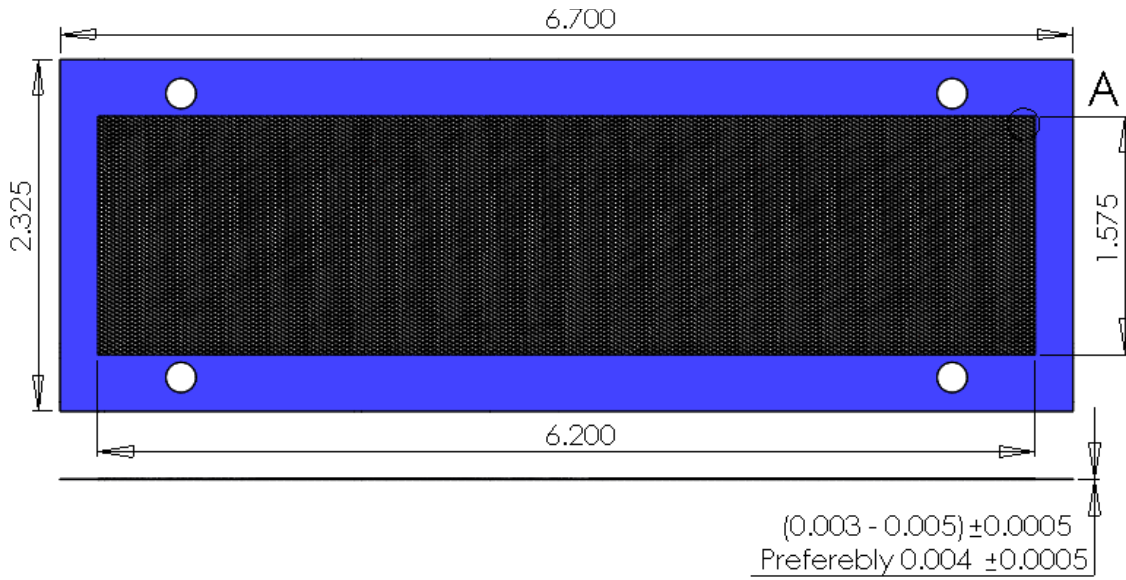


Figure 2.2. PCM structure used as the middle layer of the wicks in the 5-inch device; dimensions are in inches.

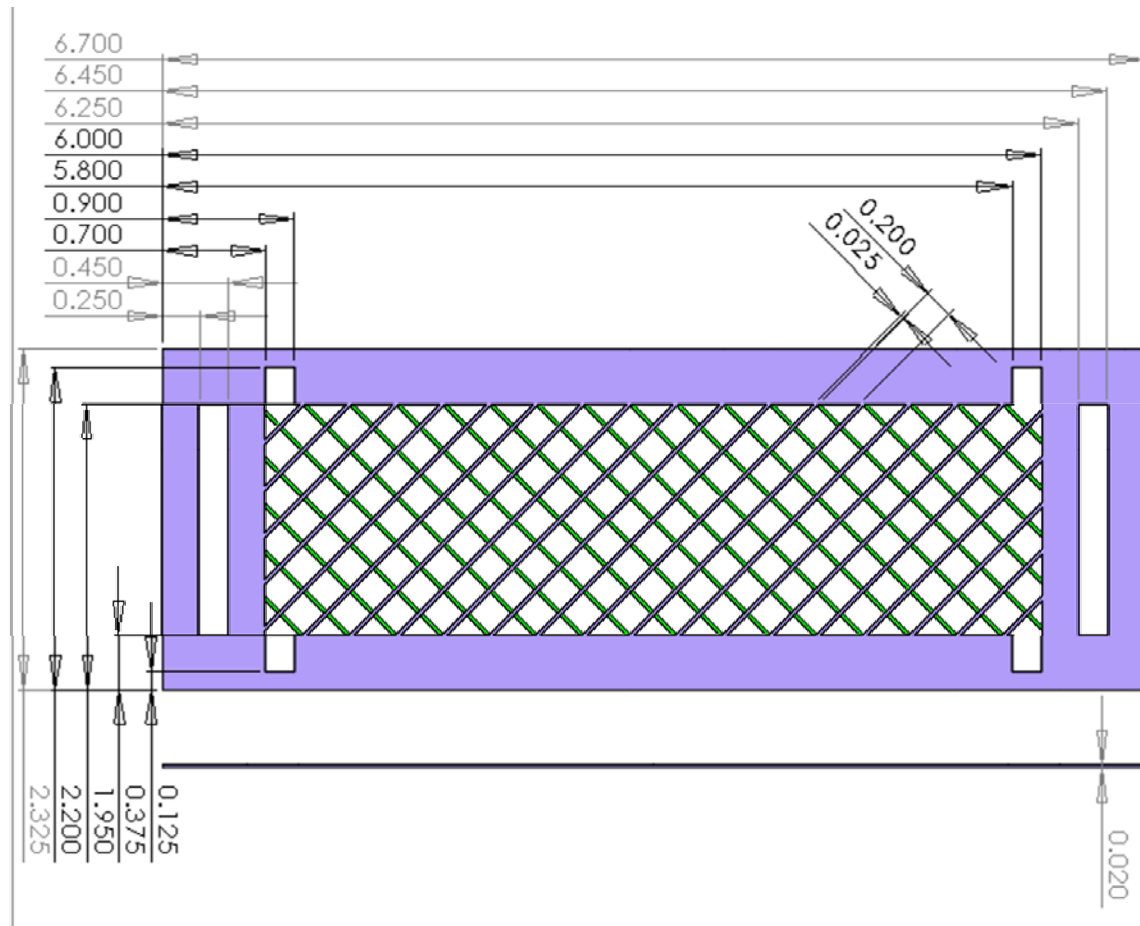


Figure 2.3. Alternative 'angled-wire' vapor channel layer; dimensions are in inches.

2.1.2 Ten-inch Test Device

The 10-inch MCD device was fabricated similarly to the 5-inch device and the assembled device is shown in Figure 2.4. However, there were subtle differences in the design and fabrication in an attempt to improve MCD performance. Design changes are represented in the PCM middle layer of the wick shown in Figure 2.5, and the vapor layer shown in Figure 2.6. First, the length was increased to improve the number of separation stages, but the increased pressure drop reduces flow capacity. Thus, in order to compensate for the decreased flow, more liquid wicks and vapor channels were necessary to achieve equivalent throughputs. The 10-inch device, therefore, contained nearly double the number of liquid wicks and vapor channels compared to the 5-inch device. In addition, the top and bottom vapor channel heights were also scaled for lower flow rates to compensate for mass exchange with only one wick. Swagelok fittings were also replaced by additional welded joints and/or VCR fittings where possible to eliminate potential leaks points.

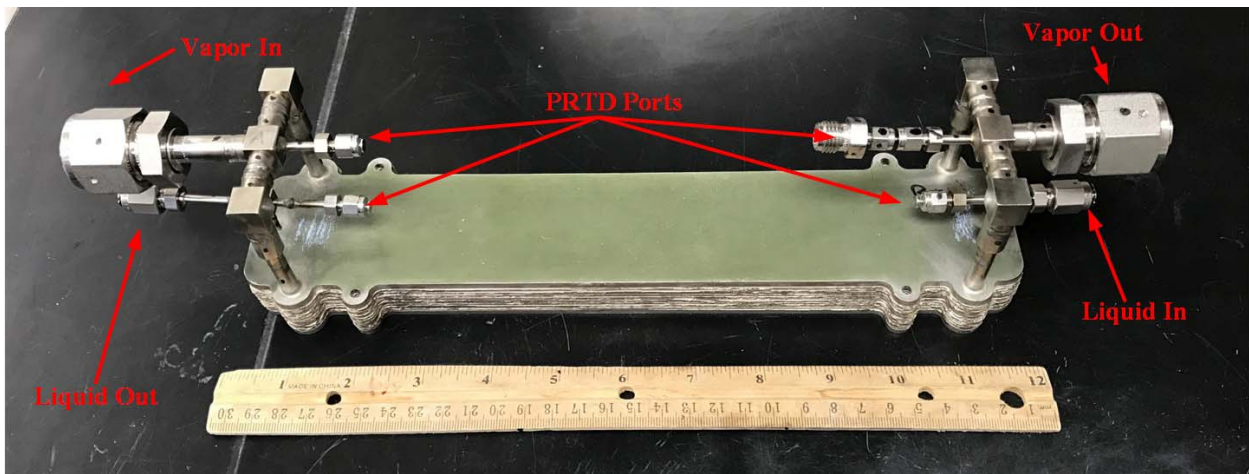


Figure 2.4. Photograph of the assembled 10-inch active length MCD devices. The different inlets and outlets along with the Platinum Resistance Temperature Detectors (PRTD) ports are labeled.

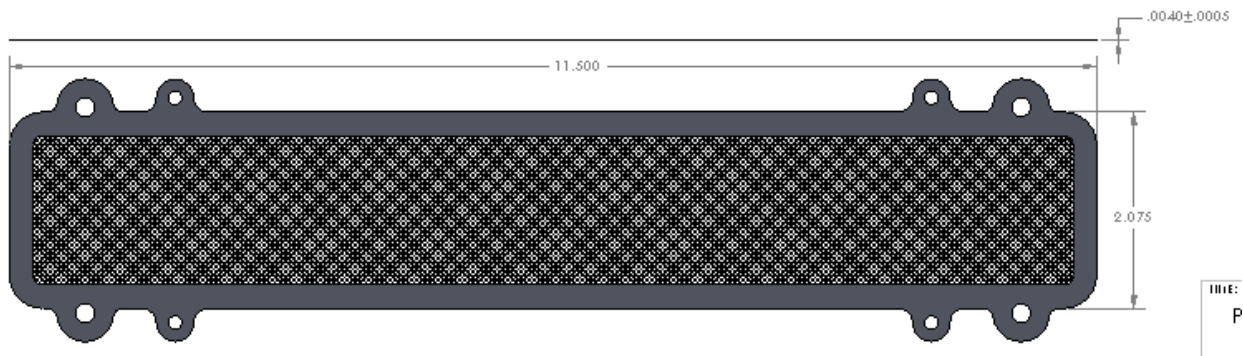


Figure 2.5. PCM structure used as the middle layer of the wicks in the 5-inch device; dimensions are in inches.

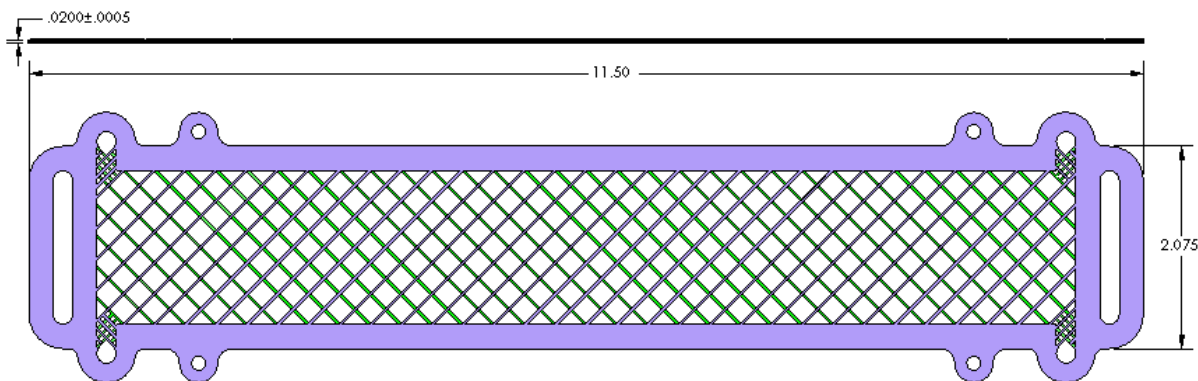


Figure 2.6. Alternative ‘angled-wire’ vapor channel layer; dimensions are in inches.

2.2 Device Functional Testing

Operational readiness testing of both the 5-inch and 10-inch devices included tests for hermeticity, functional internal seals, and flow capacity. Hermeticity tests were completed using a Varian 956 portable turbo helium leak detector. Internal seals were checked through static liquid holdup experiments which measures the requisite siphon—the amount of siphon required to drain the vapor channels—and the breakthrough pressure. Insufficient siphon causes excess liquid hold-up in the device, which increases mass transfer resistance. The requisite siphon is the point where increasing the siphon doesn’t drain additional liquid, indicating liquid is retained only in the wicks by capillarity. The breakthrough pressure is the maximum siphon that can be applied before vapor is pulled into the liquid channels and the siphon is broken. Lastly, flow rate through the device versus pressure drop—the difference between the inlet and outlet siphon heads—is measured to give an operating curve. The flow capacity corresponds to the maximum pressure drop, which theoretically occurs when the inlet is at requisite pressure and the outlet is at the breakthrough pressure. Liquid hold-up and flow rate operating curves were measured for the MCD devices at room temperature using iso-octane.

2.2.1 Hermeticity

The hermeticity of the 5-inch and 10-inch MCD devices were tested with the helium leak detector and were measured to be leak tight at or below the minimum threshold of the detector at $5.5 \cdot 10^{-8}$ atm·cm³/sec. The devices were operated in slightly positive pressure so that any leaks would be out of the device.

2.2.2 Static Liquid Holdup

Static liquid holdup experiments were performed to measure the amount of siphon required to drain the vapor channels as well as the breakthrough pressure in each device. Excess liquid in the device can increase mass transfer resistance. Initially, the device was completely filled with iso-octane at room temperature, the inlet and outlet were valved off and the device was weighed. While keeping the inlet valve closed, the outlet valve was opened and the outlet tubing was positioned at different heights below the device. At each outlet tubing position, the amount of liquid drained from the vapor channels of the device was measured, the outlet valve was closed, and the device was reweighed until the breakthrough pressure, i.e. the point at which the liquid siphon broke, was found. As can be observed from Figure 2.7, the useful operating ranges for the 5-inch and 10-inch device were ~3-13 cm of iso-octane and ~3-8 cm of iso-octane, respectively. Siphons lower than the given range for each device resulted in the inability to

completely drain the vapor channels and siphons higher than this range resulted in a loss of siphon. The results indicate that both devices could hold liquid in the wicks and that there is a usable operating range for performing MCD experiments; however, the actual working range will depend on the surface tension of the liquid and the wettability of the liquid to the stainless steel wicks at the operating temperature. The 10-inch device held 87 g versus 29 g in the 5-inch device due to the greater number of wicks and longer length. The breakthrough pressure in the 10-inch device was lower which can be partially attributed to the increased thickness of the 10-inch device.

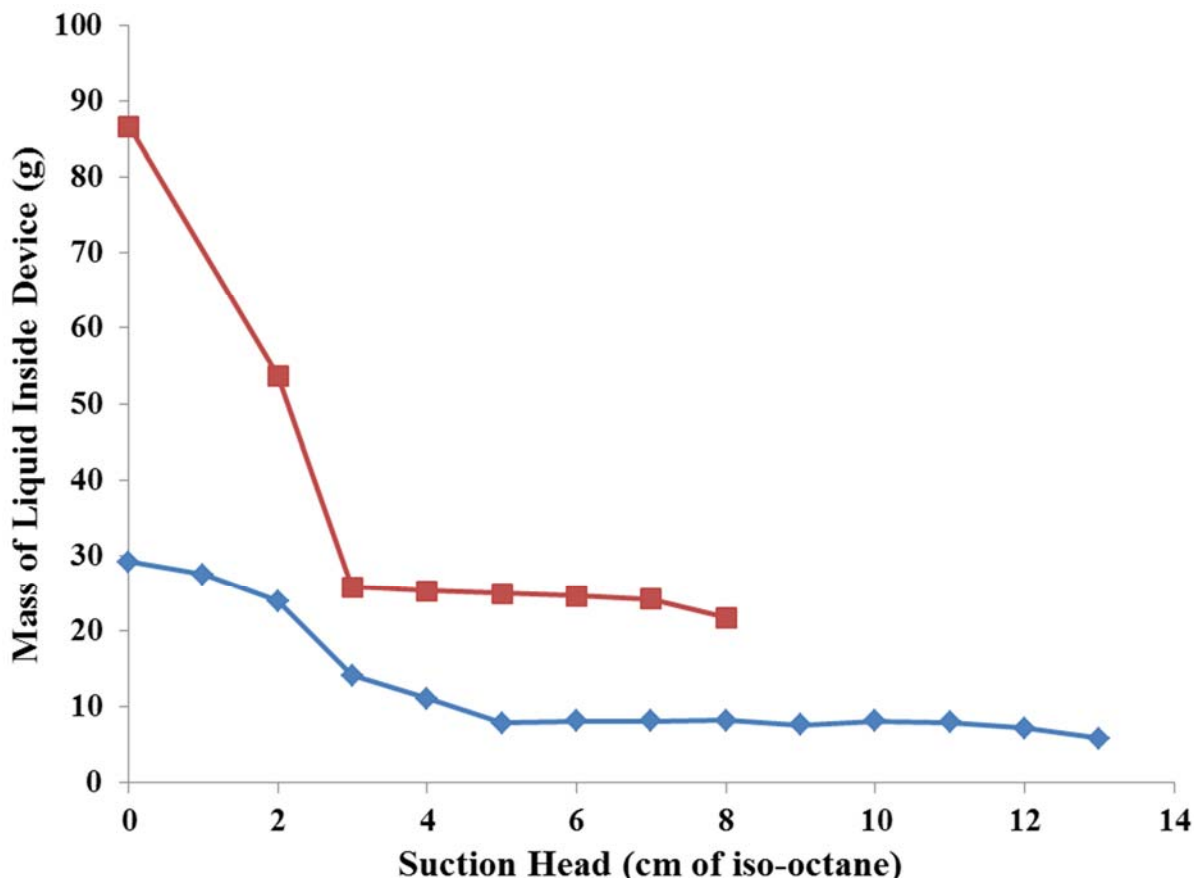


Figure 2.7. Grams of iso-octane contained in the microchannel distillation device as a function of the applied suction head. The curves end at the breakthrough pressure which was 13 cm and 8 cm of iso-octane head for the 5-inch (◆) and 10-inch (■) MCD devices, respectively.

2.2.3 Liquid Flowrate Measurements

The flowrate was measured as a function of differential suction head (ΔP_{Flow}) and indicated a linear relationship below the maximum suction head (13 cm) as shown in Figure 2.8. First, the liquid in the vapor channels was removed, similarly to the liquid holdup experiments, so that the only liquid inside the device was contained within the liquid wicks and in the inlet/outlet liquid tubing lines. Then, the liquid inlet was held at a constant siphon of 1 cm while the outlet siphon was lowered in increments of 1 cm. The flowrate through the device was measured gravimetrically. The results confirm that both devices could be used in the distillation experiments because liquid could flow through the device without breaking the siphon.

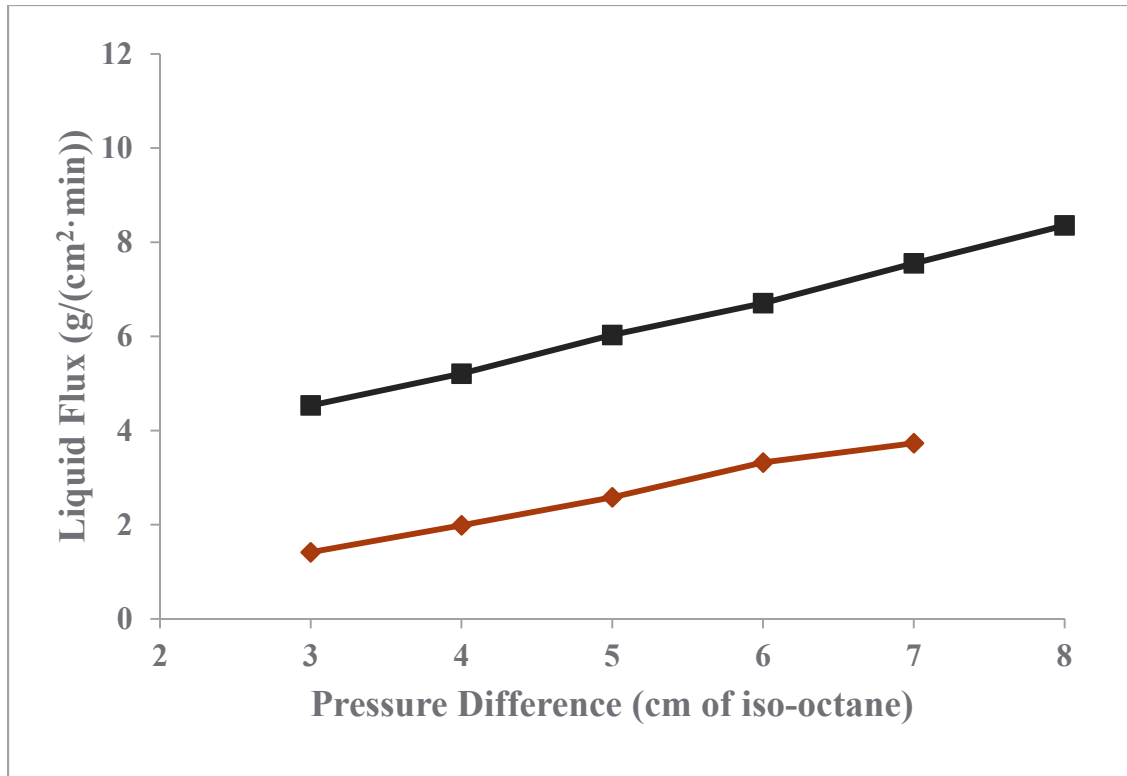


Figure 2.8. Comparison of liquid flux through liquid wicks as a function of iso-octane suction head (ΔP_{Flow}) in both the 5-inch (■) and 10-inch (◆) MCD devices in the working siphon range.

2.3 Experimental Apparatus

The MCD system was designed to deliver feed gas to the condenser where it is mixed with the recirculating vapor flow to maintain the condenser end of the device at feed concentrations as shown in Figure 2.9. The liquid is produced by condensation of the feed and recirculating vapor phase inside of the condenser. The condensation rate controls the liquid flowrate through the MCD device which is manipulated by adjusting the condenser temperature. The liquid is siphoned through the device by adjusting the relative height difference between the condenser (higher) and evaporator (lower). Vapor flow is generated in the evaporator. The liquid and vapor mass flows are balanced by maintaining a constant liquid level in the evaporator. A Solidworks assembly of the major components (MCD device, condenser, and evaporator) is shown in Figure 2.10. The vapor and liquid flow directions are indicated by the red and blue arrows and components in Figure 2.10. The system must operate adiabatically, because heat exchange with the environment will interfere with the recirculating flow.

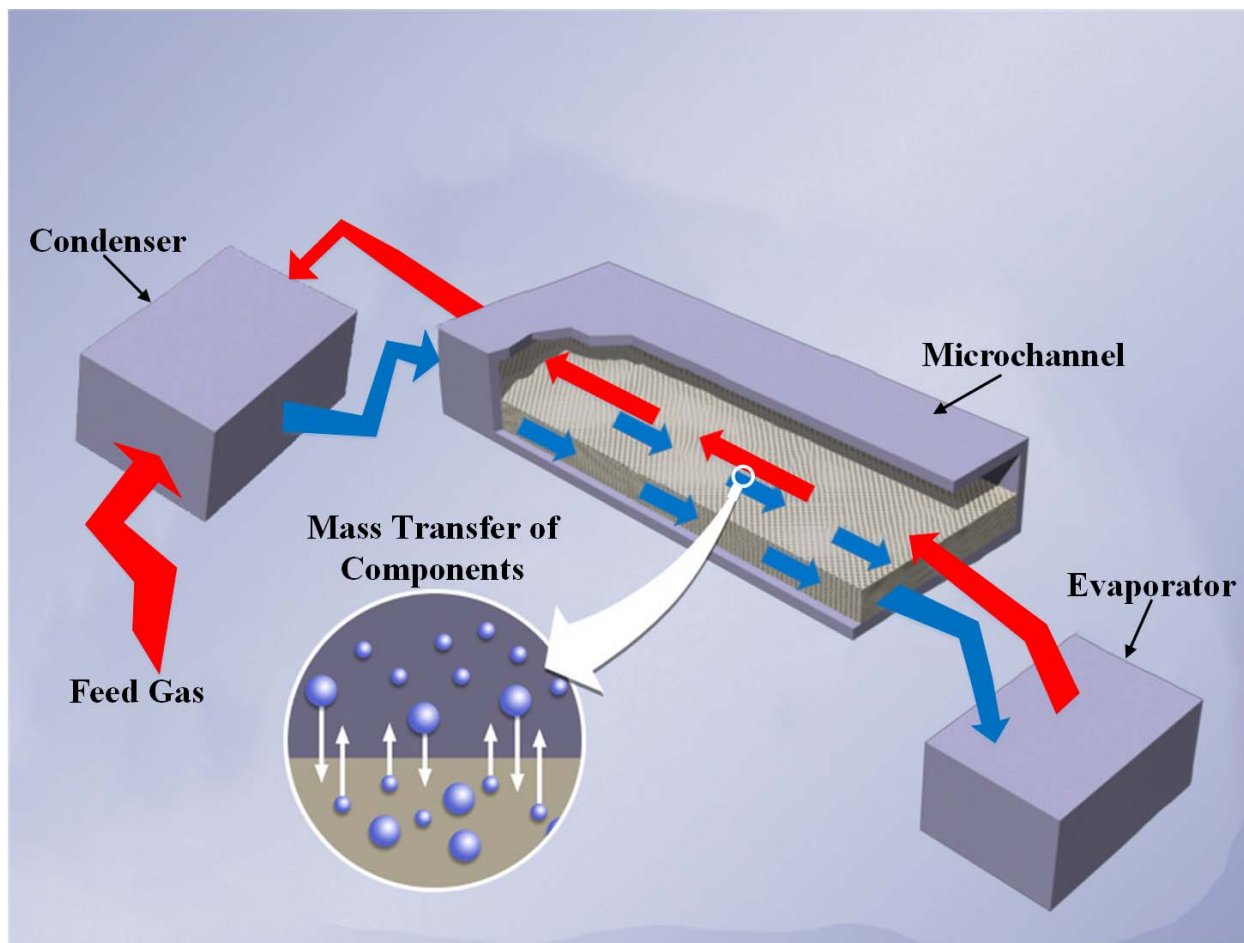


Figure 2.9. Schematic of MCD operation.

The entire system is insulated and installed in a custom-built cryogenic temperature controlled box as shown in Figure 2.11(a). The box temperature was maintained by regulating the amount of liquid nitrogen (LN_2) that was sprayed into the box. The box was designed to encase all the major components and auxiliary equipment with room to spare for position/height adjustments to control the pressure head on both sides of the MCD device. The front of the box could be removed between experiments to modify and/or reposition any components inside the assembly as necessary. The inner dimensions of the box were 24-inch tall, 18-inch wide, and 12-inch deep.

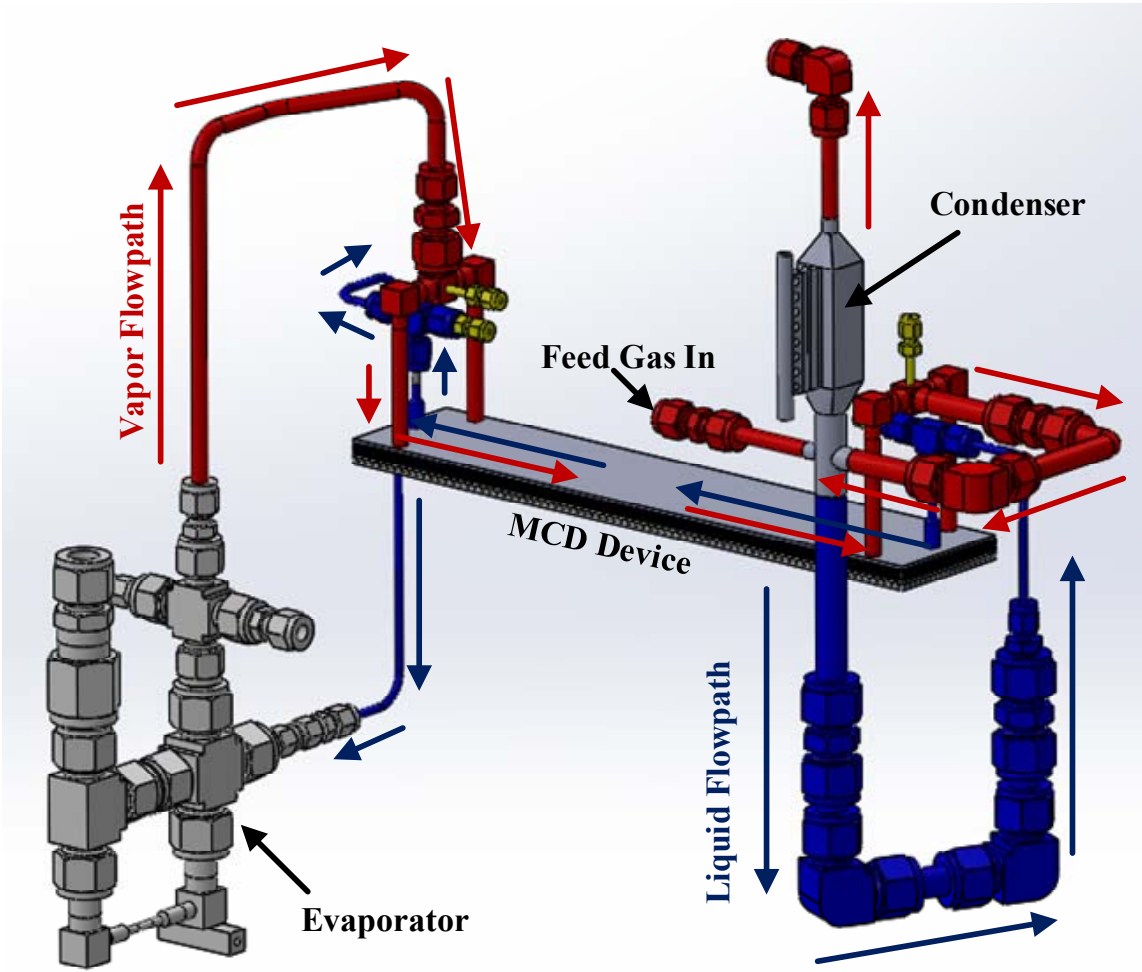


Figure 2.10. Solidworks assembly (from left to right) of evaporator, MCD device, and condenser.

The inside of the box was insulated on all sides with 10 mm thick Cryogel Z-blanket (Aerogel Technologies, LLC) and the outside with 2" thick R-7.7 rigid foam insulation plus an additional 10 mm thick Cryogel Z-blanket on all sides. All seams were sealed with foil tape to prevent heat leaks. Multiple Micronel circulation fans were positioned inside of the cold box to provide enough convective mixing to ensure isothermal conditions inside the box. All components inside the cold box, other than the aforementioned fans, were wrapped with Cryogel Z-blanket to prevent heat losses out of system components and promote adiabatic operation which is essential to successful distillation operation. Additional expanding spray foam insulation was added to the 5-inch MCD device to further minimize heat leaks into and out of the device and further help in attaining adiabatic operation. The insulated system with the front cover removed and in-place are shown in Figure 2.11(b) and Figure 2.11(c), respectively. A process & instrumentation diagram (P&ID) of the entire MCD is shown in Figure 2.12. The system was operated with process-integral-derivative (PID) control loops operated by an Allen-Bradley PLC control system.

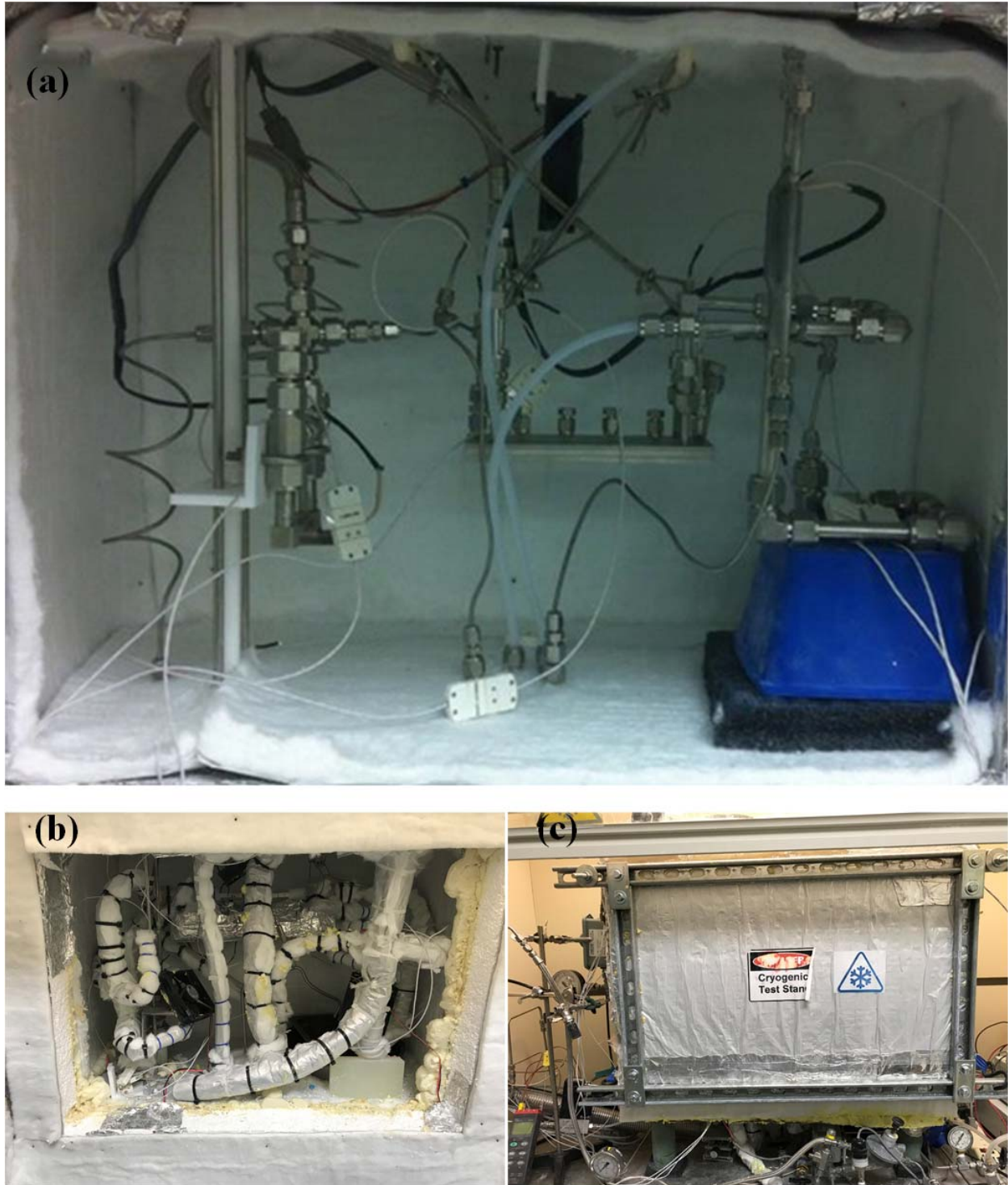


Figure 2.11. (a) The MCD system installed in a cryogenic cold box before insulating system components, (b) after insulating system components, and (c) with the front cover in-place ready for MCD operation.

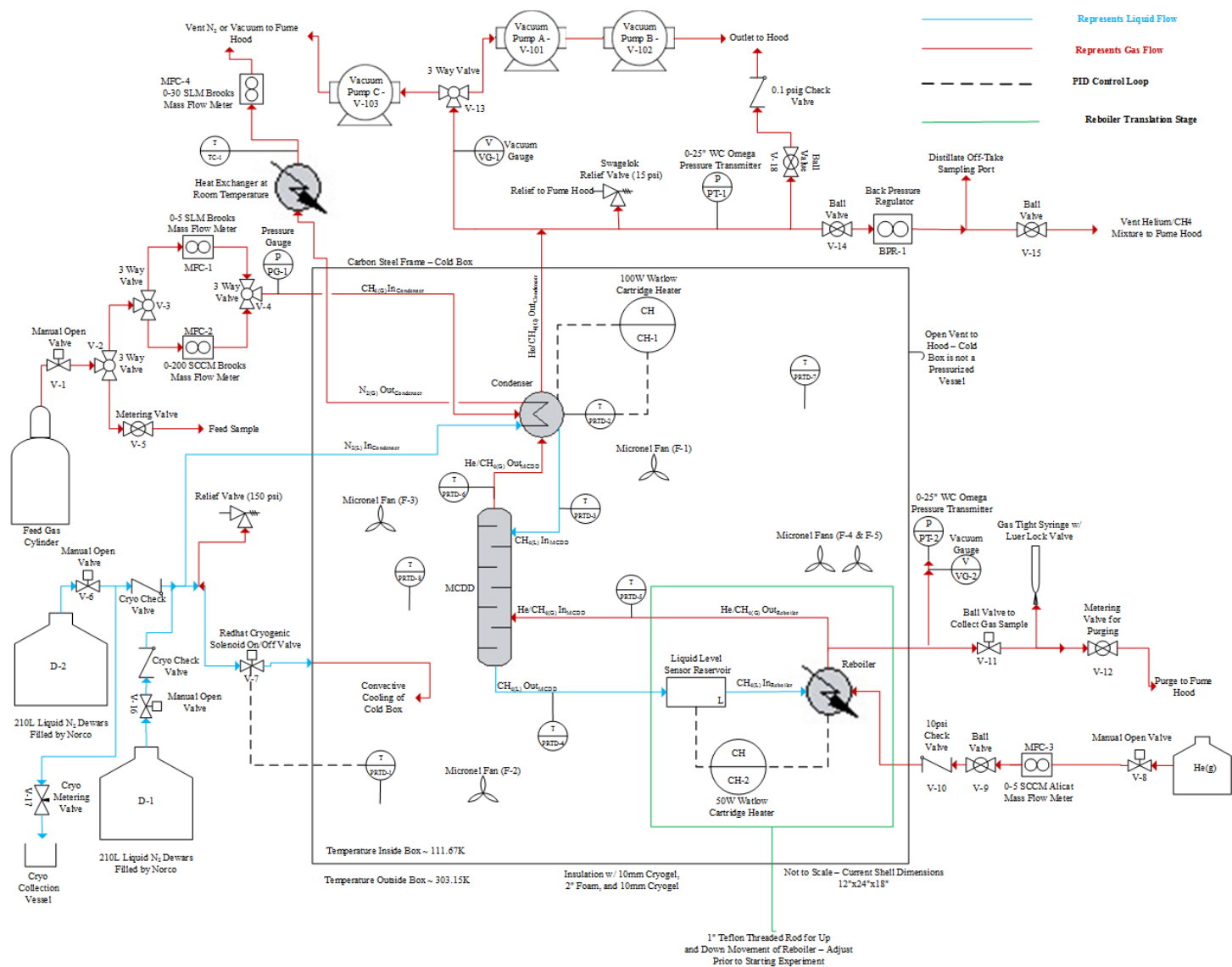


Figure 2.12. Process & instrumentation (P&ID) diagram for the MCD device test-stand.

2.3.1 Control System

An Allen-Bradley CompactLogix™ programmable logic controller (PLC) was purchased and programmed in-house and used a custom designed data acquisition control system (DACS) to monitor and log temperatures, pressures, mass flowrates, heater powers, and evaporator liquid level. The graphical user interface of the MCD control system is shown in Figure 2.13. Three proportional-integral-derivative (PID) control loops were used to aid in the MCD operation. A box temperature reading from a Platinum Resistance Temperature Detector (PRTD) was fed back to a REDHAT solenoid valve (6YEH9) to regulate the amount of LN₂ flow into the cold box in order to keep the temperature inside of the cold box constant. The condenser temperature was maintained by active heating using a 100 W cartridge heater. The condenser will be described in Section 2.3.2. The evaporator liquid level was kept constant by using a 50 W cartridge heater to provide heat to the evaporator to generate the vapor in the system and keep the liquid inventory constant. The DACS also included an automatic shutdown feature if parameter values fell outside of their established limits and a Guard It autodialer to notify the user of system abnormalities during unattended operation.

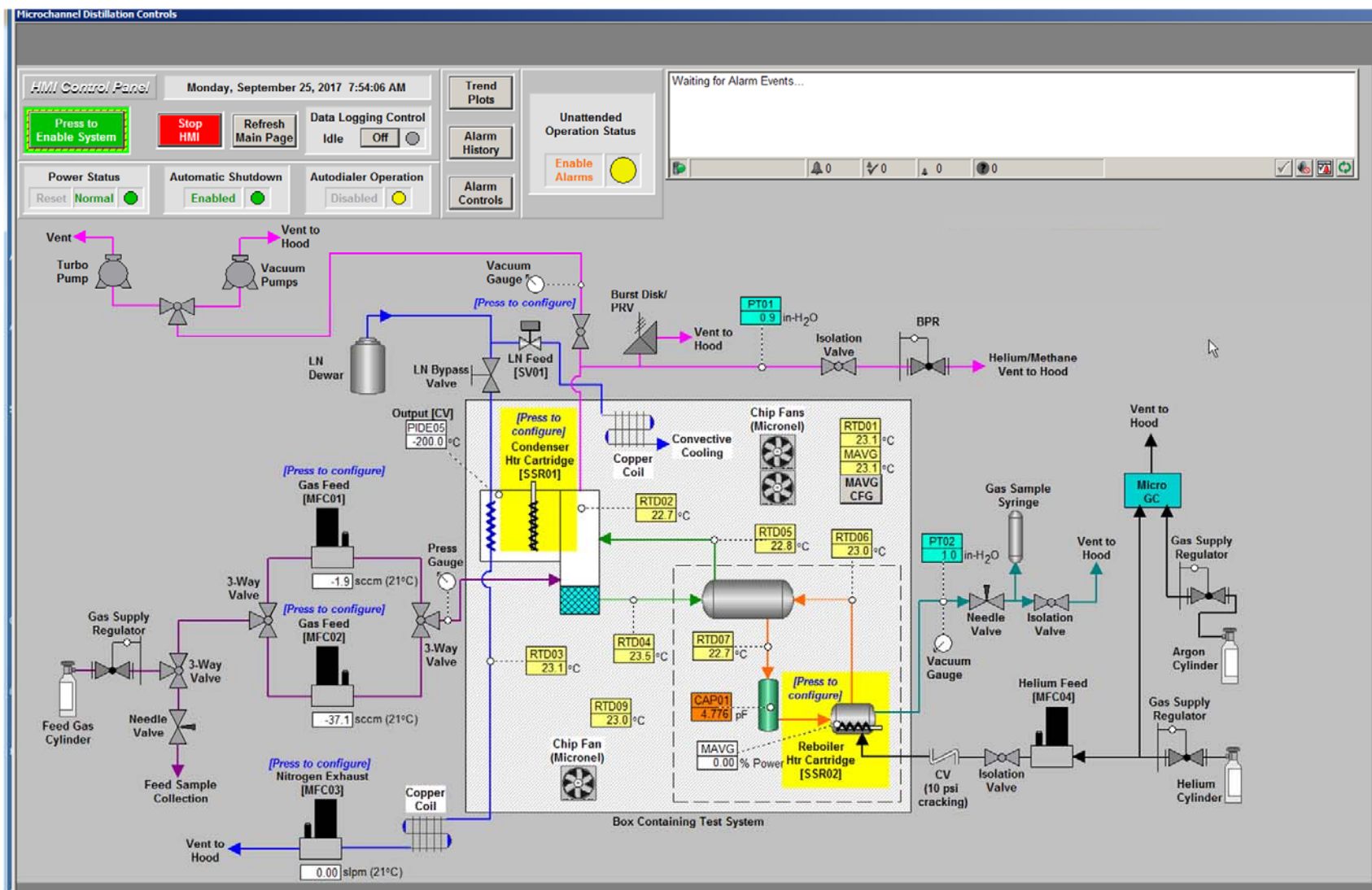


Figure 2.13. Graphical user interface of MCD control system.

2.3.2 Condenser

The condenser was additively manufactured from aluminum by selective laser melting (SLM). The condenser was designed with 8 internal fins for extended heat transfer surface area that were 2-inch tall, 0.65-inch wide, and 0.055-inch thick with 0.03-inch spacing between the fins giving a total surface area of 150 cm². The condensing compartment of the condenser was designed to provide enough surface area and cooling capacity to liquefy enough feed gas to completely fill the MCD device with liquid in a matter of minutes without freezing the process gas and blocking the flow path. The condenser was cooled using LN₂ flowing through a separate tube adjacent to and in thermal contact with the compartment where feed and process gas were condensed, as shown in Figure 2.14. The LN₂ flow was constant and the temperature of the condenser was controlled using a PRTD and cartridge heater located between the LN₂ and the condensing surfaces, as shown in Figure 2.14. The liquid nitrogen temperature (-196°C) could freeze the incoming feed or process gas, and block flow between the fins. Therefore, a PRTD was used to measure the temperature between the LN₂ and the fins that was used in a PID control loop that controlled the operation of a 100 W Firerod® Watlow cartridge heater. This allowed active control of the condenser temperature and thus the amount of liquid flow through the device while simultaneously preventing freezing of the feed or process gas. Other details of the condenser are shown in Figure 2.14.

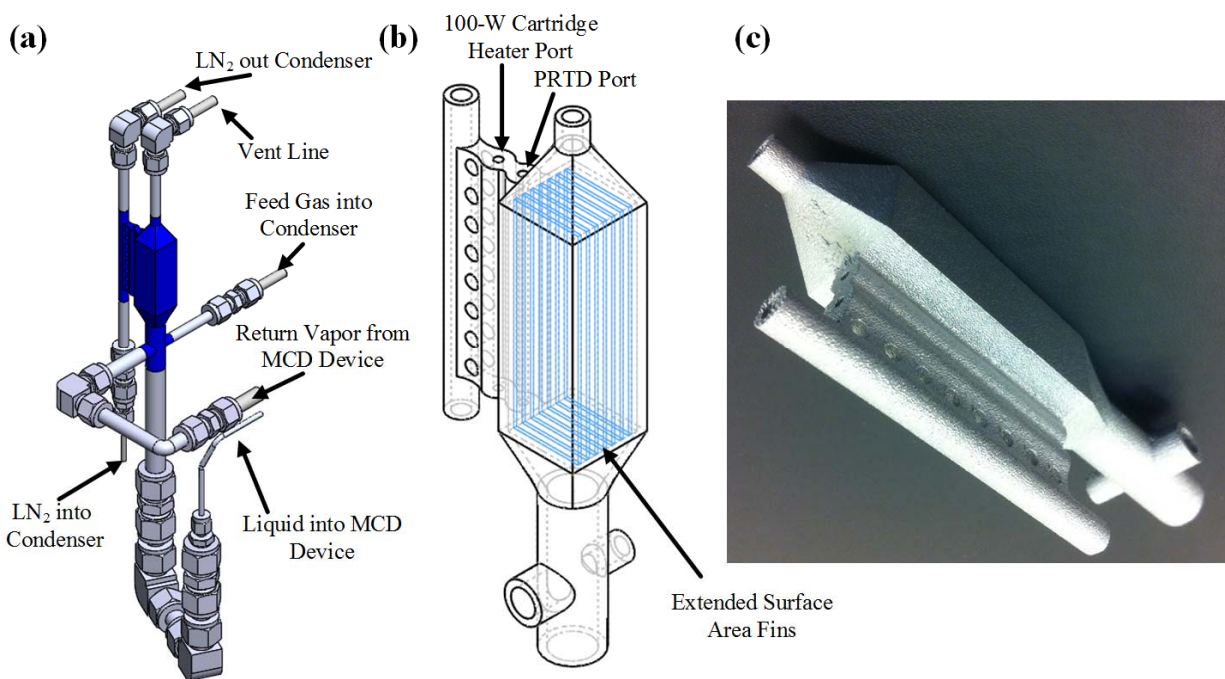


Figure 2.14. (a) CAD assembly of SLM fabricated condenser (blue) with Swagelok fittings and SS tubing showing flow inlets and outlets, (b) blow-up CAD view of condenser showing extended surface area fins, and (c) photograph of the additively manufactured condenser.

In addition, the condenser liquid hold-up volume acted as a “sink trap” below the level of the evaporator so that when the siphon was established through the device, the condenser liquid does not empty and pull vapor into the device. The liquid hold-up volume was approximately 30 mL. The condenser was designed to condense 60 mL of methane, the volume of condenser hold-up plus the 5-inch MCD device internal volume, in a few minutes. Heat transfer calculations were performed to verify this based on an average heat transfer coefficient for film condensation on flat plates [29] using the properties of methane at its normal boiling point temperature.

2.3.3 Evaporator

The evaporator was built entirely of Swagelok fittings, SS tubing, and a national pipe thread (NPT) electrical feedthrough fitting. A CAD drawing and the details of the evaporator are shown in Figure 2.15. The evaporator was designed to accommodate 1/10 the liquid volume to that of the liquid hold-up volume in the condenser (~ 30 mL) in order to decrease the residence time. The evaporator includes two hydraulically connected, but distinct compartments. It was designed accordingly to avoid boiling in the same region as where the liquid level was being monitored. Therefore, the first compartment (left of Figure 2.15) includes the location where liquid drips into the bottom of the evaporator and a capacitance based custom-built liquid level sensor. The level of the end of the liquid drip tube in the evaporator sets the siphon height. The capacitance reading was assumed to be linear with liquid level. The liquid level was set to 30-50% full during operation and the PID control loop adjusted the evaporator cartridge heater power output to achieve this desired setpoint. This allowed active liquid level control. The second compartment's outer surface (right of Figure 2.15) is attached to a 50 W Firerod® Watlow cartridge heater that provides the heat necessary to "boil off" the collected liquid. The evaporator was installed in the cryogenic cold box by attachment to a custom built Z-translation stage so that the evaporator could be manually moved up and down before or during operation to adjust the siphon height. More detailed information on the condenser and evaporator is given in **Error! Reference source not found.**

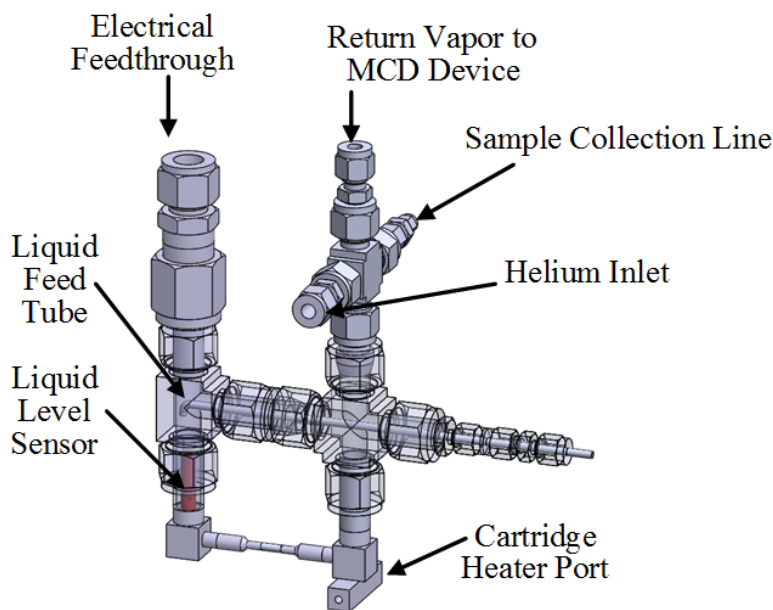


Figure 2.15. CAD assembly of evaporator indicating important components.

2.3.4 Helium Flow

Helium flow was added to the vapor stream in order to compensate for the pressure difference between the vapor and the liquid in the wicks due to the siphons. The pressure difference causes a slight shift in the boiling points of the vapor and liquid streams that previously was associated with liquid flow instability. The helium lowers the vapor phase partial pressures to correct for the boiling point disparity.

3.0 Data Analysis

3.1 Height of an Equivalent Theoretical Plate (HETP)

Distillation exploits differences in relative volatility of species in a liquid mixture to separate different components by selective condensation and evaporation. It relies on components with lower volatilities having a higher equilibrium concentration in the liquid phase, and species with higher volatilities achieve a greater equilibrium concentration in the vapor phase. Multiple stages of separation are employed to increase the level of enrichment. In each successive stage, the more volatile component is concentrated in the vapor phase and the less volatile component is enriched in the liquid phase. The minimum number of distillation stages (N_{stages}) required to achieve the desired separation for a two-component system can be calculated using the Fenske total reflux equation [30] such that,

$$N_{stages} = \frac{\ln\left[\left(\frac{X_D}{1-X_D}\right)\left(\frac{1-X_B}{X_B}\right)\right]}{\ln(\alpha)} \quad (3.1)$$

where X_D and X_B are the mole fractions of the light component in the distillate (vapor out) and in the bottoms (liquid out), respectively, and α is the relative volatility between the components. The relative volatility is the ratio of vapor pressures and is used to design distillation equipment. An average relative volatility of propane in propylene was calculated as 1.28 from CHEMCAD by averaging 9 values obtained between 10-90 mol% propane at 10 mol% increments. The relative volatility of methane isotopes $^{13}\text{CH}_4$ to $^{12}\text{CH}_4$ is 1.0028 at the normal boiling point temperature, based on a correlation in the literature [31].

A metric used for evaluating separation performance is the overall separation factor,

$$S = \left(\frac{X_D}{1-X_D}\right)\left(\frac{1-X_B}{X_B}\right) \quad (3.2)$$

Which is also used in the number of stages equation, Equation 3.1.

The distillate product composition is assumed to be equivalent to the feed composition since feed is continually added to the condenser. The bottoms product concentration was obtained from the GC/MS analysis for the propane/propylene separation and from GC/IRMS analysis for the methane isotope enrichment, as described in Section 4.4.1 and 4.5.1, respectively. From these concentrations the number of stages can be calculated. Then, as discussed in Section 1.3, the performance parameter, HETP, can be calculated as

$$HETP = \frac{L}{N_{stages}} \quad (3.3)$$

where L is the characteristic length of the microchannel distillation device.

3.2 Liquid Flow Rate

The liquid flow rate through the device was calculated from the evaporator cartridge heater output. Assuming adiabatic operation, meaning minimal heat leaks between the box and the MCD system, which was corroborated experimentally, the liquid volumetric flowrate (Q_L) is given by

$$Q_L = \frac{P_{E,CH}}{\rho_L \Delta H_{vap}} \quad (3.4)$$

where $P_{E,CH}$ is the applied power on the evaporator cartridge heater (% On·50 W), ρ_L is the liquid phase density, and ΔH_{vap} is the latent heat of vaporization at the normal boiling point. Liquid mass flux through the liquid channels of the wicks, j_L , which is used to normalize flowrate through different devices, is calculated as

$$j_L = \frac{P_{E,CH}}{\Delta H_{vap} \cdot A_L} \quad (3.5)$$

where A_L is the cross-sectional area of the liquid wicks not including the Bopp screens since most of the flow will be through the middle layer which is more open.

3.3 Comparison with Conventional Equipment

The emphasis in process intensification of distillation has been reducing the column heights, which is of particular importance for isotopic enrichment that can require thousands or tens of thousands of separations stages. However, the other aspect is throughput, which in conventional columns translates to column diameter. The drivers for column diameter are the production rate and the reflux ratio, because the liquid flow through the column is equal to the distillate (light product) flow rate times the reflux ratio. Similarly, the vapor flow is the bottoms (heavy product) flow rate times the reboil ratio. For isotopic enrichment, the low relative volatility of isotopes mandates very large reflux ratios, so liquid flow capacity is an important consideration in the size of the MCD equipment.

Conventional packed column technologies are typically evaluated by their liquid loading rate, B_{liq} which is defined as liquid flow rate through the column divided by the column cross sectional area [32]. A similar metric used by Sulzer for rating structured packings is the F-factor [20], defined as the empty bed gas velocity, w_G —gas flow divided by column cross-section—times the square root of the gas density, ρ_g .

$$F = w_G \sqrt{\rho_G} \quad (3.6)$$

The focus for this MCD demonstration is minimizing the HETP which is largely determined by the wick thickness. The height of the vapor channel is of less importance for mass transfer and was selected to insure negligible gas channel pressure drop. The vapor channel does enter into the liquid loading rate and F-factor, and an oversized vapor channel causes unnecessarily low liquid loading rate. The total cross-section of the wicks and vapor channels is 3.20 cm² and 5.58 cm² in the 5-inch and 10-inch devices, respectively. Cutting the vapor channel height in half would reduce that to 1.98 cm² and 3.47 cm², respectively, almost doubling the flow capacity without substantially changing the mass transfer or HETP. Since vapor channel height hasn't been optimized, flow capacity results will be represented by both the existing vapor channel height and channels ½ the height.

3.4 Dimensional Analysis

Dimensional analysis is used to compare and contrast MCD performance across different devices, mixtures, and operating conditions. If mass transfer is dominated by diffusion in the liquid phase, then the characteristic time for one separation stage is a function of the characteristic diffusion length scale squared, h_m^2 , divided by liquid phase diffusivity, D_l . The number of separation stages in a given device is expected to depend on the liquid residence time, τ . Assuming a linear relationship, the number of stages is

$$N_{stages} = \frac{L}{HETP} = \frac{1}{C_{eff}} \frac{\tau D_l}{h_m^2} = \frac{1}{C_{eff}} \frac{D_l}{h_m^2} \frac{\rho_l L}{j_L} \quad (3.7)$$

where L is the active length, C_{eff} is an effectiveness coefficient, ρ_l is liquid density, and j_L is liquid mass flux through the wicks. Ideally, effectiveness will be close to 1.0, but the theoretical effectiveness depends on the details of flow through the wicks. The coefficient is introduced as an inverse factor so that C_{eff} gives a factor for potential improvement relative to what is theoretically possible—a value of 10 indicates a potential for 10X reduction in HETP.

Equation 3.7 can also be written in terms of F-Factor as

$$HETP = C_{eff} \frac{h_m^2}{D_l} \frac{\sqrt{\rho_G}}{\rho_L} \frac{A_x}{A_L} F \quad (3.8)$$

where A_x and A_L are the cross sectional areas of the empty bed and the total flow area of the wicks, respectively. Since structured packing performance is typically characterized by HETP versus F , Equation 3.8 provides a means for direct comparison of MCD potential to structured packings.

Vapor phase dispersion in the flow direction is detrimental to MCD performance. An effective distillation process relies on creating concentration profiles in the flow direction in both the liquid and vapor phases. Axial diffusion, referred to as dispersion, diminishes the concentration profiles and works against the distillation process. The Peclet number (Pe) is a dimensionless group that indicates the relative importance of convection to diffusivity. Using HETP as the characteristic length scale, the Peclet number is defined for either the vapor or liquid streams as

$$Pe = \frac{v HETP}{D} = \frac{m HETP}{\rho AD} \quad (3.9)$$

where v is average flow velocity, m is mass flow, ρ is stream density, and A is flow area. In general, $Pe \gg 1$ is desired to prevent dispersion from becoming destructive to the distillation process. In general, dispersion is more important in the gas phase, because the increase in diffusivity is greater than the decrease in density. Furthermore, in the MCD devices, the vapor channel flow area is much larger than the liquid flow area. Consequently, analysis of dispersion is therefore focused on the gas phase.

4.0 Experimental Procedure and Results

The first three sections describe the experimental procedures, which are applicable to both propane/propylene separation and isotopic enrichment of methane with examples provided from one or the other. The remaining sections provide experimental results, analysis, and interpretation of data for each of the two systems.

4.1 Experimental Procedure and Start-up

Startup of the MCD device required filling the entire device with liquid from the condenser until the liquid overflowed into the evaporator. The evaporator, condenser, and MCD device were positioned in the cold box to provide enough suction on the condenser side to prevent flooding and enough pressure difference on the evaporator side to siphon liquid from the condenser through the device as described previously in Figure 1.1. However, too large of a ΔP_{Flow} would cause flooding which adversely effects mass transfer ruining the separation process. Therefore, initial positioning of these individual components was critical to successful distillation experiments.

The system was held under vacuum during the initial cooling down of the device. The box temperature was set to slightly below the feed gas boiling point temperature to cool down system components, the condenser temperature was set 10-20°C below the feed gas boiling point temperature, and LN₂ flow through the condenser was initiated to cool down the condenser. Then, feed flow was started and maintained until the entire device was filled and liquid overflowed into the evaporator as observed by a rapid increase in the liquid level sensor in the evaporator (indicating full). Then, the following steps were performed,

1. feed flow was reduced,
2. box temperature was increased to near the feed gas boiling point temperature,
3. LN₂ flow through the condenser was decreased,
4. evaporator cartridge heater was turned on to a fixed power to begin producing vapor flow back into the device,
5. the condenser temperature was increased to within a few degrees of the feed gas boiling point temperature to slow down the condensation rate and reduce liquid flow being siphoned through the device into the evaporator, and
6. helium flow was started and set to 5 sccm.

The prior six steps were necessary in order to establish a vapor path so that mass transport could occur between the two phases and MCD could commence. The evaporator was initially flooded by liquid overflow from the device, so the evaporator heater was set to a constant power while the excess liquid was boiled off. Once the liquid level in the evaporator was within the operating range of the level sensor, PID control of the liquid level was initiated. Evaporated vapor flowed back into the MCD device, displacing the liquid in the vapor channels until it exited the vapor outlets of the MCD device and into the condenser. Vapor from the device either condensed or flowed out of the system vent line with the accompanying non-condensable helium. At this point, the liquid wicks were filled with only liquid and the vapor channels contained only vapor, and distillation was achieved by mass transfer between the two phases flowing counter-current. The start-up process is illustrated for a methane experiment performed in the 10-inch MCD device in Figure 4.1, Figure 4.2, and Figure 4.3 showing the evolution box temperature,

pressure difference between the two ends of the MCD system, and liquid level as measured by the capacitance probe, respectively. The fluctuations that are observed at approximately 15 hours were a result of an LN₂ Dewar exchange whereby the system dynamics, i.e. cooling, was disturbed. Multiple LN₂ Dewars were necessary to increase run-times and achieve steady-state operation. Soon thereafter the system resumes stable operation and the MCD continues for an additional 8-10 hours.

The box temperature was relatively constant at the normal boiling point of methane during stable-operation as shown in Figure 4.1. Some temperature fluctuations inside the cold box were observed due to pulsing of the LN₂, however, they did not impact the device temperatures as monitored by the PRTDs inside of the device which were relatively constant ($\pm 0.1^\circ\text{C}$) during stable operation. These results are evidence of adiabatic operation, because if significant heat leaks existed, changes in box temperature would result in fluctuations in device temperature, and this was not observed.

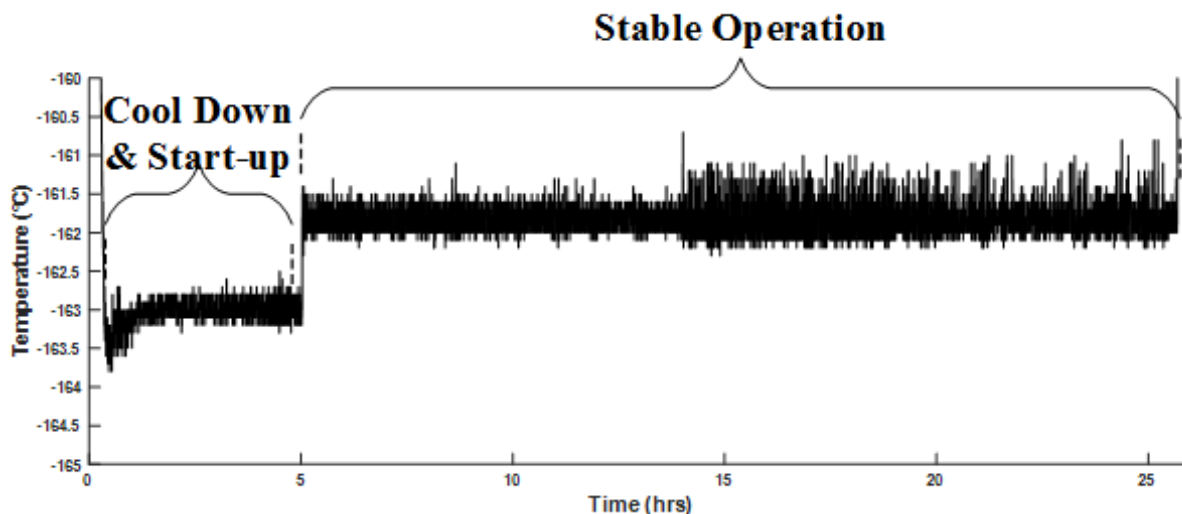


Figure 4.1. Box temperature versus time for a sample distillation experiment of methane isotopic enrichment in the 10-inch device.

After start-up and subsequent displacement of the liquid in the vapor channels, stable operation proceeded and the pressure readings tracked and were equal to one another as observed in Figure 4.2. This verified that excess liquid had been removed from the vapor channels and a continuous vapor path through the MCD device had been established. The six negative pressure spikes during stable operation indicate times when gas phase samples were manually withdrawn from the evaporator for analysis.

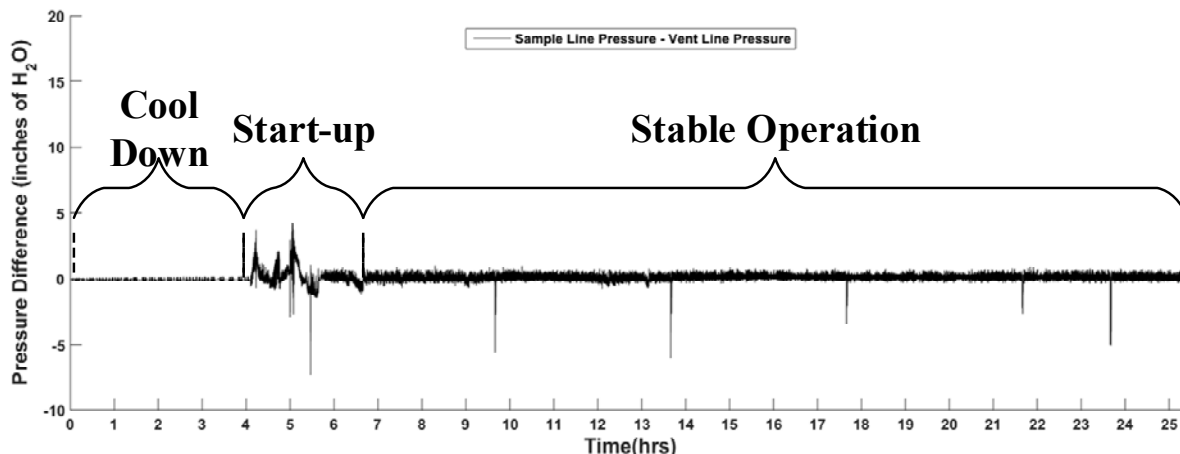


Figure 4.2. Pressure difference through the 10-inch MCD device, measured between the condenser vent line and the evaporator sample line, for a sample distillation experiment of methane isotopic enrichment.

The capacitance-based liquid level in the evaporator is also stable after start-up as shown in Figure 4.3. The figure indicates the lower and upper limits of the capacitance based liquid level sensor that occur at a reading of ~ 4.5 pF (empty) and 7.5 pF (full), respectively for liquid methane. The start-up time to completely fill the device and overflow into the evaporator was about 5 hours and the time necessary to achieve stable operation between empty and full was an additional 1 hour. During stable operation, the liquid level was within $\sim 10\%$ of its setpoint.

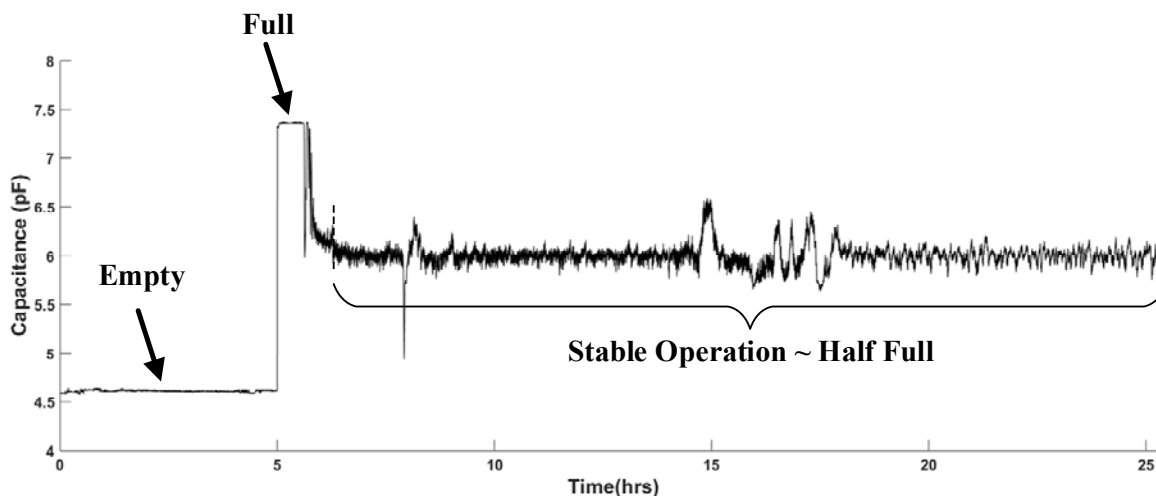


Figure 4.3. Capacitance reading from the liquid level sensor in the evaporator versus time for a sample distillation experiment of methane isotopic enrichment in the 10-inch device.

4.2 Flow Rate

Initial experiments included verifying contiguous flow between the condenser and the evaporator which is a prerequisite for successful distillation operation. The condenser temperature controls the condensation rate and therefore the liquid flow through the device into the evaporator. For a constant evaporator liquid

level at steady-state operation, the evaporation rate that is proportional to evaporator power must be equal to the condensation rate. This was validated by varying the condenser temperature and observing an inversely proportional response from the cartridge heater power in the evaporator. For instance, an increase in the condenser temperature setpoint (warmer) resulted in a decrease in the evaporator cartridge heater output. When the condenser temperature is increased, less feed gas is condensed, the liquid level in the condenser decreases, and the driving force for flow (ΔP_{Flow}) through the device is decreased. This indicates that less power from the evaporator cartridge heater is needed to reboil the liquid in the evaporator to keep a consistent liquid level in the evaporator. A calibration curve is shown in Figure 4.4 relating the condenser setpoint temperature to the evaporator cartridge heater output (red curve with red data points) on the secondary y-axis for propane/propylene experiments.

Liquid mass flux through the wick as a function of condenser temperature is also shown in Figure 4.4 (blue curve with blue data points) on the left ordinate axis. Thus, the liquid flow through the device was controlled by modulating the condenser temperature setpoint. Further, a condenser temperature of $\sim -51.35^\circ\text{C}$ would stop liquid flow through the device in the propane/propylene experiments. By verifying a corresponding response by the the condenser and evaporator, MCD distillation could be optimized by performing experiments at different flowrates to evaluate performance.

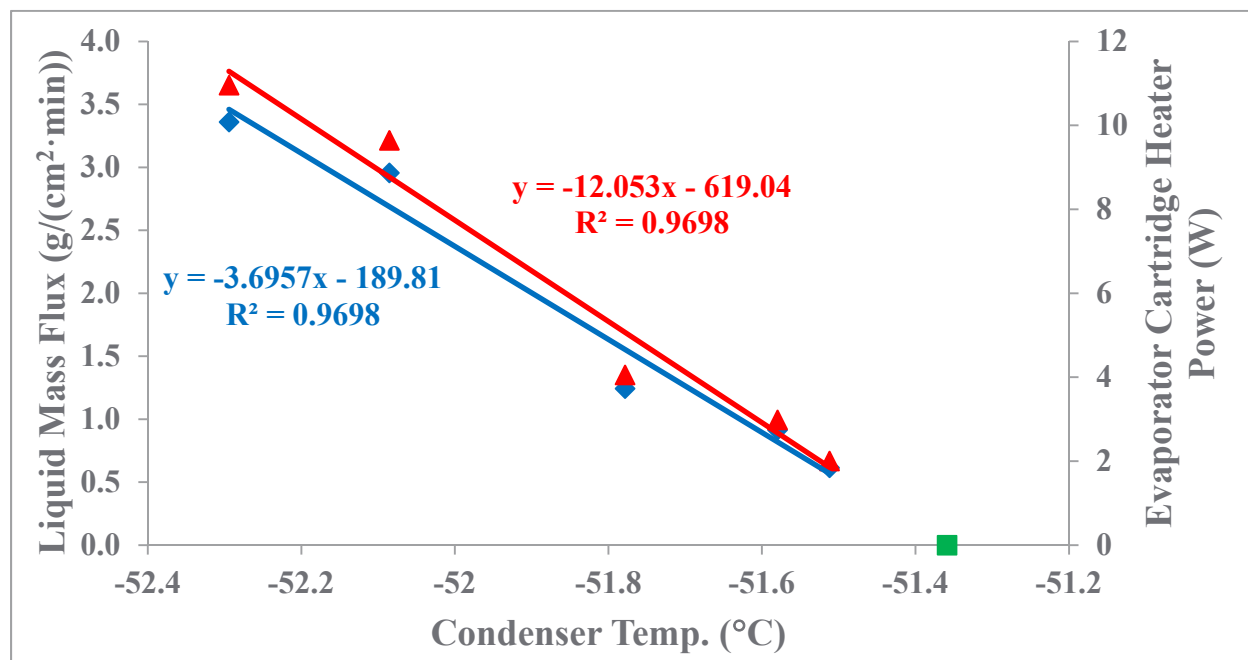


Figure 4.4. (a) Calibration curve of liquid mass flux (blue diamonds (\blacklozenge) and fit) and evaporator cartridge heater output (red triangles (\blacktriangle) and fit) vs. condenser setpoint temperature for propane propylene in the 5-inch device. Both curves intersect at the zero flow condition (green square (\blacksquare)) at a condenser temperature of $\sim -51.35^\circ\text{C}$.

4.3 Approach to Steady-State Operation

Approach to steady-state performance is shown in Figure 4.5 for a sample propane/propylene experiment at a flowrate of 1 mL/min. An HETP of 1 cm was achieved after 20 hours of stable MCD operation. From the results shown in Figure 4.5, it was not evident that equilibrium had been achieved. As a result, the HETP data as a function of time was fit to an exponential to determine the equilibrium time constant. In

addition, experiments were performed for a longer duration to determine if longer run times were necessary to obtain steady-state performance.

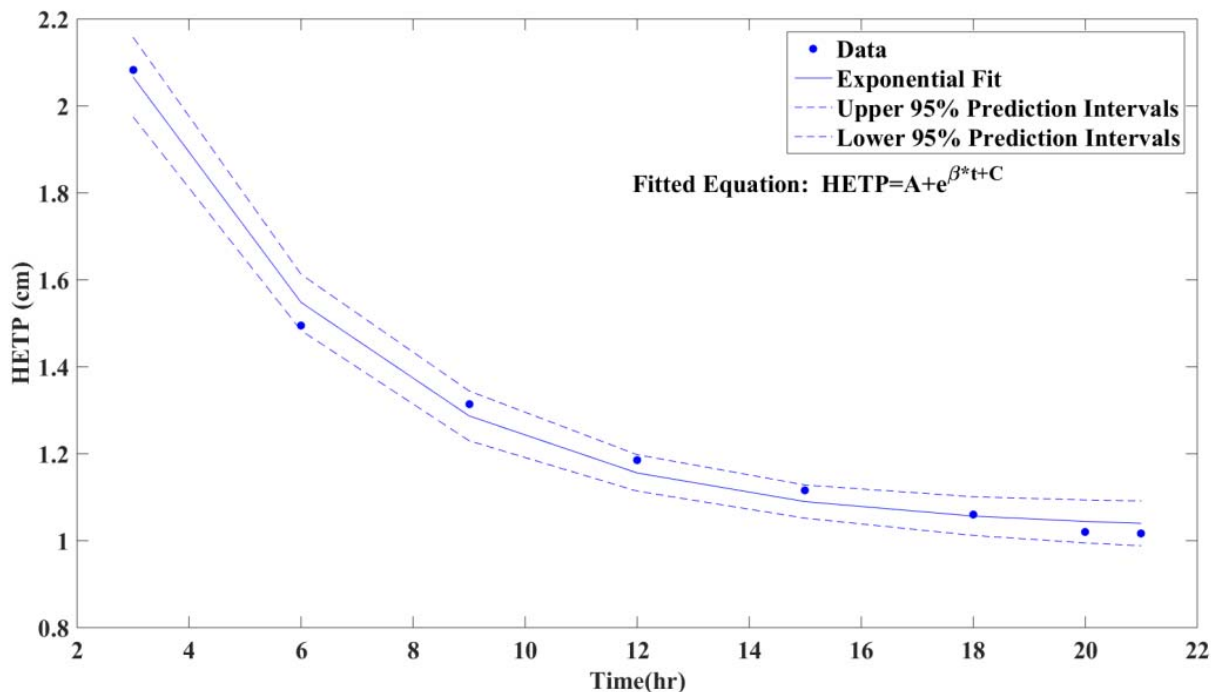


Figure 4.5. Calculated HETP vs time for a propane/propylene experiment in the 5-inch device at 1 mL/min liquid flow; the results (●) are fit to an exponential function (—) to obtain the characteristic time, $-1/\beta$, and 95% prediction intervals are also shown (- -). The calculated flowrate for the experimental data was.

The calculated characteristic time from the fit was 4.4 hours. Conservatively, the operating time should be at least 10X the characteristic time. Thus, MCD was performed for an extra 9 hours (30 hours stable operation + 4 hours of start-up) to determine if additional time was necessary. Only minimal improvement was obtained when comparing 21 hours and 30 hours of stable operation (25 hours and 34 hours of total operation with 4 hours of startup), as shown in Figure 4.6.

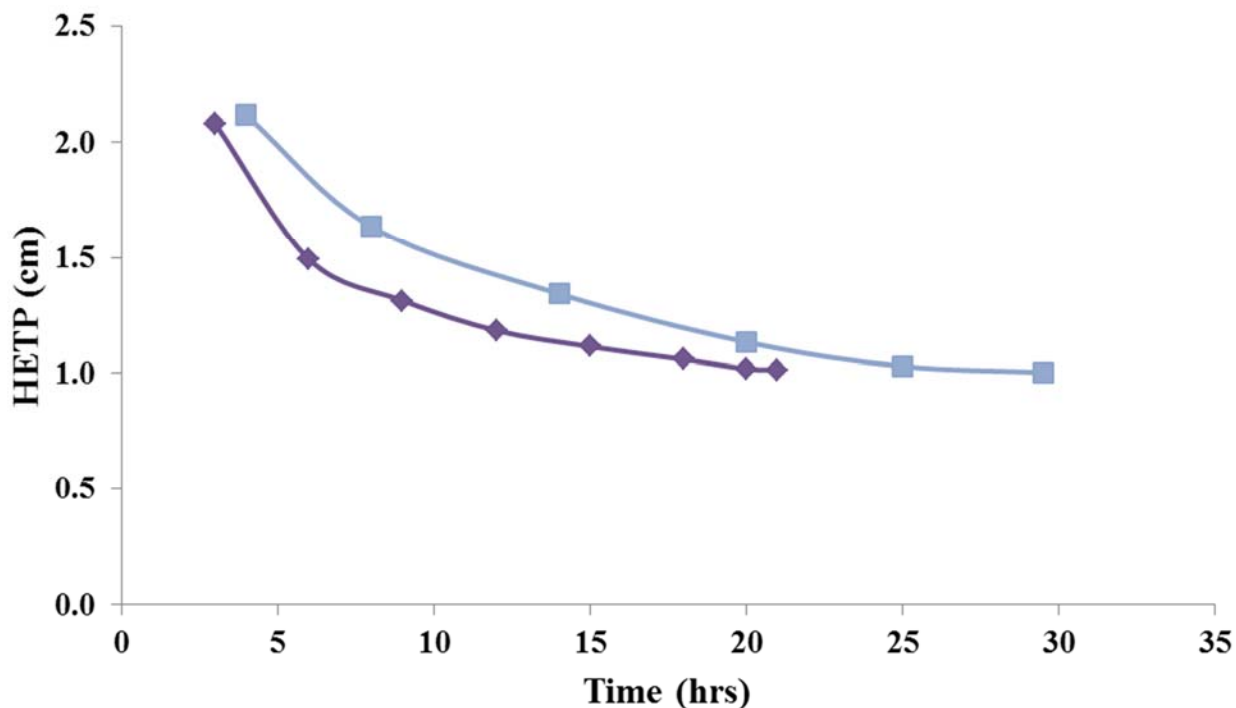


Figure 4.6. Calculated HETP from consecutive measurements of the bottoms (evaporator) composition as a function of time with all other operating conditions equal after 21 (◆) and 30 (■) hours of stable operation for a propane/propylene experiment in the 5-inch device at 1 mL/min liquid flow.

4.4 Propane/Propylene Chemical Separation

Initial MCD experiments were performed with a feed mixture of 1 mol% propane in propylene. This is a separation performed routinely in the chemical industry and has well-characterized vapor-liquid equilibria. Furthermore, analysis of sample compositions could be performed more expeditiously using GC/MS than the isotopic analyses required for enrichment of methane, and thereby, provide quicker feedback on performance and a faster turn-around of experiments. The higher confidence in VLE also provided a more reliable calculation of the number of separation stages and therefore, HETP.

4.4.1 Propane Propylene Concentrations by GC/MS

Each feed and product gas sample was injected into a gas chromatograph coupled to a mass spectrometer (GC/MS). Analysis was performed on an Agilent 6890/5975 GC/MS detector equipped with a DB1 capillary column, 40 m long x 0.1 mm I.D. x 0.4 μ m film. Sample was injected into a split/splitless injector at 150°C, split 100:1, and 4 mm deactivated glass wool. The carrier gas was helium at a constant pressure of 100 psi (linear velocity of 28 cm/sec). Samples were analyzed at an isothermal temperature of -40°C. The mass spectrometer source and interface temperatures were set at 220°C and 150°C, respectively; acquired in 70 eV EI mode with a scan mode from 10 to 150 m/z. The peak areas from the chromatograms for both propane and propylene were measured and the composition was determined from the relative ratio of peak areas.

Chromatographs are overlaid in Figure 4.7 of the feed and an evaporator sample obtained after 20 hours of stable operation for an experiment with the 5-inch device at a flowrate of ~ 1mL/min. Baseline

chromatographic resolution between propylene and propane was achieved with retention times of 5.05 and 5.30 min, respectively. The inset of Figure 4.7 shows a 10x magnification of the y-axis demonstrating the increase of the propane peak after MCD. The feed concentration was calculated as 0.9 mol% and the concentration after distillation was calculated as 8.5 mol% by comparing the peak areas of propane and propylene, respectively. Therefore, the MCD device was able to increase the concentration of propane by a factor of 9.4 for this particular case, which represents an overall separation factor of 10.2.

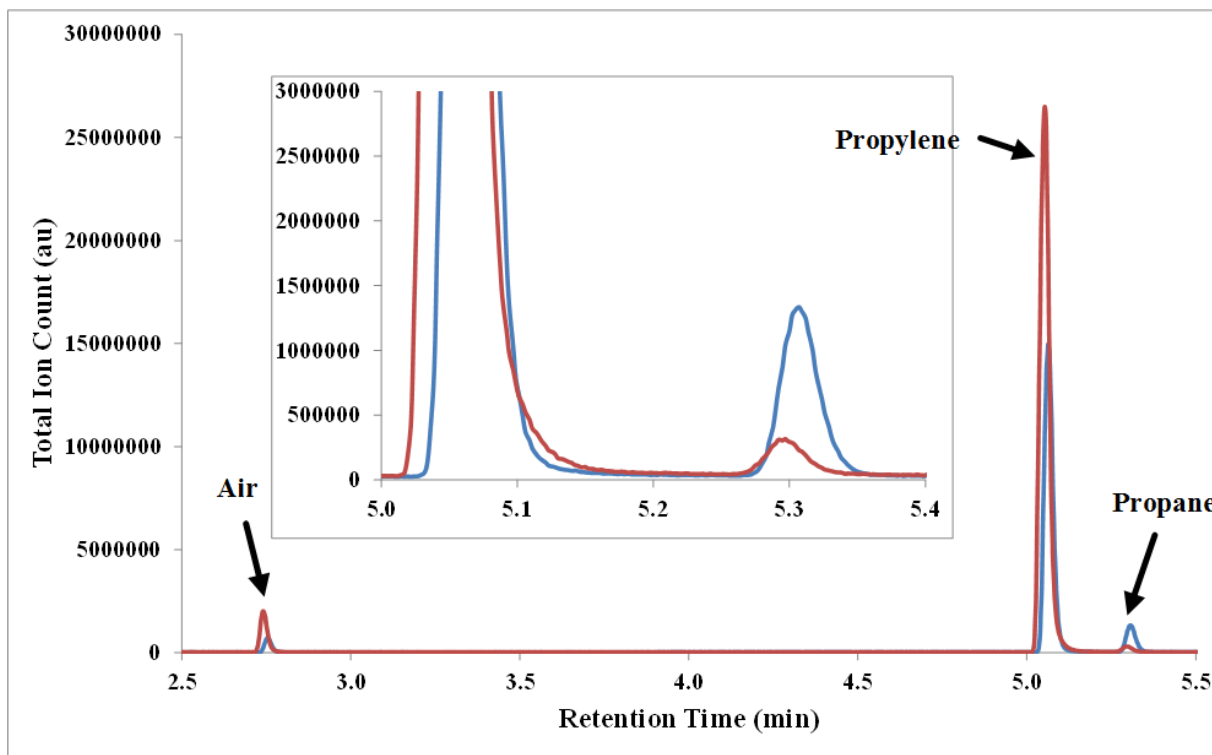


Figure 4.7. Comparison of gas chromatographs for a feed gas sample (—) and an evaporator sample obtained after 20 hours of operation of the 5-inch device at 1 mL/min liquid flow (—).

4.4.2 Propane Propylene Results

Five extended duration experiments were performed at different flowrates which were adjusted by varying the condenser temperature as described above. The results at the end of 20 hours of stable operation in the 5-inch device are tabulated in Table 4.1 and depicted in Figure 4.8. The lowest HETP value achieved was 1 cm, which is a significant achievement in the field of cryogenic MCD. Results gave an optimal liquid mass flux of between 1.5 and 1.7 g/(cm²·min). TeGrotenhuis and Powell [28] showed a similar leveling off of performance in distilling n-octane in the same device, but at higher flowrates between 2.7 and 5.5 g/cm²·min. The much wider flowrate operating range resulted in a factor of 2-4X higher throughput at HETPs that were a factor of 3X lower than what was achieved here. Previous attempts at MCD at cryogenic temperatures achieved an HETP of 1.7 inches in the C-2 splitting of ethane and ethylene [19]. In addition, the same group reported an HETP of 0.5 inch between cyclohexane and hexane at much higher temperature which, coincidentally, is about 3X lower than the HETP achieved in the cryogenic experiments. Anecdotally, there is a trend of higher HETPs at cryogenic temperatures in the same device. Dimensional analysis of the liquid phase mass transfer does not support liquid phase diffusivity as being the cause.

Table 4.1. Summary of results separating 1% propane in propylene using the 5-inch MCD device.

Stable Operating Time	Condenser Temperature (°C)	Liquid Flux (g/(cm ² ·min))	Bottoms conc. mol % C ₃ H ₆	# of Stages	HETP (cm)	Overall separ. factor
20 hours	-51.4	0.8	93.3	8.9	1.1	10.6
20 hours	-51.9	1.5	91.6	9.9	1.0	10.1
21 hours	-51.9	1.7	91.5	10.0	1.0	10.3
20 hours	-51.8	2.9	97.0	5.5	1.9	3.4
20 hours	-52.3	3.9	98.2	3.3	3.1	1.8

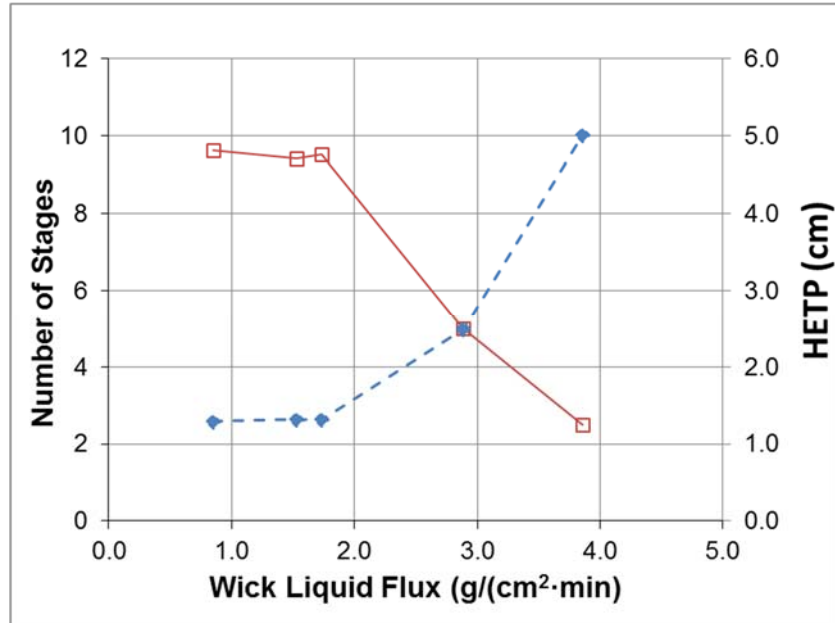


Figure 4.8. Number of separation stages (■) and HETP (◆) as a function of liquid flux through the wicks in the 5-inch MCD device after 20 hours of stable operation.

4.4.3 Effect of Box Temperature

The box temperature was initially set to (-47.0°C) which is slightly above the boiling point of the propane/propylene mixture at an operating pressure of 4 in.H₂O. The temperature profile inside the device corresponds to the composition along the axially length of the device dictated by the vapor liquid phase equilibrium curve as shown in Figure 4.9. However, if heat leaks occur then the performance will suffer because the vapor/liquid contact length along the axial length of the device will decrease. Thus, if heat leaks were occurring between the MCD device and the cold box, then the device would not be operating adiabatically and, thus, performance would suffer. Thus, great care in insulating the MCD, the evaporator, and the condenser was taken to ensure adiabatic operation. Experiments at a box temperature of -47.0°C and -45.5°C, under otherwise identical conditions including liquid flowrate through device, were conducted and the HETP curves vs time results are shown in Figure 4.10. The curves were nearly identical after 5 hours of stable operation and indicate that the MCD device is operating adiabatically and that box temperature does not impact performance as indicated by a final HETP of ~ 1 cm for both cases after 20 hours of MCD.

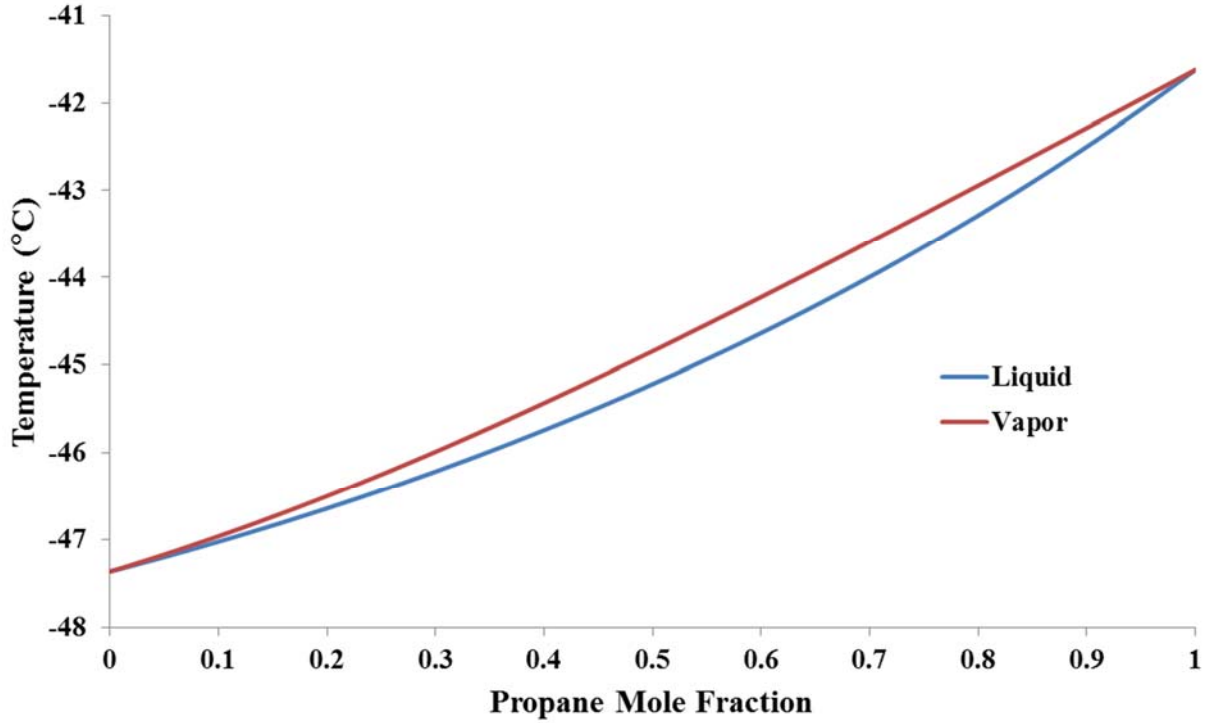


Figure 4.9. Txy diagram for propane in propylene at an operating pressure of 4 in.H₂O taken from ChemCad.

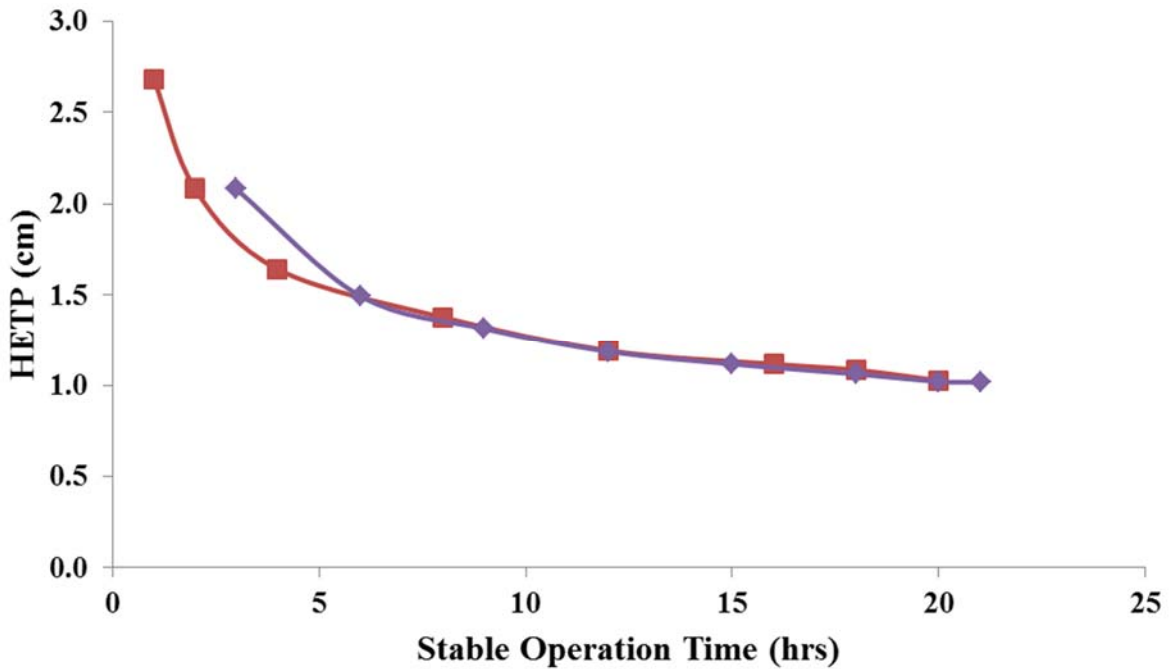


Figure 4.10. Effect of box temperature on performance after > 20 hours of stable operation. The trend lines follow the same path after ~ 5 hours of operation for box temperatures of -47.0°C (◆) and -45.5°C (■), respectively, and the final HETP for both cases was ~ 1 cm.

4.4.4 Effect of Helium Flow

When helium flow was not added to the reboiled vapor entering the MCD device, the evaporator liquid level was very difficult to control consistent with “pulsing” liquid flow which causes dispersion that decreased performance (HETP = 1.5 cm after 20 hours of stable operation) at a flowrate of ~ 1 mL/min. It was shown that the MCD test-stand could be successfully operated without helium flow, however, the system was more difficult to control and resulted in a 50% decrease in performance.

4.5 Methane Isotopic Enrichment

Isotopic enrichment of methane was performed using ultra high purity natural abundance methane feed. Samples were collected from the evaporator as before and analyzed for isotopic enrichment using GC/IRMS. Previous attempts to perform the isotopic separation chromatographically were marginally successful and are discussed in Section 6.

4.5.1 Methane Isotopic Analysis by GC/IRMS

Methane samples were prepared by first flushing a muffled 125 mL bottle with cap and septum with helium. The sample was injected into the bottle just prior to analysis. In house standards were prepared by adding 5 ml of compressed methane to a muffled, flushed 125 mL bottle.

Samples were analyzed by gas chromatography-isotope ratio mass spectrometry (GC/IRMS) with an Agilent 7890B GC and a Sercon 20-22 IRMS. The GC column was an HP-5 (30 m x 0.32 mm x 0.25 μ m). Helium was used as the carrier gas. The oven program was isothermic at 50°C and inlet was splitless at 250°C. The carbon isotope value of the standard used was determined in house by a prior scientist. Carbon dioxide (CO₂) was used as a reference gas at the beginning and end of each run. Five to six injections were made for each run of the sample and standard used. The in house methane standard was run at the beginning and end of each day and various times in between. Data was collected and integrated by the Sercon software. Integrated values were corrected by the in house value and the daily standard run.

4.5.2 Methane Isotopic Separation

Five experiments in each of the 5-inch and 10-inch devices were performed to produce performance curves of number of stages and resulting HETP versus liquid mass flux through the device. All of the experiments were performed with naturally enriched methane, and were analyzed for ¹²CH₄ and ¹³CH₄. Other minor isotopes of carbon and hydrogen were assumed to be negligible. A feed sample was obtained during each run and analyzed along with samples from the evaporator taken periodically during the runs. Feed samples varied between 0.001075 and 0.001087 atomic% of ¹³C, while the maximum value obtained for an enriched evaporator sample was 0.01286 atomic%. The results are summarized in Table 4.2 and graphically depicted in Figure 4.11. Even with 60 stages of separation, the overall separation factor was less than 1.2, due to the small relative volatility of the methane isotopes. This illustrates the need for thousands of stages to achieve substantial enrichment.

In general, lower fluxes resulted in lower HETP, as expected. However, too low of a liquid flux (< 0.22 g/(cm²·s)) resulted in unstable operation due to the limits on the control system’s resolution. For instance, at this low of a flux, the evaporator cartridge heater power was 1.6% “on” in the 5-inch device and 3% “on” in the 10% device. Since the resolution on the cartridge heater was 2%, the system operated much less stably, causing higher uncertainty in the lowest flux result in the 5-inch device.

Table 4.2. Summary of results separating methane isotopes using the 5-inch and 10-inch MCD devices.

Operating Time (hours)	Condenser Temp. (°C)	Liquid Flux (g/cm ² ·min)	Bottoms conc. atomic % ¹³ C	# of Stages	HETP (cm)	Overall separ. factor
5-inch Device						
24.0	-167.4	1.56	0.011315	12.03	0.84	1.042
25.0	-163.8	1.32	0.011501	17.51	0.58	1.061
19.7	-167.5	0.67	0.011310	17.96	0.57	1.053
10.0	-168.1	0.51	0.011297	20.60	0.49	1.051
23.9	-166.7	0.22	0.011123	14.35	0.71	1.035
10-inch Device						
6.0	-164.2	1.46	0.011690	28.27	0.90	1.084
13.0	-163.6	1.13	0.012465	50.96	0.50	1.157
20.0	-162.9	0.74	0.012541	54.42	0.47	1.168
27.8	-162.5	0.35	0.012737	60.19	0.42	1.187
20.0	-162.0	0.21	0.012855	61.78	0.41	1.193

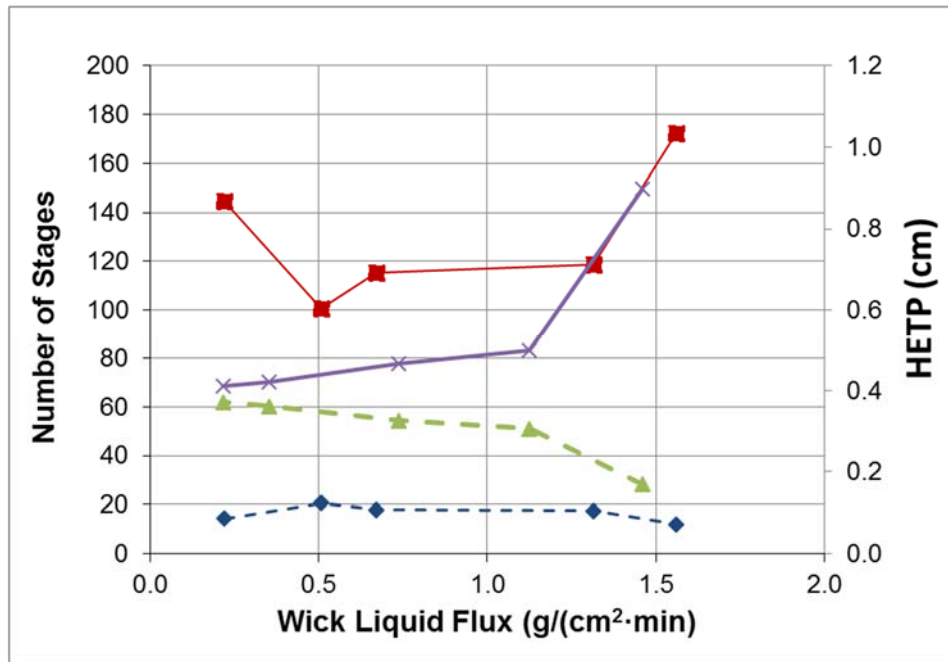


Figure 4.11. Number of separation stages (◆) and resulting HETP (■) in the 5-inch device and the number of separation stages (▲) and resulting HETP (X) in the 10-inch device as a function of liquid flux for methane isotopic enrichment.

The results indicate a maximum of 20.6 separation stages and a minimum HETP of 0.49 cm in the 5-inch device. Simply scaling the 5-inch distillation device to 10-inch would result in a maximum number of stages of 51.5 and an equivalent HETP; however the improved performance was seen in both parameters. The maximum number of stages in the 10-inch device was 61.8 which corresponded to an HETP of 0.41 cm. The improved performance was attributed to improved design using lessons learned from the 5-inch MCD device. For instance, the top and bottom vapor channel heights were scaled for lower flow rates to compensate for mass exchange with only one wick. In addition, the longer length reduced end effects

yielding better vapor flow distribution and more uniform contact along the entire length of the device as shown in Figure 4.12. The vapor flow lines are not evenly distributed across the entire length of the liquid: vapor contact area. This effect is reduced as the length of the device is increased.

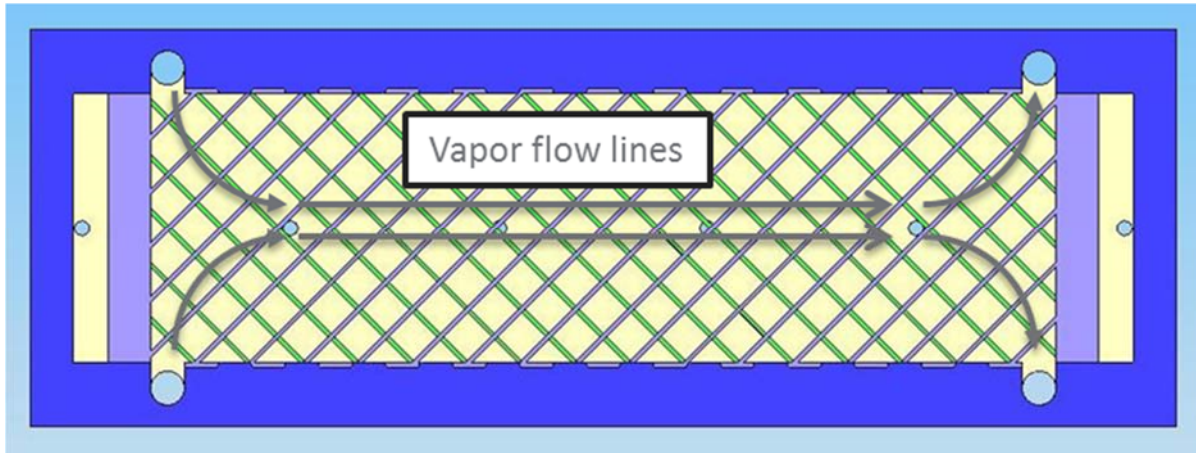


Figure 4.12. Vapor channels showing the vapor path flow lines. Part of the inlet and the outlet flow of the vapor headers are not fully counter-current. As the device length increases, this end effect is reduced.

These improvements resulted in a single device capable of > 60 stages of separation which is double what was achieved previously at elevated temperatures in a similar device [28] and significantly more than any other device in the literature. An HETP of 0.41 cm is also an order of magnitude better than the only other MCD device operated at cryogenic temperatures [19] and two orders of magnitude smaller than commercial packing [19]. In addition, isotopic enrichment was achieved.

4.6 Analysis of Results

The analyses include dimensionless parameters that depend on physical properties of the fluids that are given in Table 4.3.

Table 4.3. Diffusion coefficients and densities at the boiling points of the fluids used in MCD testing.

System	Liquid density (g/ml)	Liquid diffusivity (cm ² /s)	Gas density (g/ml)	Gas diffusivity (cm ² /s)
Methane	0.422	5.23x10 ⁻⁰⁵ (a)	0.00182	0.0316 (c)
Propane/Propylene	0.610	3.42 x10 ⁻⁰⁵ (b)	0.00236	0.040 (d)

^a Liquid phase propane diffusivity in propylene obtained from the Tyn-Calus correlation [34]

^b Gas phase propane diffusivity in propylene obtained from the Chapman-Enskog theory [35]

^c Self-diffusivity of methane liquid obtained from Dymond [36]

^d Self-diffusivity of methane gas obtained from Lee and Thodos [37]

The data from MCD testing is compiled in Figure 4.13, showing the effect of liquid flow through the device on HETP. Data are also included from computation fluid dynamics (CFD) modeling using COMSOL Multiphysics software of the 5-inch device for the propane in propylene system. The CFD model is described in Section 5.0. The results are plotted on a log scale so the magnitude of differences could be discerned between measured performance and that predicted from modeling. The MCD device results show at least a factor of 5 to greater than 10X larger HETP than what the model supports. The data

all show the expected trend of decreasing HETP with decreasing flowrate, consistent with conventional packed columns. However, at low flow the HETP levels out and possibly even starts increasing, which is also observed in the model results. The potential for improvement is significant.

The MCD test results are plotted in Figure 4.14 as number of separation stages versus the dimensionless residence time. As described in Section 3.0, if mass transfer is dominated by liquid phase diffusion, the data are expected to be linear with a slope of C_{eff} . A C_{eff} of 1 gives the 45° line shown in Figure 4.14. The model is in agreement with $C_{eff}=1$ at low residence time corresponding to higher flow rates, but deviates as residence time is increased and eventually plateaus at a little over 100 separation stages. The MCD devices also plateau at different numbers of stages and never reaches $C_{eff}=1$ within the operating range of the devices. Another view of the data is given in Figure 4.15 as C_{eff} versus dimensionless residence time. The modeled efficiency coefficient of the 5-inch device with propane and propylene starts at 1 at low residence time and climbs to almost 5 over the range of flows. The MCD devices all have a minimum efficiency factor of < 10 at varying dimensionless residence times.

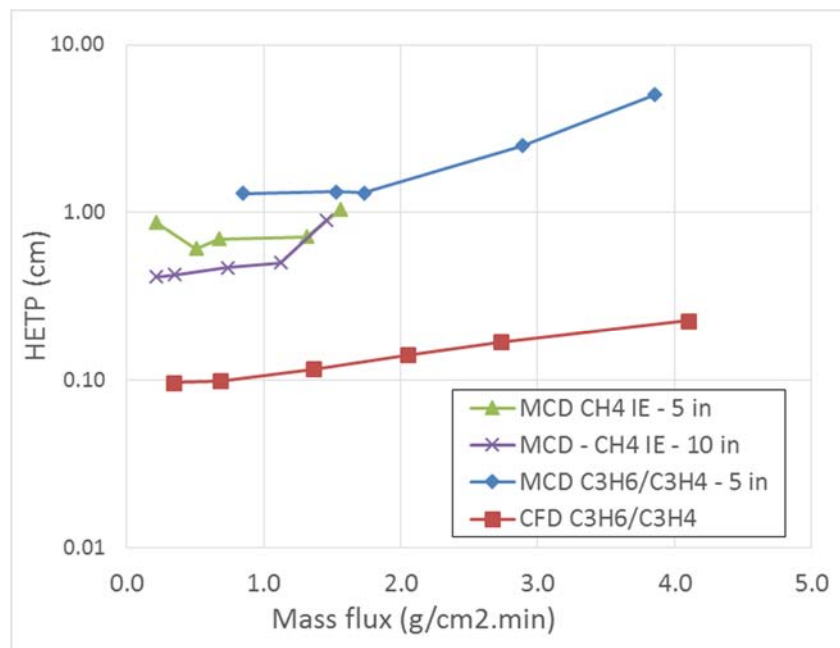


Figure 4.13. Compilation of HETP results from MCD testing with 1% propane in propylene in the 5-inch device (\blacklozenge), for methane IE in the 5-inch device (\blacktriangle), and for methane IE in the 5-inch device (\times), along with CFD results for 1% propane in propylene in a 5-inch model device (\blacksquare).

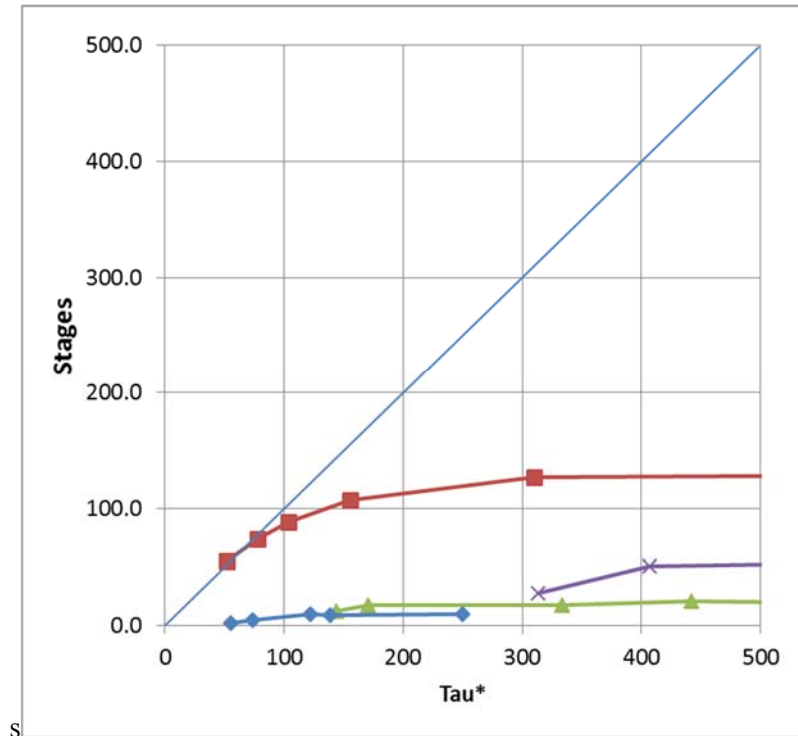


Figure 4.14. Compilation of Stages versus dimensionless residence time, $Tau^* = \tau D_L / h_m^2$, from MCD testing with 1% propane in propylene in the 5-inch device (\blacklozenge), for methane IE in the 5-inch device (\blacktriangle), and for methane IE in the 5-inch device (\times), along with CFD results for 1% propane in propylene in a 5-inch model device (\blacksquare).

As explained in Section 3.0, vapor phase axial dispersion is detrimental to the distillation process, and is assessed using the vapor phase Peclet number (Pe_g). The issue is best illustrated by the model results in Figure 4.16. When Pe_g is greater than 10, the efficiency coefficient is close to 1, but increases when $Pe < 10$. The MCD experimental results presented in Figure 4.16 show similar behavior at low Peclet number. However, dispersion does not explain the more significant deviation when $Pe > 10$. However, it is not possible to rule out axial dispersion or mixing in either phase without further detailed analysis. The CFD model assumes fully-developed laminar flow in straight channels in both phases and does not capture the detailed geometry of the vapor and liquid shims. The flow obstructions in these channels could be creating eddies and other flow non-uniformities that are detrimental to performance.

The flow capacity of the MCD devices is represented in Figure 4.17 to Figure 4.19 by plotting HETP versus F factor. Figure 4.17 uses the F factors calculated from the as built devices, while Figure 4.18 assumes the vapor channels are half the current height. Figure 4.19 is overlaid on a figure extracted from the Sulzer literature which represents their lowest HETP advanced structure packings that is limited to 8 cm in diameter. Clearly, MCD devices are performing in a regime at lower HETP and flow capacities than what is achievable with best available commercial technology. Optimization of the vapor channel should be pursued if flow capacity is an important metric.

All of the MCD experiments were performed with the MCD devices oriented horizontally. In this orientation, the flow capacity is limited by the maximum suction that can be applied to the MCD device without breaking the siphons at the two ends. Alternatively, the devices can be operated at an inclination from the condenser end to the evaporator end in order to use gravity to augment flow, which would increase flow capacity and move the operating window to the left in Figure 4.17 to Figure 4.19.

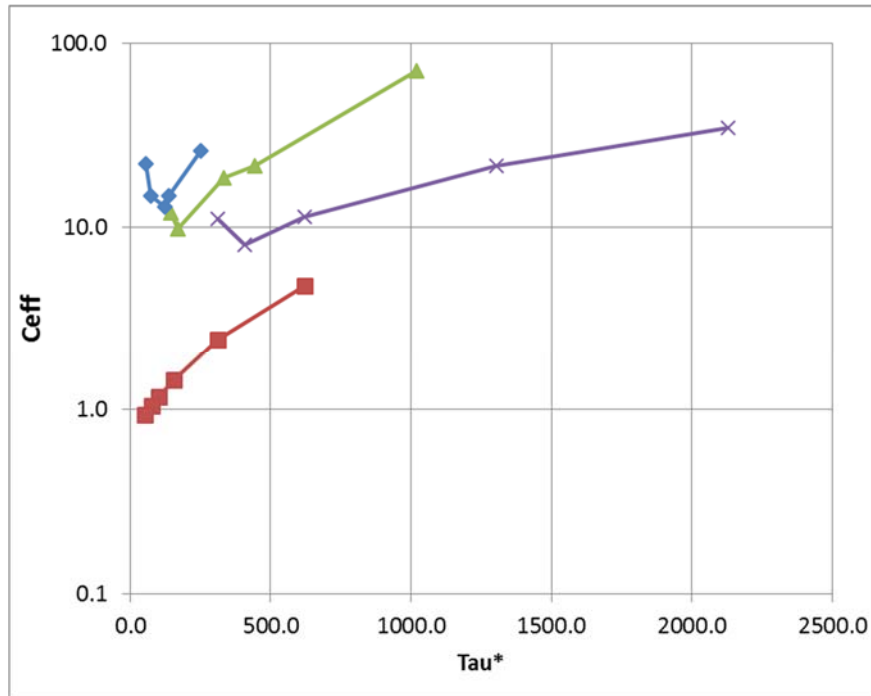


Figure 4.15. Compilation of C_{eff} versus dimensionless residence time, $Tau^* = \tau D_L / h_m^2$, from MCD testing with 1% propane in propylene in the 5-inch device (\blacklozenge), for methane IE in the 5-inch device (\blacktriangle), and for methane IE in the 5-inch device (\times), along with CFD results for 1% propane in propylene in a 5-inch model device (\blacksquare).

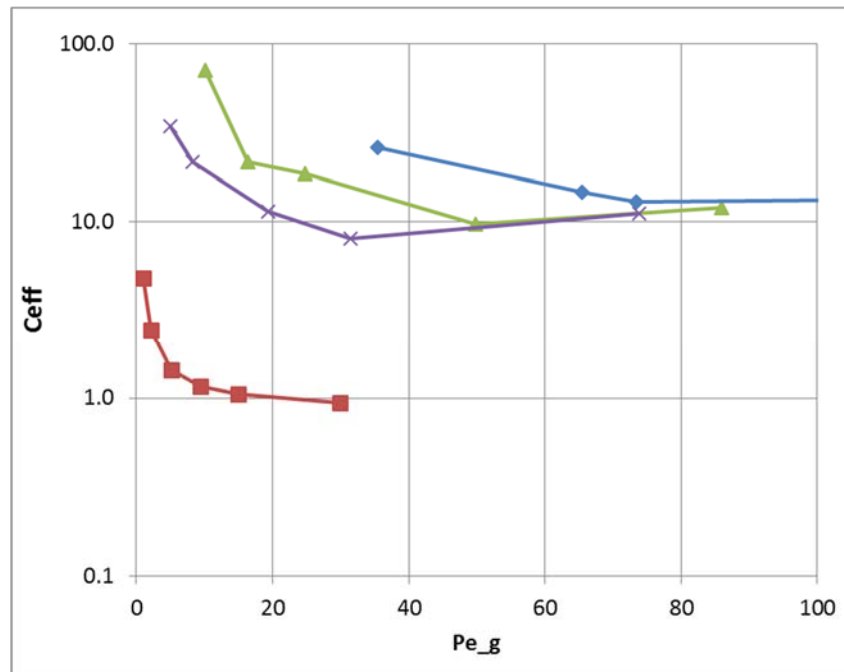


Figure 4.16. Compilation of C_{eff} versus Pe_g , from MCD testing with 1% propane in propylene in the 5-inch device (\blacklozenge), for methane IE in the 5-inch device (\blacktriangle), and for methane IE in the 5-inch device (\times), along with CFD results for 1% propane in propylene in a 5-inch model device (\blacksquare).

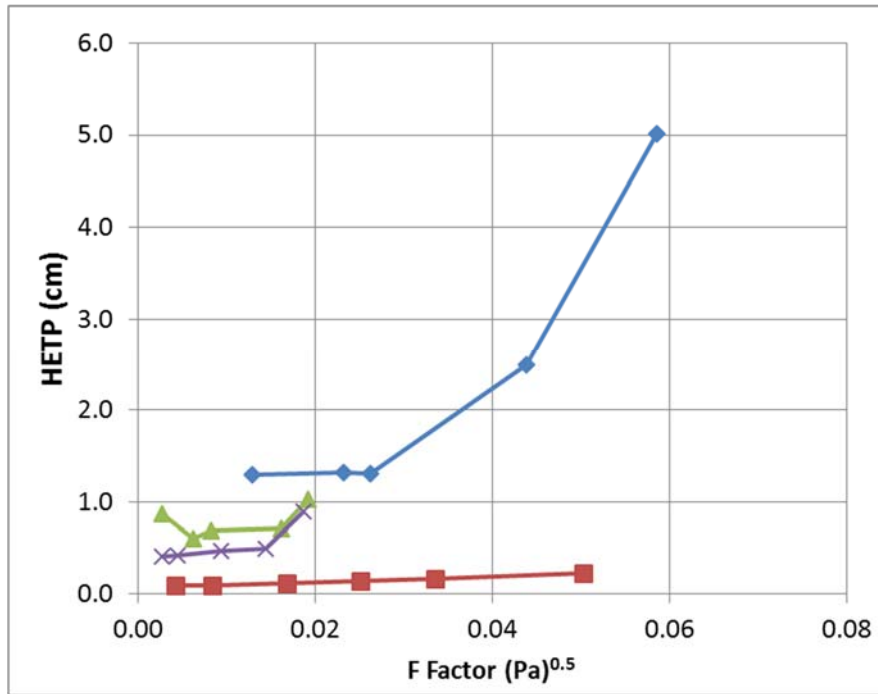


Figure 4.17. Compilation of HETP versus F factor from MCD testing with 1% propane in propylene in the 5-inch device (\blacklozenge), for methane IE in the 5-inch device (\blacktriangle), and for methane IE in the 5-inch device (\times), along with CFD results for 1% propane in propylene in a 5-inch model device (\blacksquare).

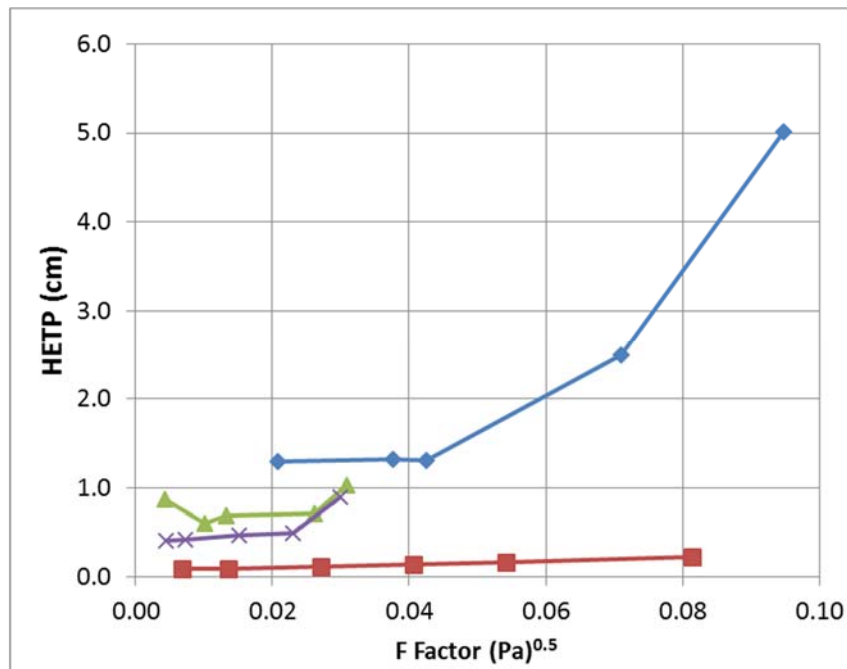


Figure 4.18. Compilation of HETP versus F factor from MCD testing with 1% propane in propylene in the 5-inch device (\blacklozenge), for methane IE in the 5-inch device (\blacktriangle), and for methane IE in the 5-inch device (\times), along with CFD results for 1% propane in propylene in a 5-inch model device (\blacksquare) at $\frac{1}{2}$ vapor channel thickness.

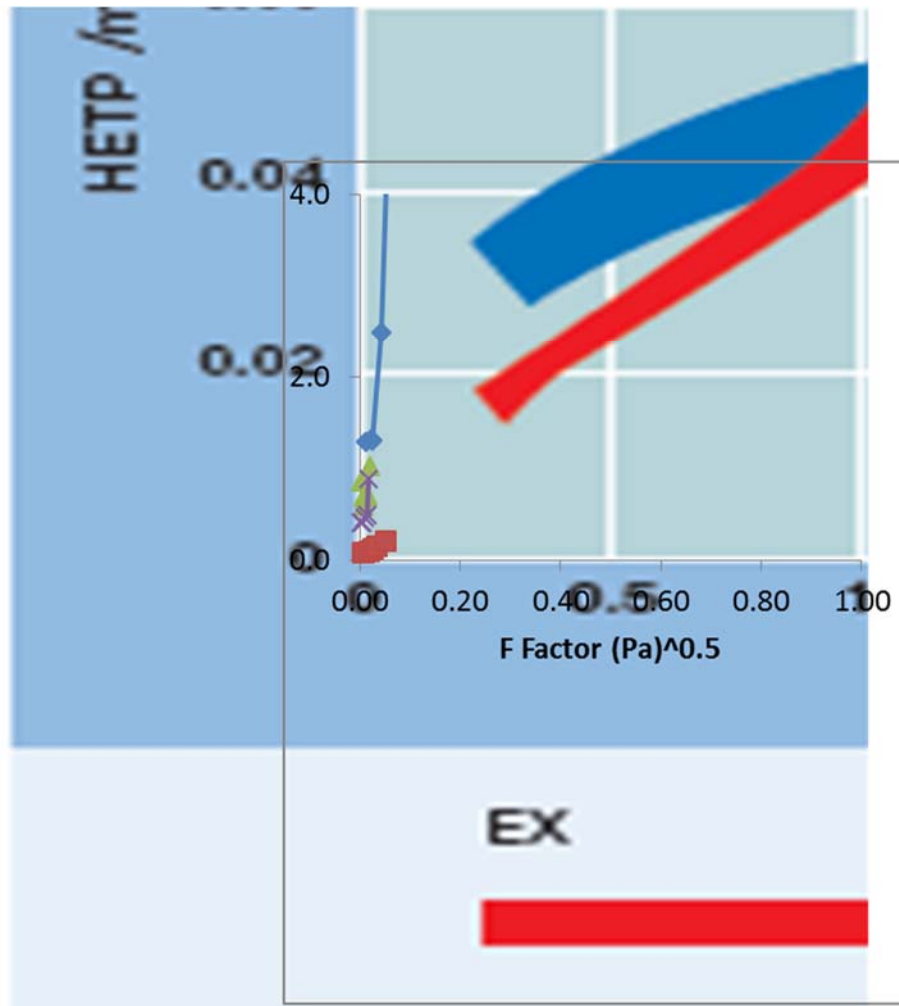


Figure 4.19. Comparison of HETP versus F factor between Sulzer laboratory packing [20] and MCD results with 1% propane in propylene in the 5-inch device (◆), for methane IE in the 5-inch device (▲), and for methane IE in the 5-inch device (X), along with CFD results for 1% propane in propylene in a 5-inch model device (■).

5.0 Modeling

5.1 Model Description

A computational fluid dynamics (CFD) model was developed to predict the performance of MCD devices. The model was developed and run using the commercial software packaged COMSOL Multiphysics. A simple two dimensional geometry of a single wick was used that is depicted in Figure 5.1. Simulating one half of the repeat unit in the stack structure of a MCD devices was adequate for predicting performance due to planar symmetries. The model contained 3 domains: (1) half of a vapor channel, (2) half of a liquid channel, and (3) a domain between the two representing the outer screen of the wick structure. The convective-diffusive mass transfer equations were solved, assuming fully-developed laminar flow in the liquid and vapor channels with a symmetry plane as the outer boundary condition. Dispersion in both the vapor and liquid phases was included. The outer screen that maintains phase segregation has much lower lateral permeability than the middle PCM layer. Consequently, outer screen layer was modeled as a stagnant liquid layer. Furthermore, the wires of the screens and the internal structures of the flow channels impede mass transfer, which was accounted for by reducing the liquid diffusivity in the stagnant layer by half.

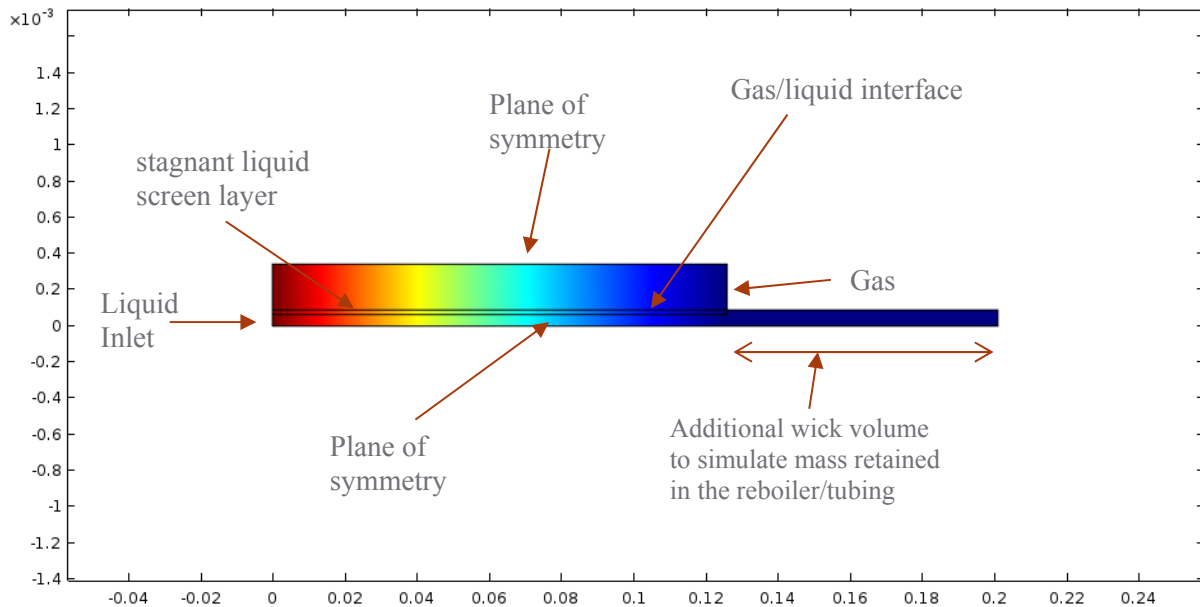


Figure 5.1. 2D geometry for simulating the distillation process in MCD devices.

Concentration and flow rate were specified at the liquid inlet. The mass flow of the gas inlet was set to 99% of the liquid outlet, consistent with a reboil ratio of 99 at steady-state operation. The gas inlet concentration was matched to the liquid outlet average concentration. Convective-diffusive mass transport differential equations were solved with velocities set to fully-developed laminar flow in the liquid and vapor domains and zero (diffusive only) in the stagnant screen layer. The flux continuity boundary condition was used at the internal boundaries to maintain mass balance. Vapor-liquid equilibrium using a constant relative volatility was used as a boundary condition between the vapor channel and the stagnant layer, and concentration continuity was set between the stagnant layer and the liquid channel. The feed concentration was set to 145 mole/m^3 , consistent with 1% propane in propylene. The liquid phase density and diffusivity were set to 0.610 g/cm^3 and $3.5 \times 10^{-5} \text{ cm}^2/\text{s}$, respectively, and 0.002245 g/cm^3 and 4.0×10^{-6}

m²/s for the vapor phase. The baseline relative volatility was set to 1.01, and the liquid flow was 1 ml/min.

The model was constructed for dynamic time-dependent simulations as well as for steady-state operation. Dynamic simulations were used to evaluate start-up time, the time it takes for the system to develop concentration profiles for steady-state. Start-up time is lengthened by hold-up volumes in the system, particularly liquid inventories. When the entire system is initially filled with feed material, the hold-up volumes gradually evolve from the feed composition to their steady-state concentrations. For the MCD system, liquid hold-up volumes are located in the condenser and evaporator, the liquid headers of the MCD device, and interconnecting liquid tubing. Dynamic simulations were performed with the geometry in Figure 5.1 initially filled with feed composition. To simulate the effect of liquid hold-up on start-up time, the liquid channel length was extended beyond the end of the gas channel an appropriate length, as shown in Figure 5.1. Since fresh feed was continually added at the liquid inlet end, the extra liquid length was added to only the liquid outlet. Dynamic simulations predicted start-up times consistent with experimental results.

The two-dimensional CFD model does not fully represent the processes occurring in the MCD devices. The details of the structures in the liquid and vapor channels that will alter the flows from the assumed fully-developed Poiseuille flow. Lateral gas flow in the 3rd dimension to and from the vapor headers is not represented in the two-dimensional model. This lateral flow that was also described in Section 4.0, prevented true counter-current flow over the full active length. Even though the CFD model is simplified, it predicts the theoretical potential of the MCD technology and provides targets for improving the performance of actual devices.

Predicted HETP versus liquid flow rate for propane/propylene separation in the 5-inch MCD device is shown in Figure 5.2. The data predict a nearly linear decrease in HETP with flow rate until the flow rate is below 1 ml/min. These results were compared to experimental results in Section 4.0. Parametric studies were performed for other variables, as well.

The effect of vapor phase dispersion was investigated by varying gas diffusivity at a flow rate of 1 ml/min, and results are shown in Figure 5.3. At this flow rate, HETP is at a minimum for propane/propylene distillation. At higher diffusivities, vapor phase dispersion begins to adversely affect performance, while HETP rises at lower gas diffusivities because vapor phase mass transfer resistance becomes important.

HETP is also affected by relative volatility as shown in Figure 5.4, again for a flow rate of 1 ml/min. The 1.01 relative volatility ($\log_{10}(\alpha-1)=-2$) of propane and propylene is near the optimum, but will continue to increase at lower relative volatility. The curve in Figure 5.4 is influenced by other properties and parameters of the system, including shifting with flow rate. Figure 5.3 and Figure 5.4 imply there are optimal conditions for minimizing HETP for any given separation.

The benefits of this relatively simplified model include performing sensitivity analyses, gaining an understanding of the relative importance of parameters, and for optimizing design. More importantly in the current context, modeling provides a benchmark for evaluating the capability of an MCD device to attain theoretical performance, and for gaining insights on potential causes of deficiencies.

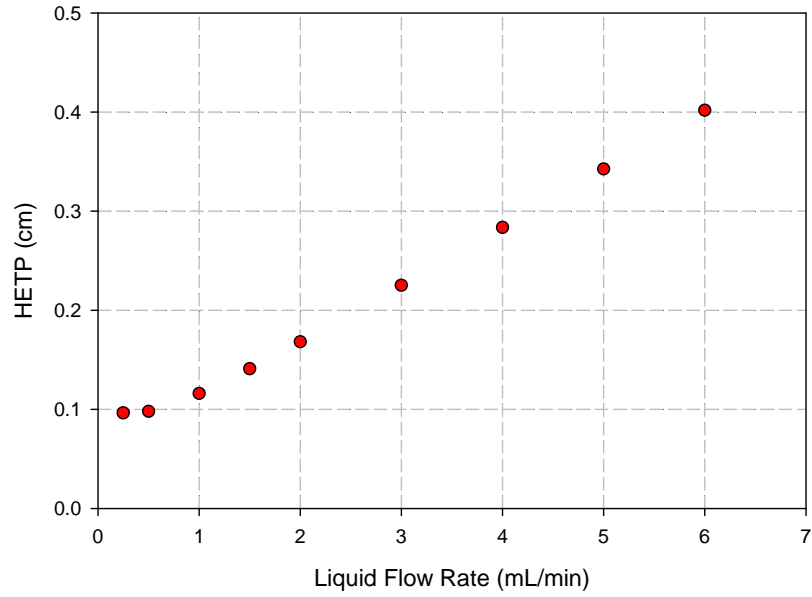


Figure 5.2. Predicted effect of flow rate on HETP for propane/propylene separation in the 5-inch MCD device.

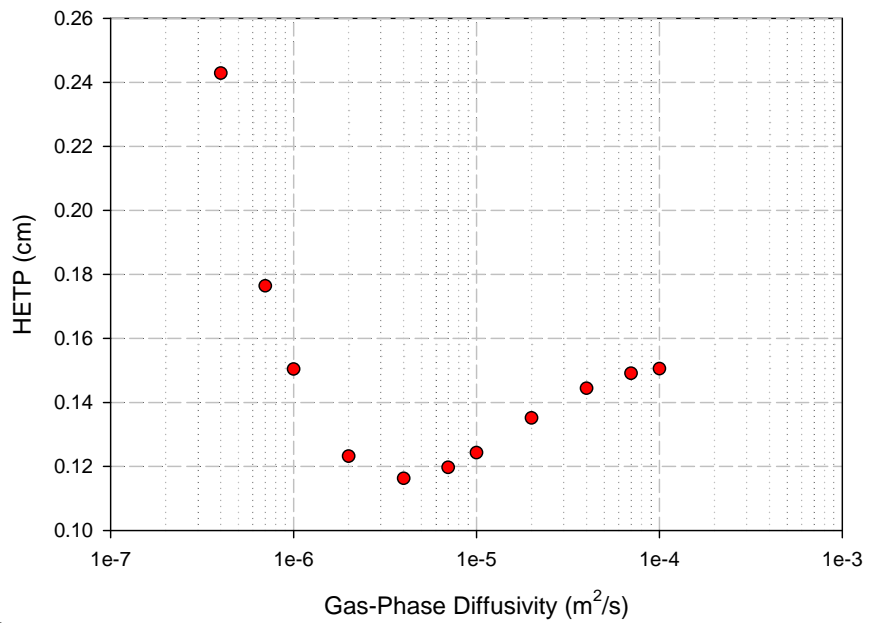


Figure 5.3. Predicted effect of gas diffusivity on HETP for propane/propylene separation in the 5-inch MCD device.

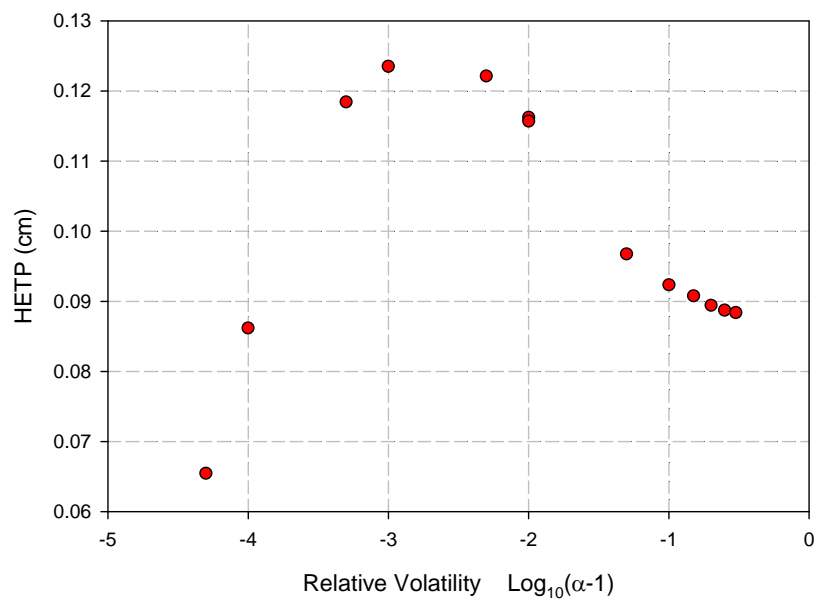


Figure 5.4. Predicted effect of relative volatility on HETP for propane/propylene separation in the 5-inch MCD device.

6.0 Germane Isotopic Enrichment

The scope of enriching germanium by chemical boiling point separation using microchannel distillation is projected in this section. The focus is on separating fully hydrogenated germanium species, and the confounding effects of deuterated or tritiated species present at very low levels in naturally occurring materials are neglected. Relative volatilities of chemical isotopes of germanium are required to calculate the number of theoretical stages and minimum reflux ratio of a distillation process. The number of stages and reflux ratio can then be used to project the size of the equipment and energy requirements of a production process.

Any volatile chemical species containing germanium is a viable candidate for isotopic enrichment by distillation. The general rule is that lower molecular weights have higher isotopic effects, however, halogenated compounds have been shown to have larger relative volatilities.

6.1 Relative Volatility

Relative volatilities of germane isotopes are needed to calculate the number of stages needed to produce material enriched to 86% ^{76}Ge . Chromatographic separation of isotopes holds promise in that it allows the determination of the relative volatilities without requiring the separated isotopes to perform the measurement. Separate isotopes are often not available and those that are can be very expensive. The chromatographic method is based on the ASTM D2887 method for determining boiling points but is performed in a very narrow temperature region appropriate for the target species. Known boiling point standards are used to bracket the unknown mixture. Extremely high resolution chromatography should separate the isotopes based on their boiling point. The results would not only provide relative volatility of the isotopes but the number of theoretical plates required to affect a separation.

Before attempting to obtain relative volatility and/or boiling point measurements of germane isotopes using GC/MS methods, efforts were made to measure relative volatility of $^{12}\text{CH}_4$ and $^{13}\text{CH}_4$ as a surrogate. A commercial GCMS system (Agilent 6890/5975) was used and fitted with a variety of commercial columns. Although they were tried, bonded liquid phase columns such as a DB-1 were quickly ruled out since the temperatures required for the separation were below the columns operating range of -60°C due to freezing of the stationary phase. PLOT columns of varying diameter and length and at temperatures down to -80°C were also used with limited success despite up to 350,000 theoretical plates predicated on the certificate of analysis for the columns. The column operating temperature was limited to -80°C by the chromatograph. Efforts were then focused on operating extremely long stainless steel capillary columns at cryogenic temperatures. Figure 6.1 shows a chromatogram obtained at the lowest operating temperature of the chromatograph. Note that limited separation of the carbon 12 and 13 methane isotopes is observed. Based on this chromatogram the number of theoretical plates are

$$N = 5.545 (t_R/w_h)^2 \quad (6.1)$$

where N is the number of theoretical plates, t_R is retention time, and w_h is peak width at half height. For $t_R=7.73$ minutes and $w_h=0.03$ minutes, the number of theoretical plates is 368,000.

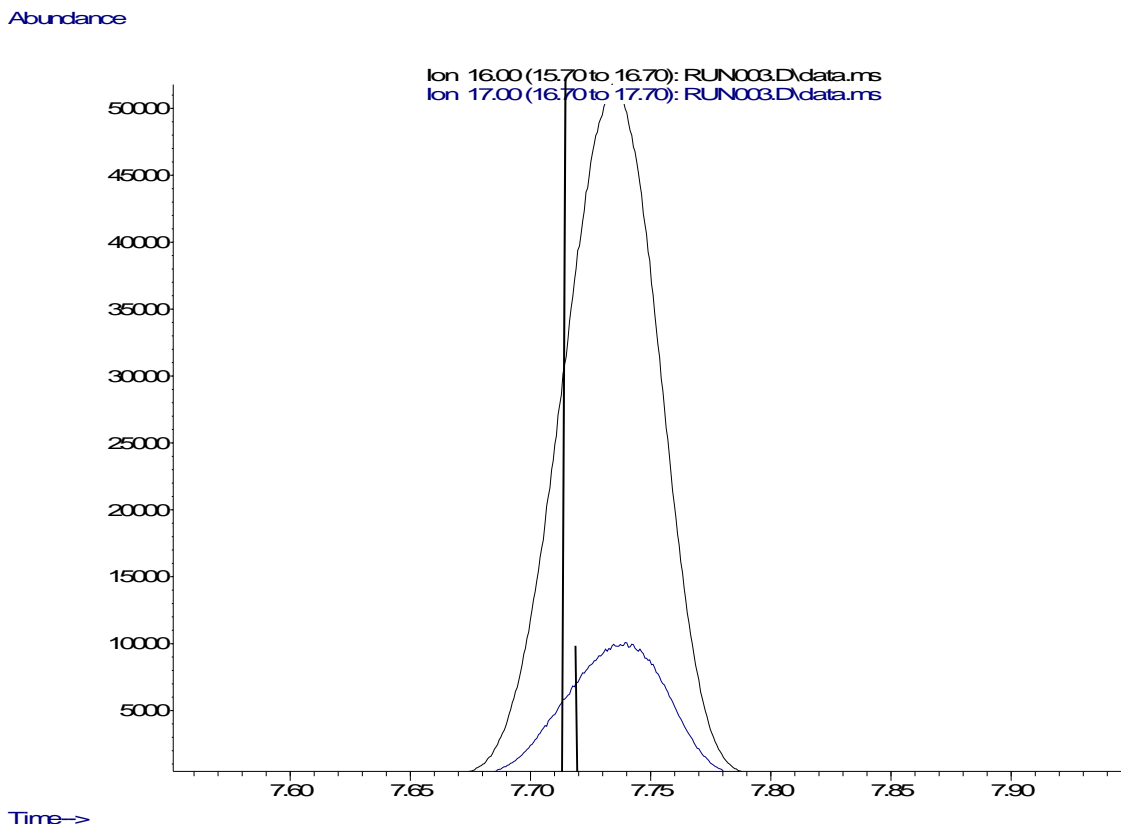


Figure 6.1. Chromatographic separation of ^{12}C methane enriched with ^{13}C methane on a 100 m x 0.25 mm ID stainless steel column at -80°C with a helium carrier gas at 25 cm/sec flow velocity.

The height equivalent to a theoretical plates (HETP) is

$$H = L/N \quad (6.2)$$

where L is column length and H is plate height. For this 10 meter column, the HETP is 0.027 cm.

Improved separation would be achieved by lowering the column operating temperature. Attempts to run at lower temperatures resulted in mechanical problems and temperature instability. An improved cryogenic chamber and temperature controller would have been required. Direct immersion of the column in liquid nitrogen caused the methane to freeze out in spite of the carrier gas flow. Although the method shows promise, no further development was attempted due to budget constraints.

Isotope effects on VLE curves have been predicted and measured for numerous compounds [38]. Simple theories assume molecules in a liquid are trapped in a potential energy well, and boiling points are calculated by determining the energy required for molecules to escape the liquid phase into the gas phase. A simple harmonic oscillator potential of finite depth gives rise to a $A - Bm^{-1/2}$ dependence of the boiling point on molecular weight, m [39]. This theory implies that lower molecular weight chemicals are preferred for larger isotope effects. A more rigorous treatment using the more realistic Morse intermolecular potential yields two terms, one dependent on $m^{-1/2}$ and the other on m^{-1} [40].

However, predicting VLE IE is more complicated than a simple molecular mass dependence, as evidenced by contradictions to the rule of thumb that lower molecular weight isotopes are more volatile. The vapor pressure of CD_4 is higher than CH_4 over the entire boiling range, while the vapor pressure versus temperature curve of D_2O crosses the H_2O curve [41]. The relative volatility of $^{12}\text{CO}/^{13}\text{CO}$ is

greater than $^{12}\text{CH}_4/^{13}\text{CH}_4$ despite the larger molecular weight [18]. Bradley [42] provided an explanation that the increase in intermolecular attractions in the condensed phase with size and number of atoms is counteracted by increased translation entropy in the gas phase. This causes replacement of the inner atoms with heavier isotopes to more likely increase volatility, whereas heavier outer atoms are more likely to decrease volatility.

There have been numerous studies to predict isotope effects on thermodynamic properties, critical properties, and even surface tension [43, 44]. One of the more comprehensive efforts at predicting VLE IE is the corresponding states theory presented by Van Hook, et al. [41]. They adopted the acentric factor of Pitzer, et al. [45-47] in a modified Van der Waals equation of state to obtain a good prediction of VLE IE over the full range of boiling temperatures.

Predicting VLE IE for germane from intermolecular forces or physical properties is outside the scope of the project and property information for germane is not readily available. Instead, relative volatilities are estimated by observing IE of related compounds. Carbon and silicon are directly above germanium in the periodic table, and VLE IE of several compounds containing these elements are shown in Table 6.1 along with other similar compounds [38, 48]. Halogenated compounds and methylated silane show a reverse IE effect, while the hydrides show the trend of larger masses having lower volatility.

The absolute value of $1-\alpha$ indicates how easily isotopes can be separated by distillation, which is shown in the last column and plotted in Figure 6.2 as $|1-\alpha|$ versus mass difference divided by mean mass. The normal VLE IE effects are blue symbols, and the orange symbols are used for the reverse IE where relative volatility decreases with increasing mass. Predicting VLE IE effects for germane from trends in molecular mass or mass difference is problematic. Surmising that germane VLE IE will follow the trend of silane and the two other lower points in Figure 6.2 and that they display normal isotope effects, then the linear fit in Figure 6.2 gives the ‘high’ α values in Table 6.2. On the other hand, if the factor of ~ 4 change in $|1-\alpha|$ from methane (0.0028) to silane (0.00061) continues to germane, then the ‘low’ values in Table 6.2 are projected. The ‘low’ and ‘high’ values proved a reasonable bound on the VLE IE for germane. However, observing the very high relative volatility for the 46/50 TiCl_4 in Table 6.1 gives hope that the actual values for germane are closer to the high projected values.

Table 6.1. VLE data for selected isotopic compound pairs, including relative volatility (α) and absolute value of $1-\alpha$ [38, 48].

	M1	M2	M2/M1	$\Delta M/M$	α	$ 1-\alpha $
28/30 SiH ₄	32.03	34.03	1.062	0.0605	1.00061	0.00061
28/29 SiH ₄	32.03	33.03	1.031	0.0307	1.00035	0.00035
12/13 CH ₄	16.03	17.03	1.062	0.0605	1.0028	0.0028
12/13 CCl ₄	153.81	154.81	1.0065	0.0065	0.99797	0.0020
12/13 CHCl ₃	119.37	120.37	1.0084	0.0083	0.9992	0.00080
28/30 SiCl ₄	169.81	171.81	1.012	0.0117	0.99964	0.00036
28/30 SiH ₃ CH ₃	44.04	46.04	1.045	0.0444	0.99935	0.00065
28/30 SiF ₄	103.99	105.99	1.019	0.0190	0.9982	0.00180
32/34 SF ₄	160.26	162.26	1.012	0.0124	0.9992	0.00080
46/50 TiCl ₄	187.81	191.81	1.021	0.0210	0.997	0.00300

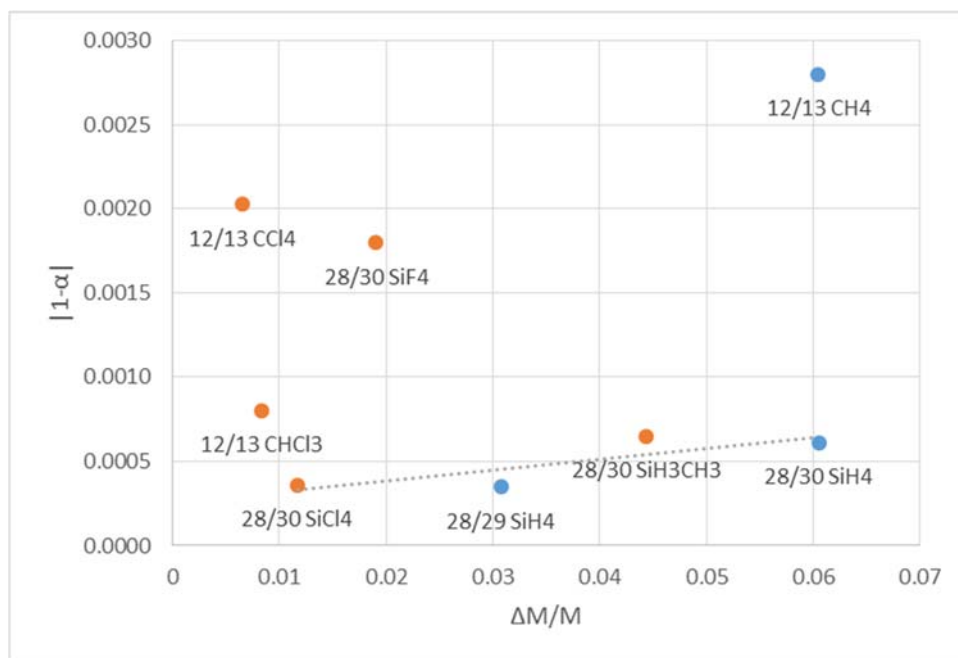


Figure 6.2. Relative volatilities in the form of $|1-\alpha|$ for various compounds containing carbon and silicon.

Table 6.2. Germanium natural isotope abundances and mass as GeH₄ versus ⁷⁶GeH₄.

	Natural Abundance	GeH ₄ IE from ⁷⁶ GeH ₄					
		M1	M2	M2/M1	ΔM/M	High α	Low α
70 Ge	20.57%	74.03	80.03	1.081	0.0779	1.00079	1.00020
72 Ge	27.45%	76.03	80.03	1.053	0.0513	1.00062	1.00016
73 Ge	7.75%	77.03	80.03	1.039	0.0382	1.00054	1.00014
74 Ge	36.50%	78.03	80.03	1.026	0.0253	1.00046	1.00012
76 Ge	7.73%						

6.2 Column Height

Estimates for the relative volatilities of germane isotopes given in Table 6.2 are used to estimate the number of separation stages and reflux ratio—liquid flow through the column divided by the flow of distillate product depleted in ⁷⁶Ge. The height of a theoretical plate (HETP) is used to translate separation stages to column height. Reflux ratio is used to calculate how big of a column is needed for a given production rate, which is addressed in the next section.

The product requirement is 86% ⁷⁶Ge, which specifies the concentration at the bottom of the column. To size the column, a concentration must also be specified at the top of the column in the distillate product stream, which is arbitrary but effects the recovery of ⁷⁶GeH₄ from the natural feed material. While germane is a costly material, it is assumed that the depleted byproduct can be repurposed to recover cost, so recovery is not a priority. It is assumed that the distillate byproduct is depleted from 7.73% in the feed to 5% in these calculations.

The number of separation stages and reflux ratio are calculated using the Fenske-Underwood-Gilliland method [49]. The Fenske equation is used to distribute the isotopes between the distillate stream, denoted by a **D**, and the bottoms stream, denoted by a **B** [49]:

$$\frac{x_{iD}}{x_{iB}} = (\alpha_i)^{N_{min}} \frac{(x_{HK})_D}{(x_{HK})_B} \quad (6.1)$$

where x_i is the concentration of component i in the liquid phase, HK refers to the heavy key which is the ⁷⁶GeH₄, α_i is the relative volatility between component i and ⁷⁶GeH₄, and N_{min} is the minimum number of stages required at total reflux—all liquid is fed back down the column and there are no product or feed flows. Overall and component mass balances are solved in conjunction with Equation 6.1 to determine the minimum number of stages required. Starting from natural abundances of germane isotopes and using the High α values from Table 6.2, the minimum number of stages required is 8,925. The resulting bottoms product contains 86% of ⁷⁶GeH₄ as well as 10.7% of ⁷⁴GeH₄, 1.1% of ⁷³GeH₄, 1.9% of ⁷²GeH₄, and 0.3% ⁷⁰GeH₄.

The next step is to calculate the minimum reflux ratio—the liquid flow in the column divided by the distillate product flow—using the Underwood method. The method first solves for the θ parameter using the equation [49]:

$$\sum_{i=1}^n \frac{\alpha_i x_{iF}}{\alpha_i - \theta} = 1 - q \quad (6.2)$$

where F refers to the natural abundance feed, and q depends on the fraction of vapor and liquid in the feed, which is of little consequence in these calculations. Using a saturated liquid feed, $q=1$, the calculated θ is 1.0000422. The minimum reflux is then calculated using the equation [49]:

$$R_{\min} + 1 = \sum_{i=1}^n \frac{\alpha_i x_{iD}}{\alpha_i - \theta} \quad (6.3)$$

Again using the High α values from Table 6.2, the minimum reflux ratio is 645, implying that for every L/min of distillate product flow, at least 645 L/min of liquid is flowing through the column.

The actual number of separation stages and the reflux ratio must both be greater than their minimums to produce a product. The general rule-of-thumb is that the actual reflux ratio should be 1.1 to 1.4 times the minimum reflux ratio [49], so a value of 1.4 is used here to give a reflux ratio of 904. The number of stages is finally calculated to be 14,423 from the Gilliland correlation:

$$\frac{N - N_{\min}}{N + 1} = 0.75 \left(1 - \left[\frac{R - R_{\min}}{R + 1} \right]^{0.566} \right) \quad (6.4)$$

where N is the number of stages.

The height (or length) of the distillation column can then be calculated from the HETP. The best HETP obtained for isotopic enrichment was 0.41 cm in the 10-inch device, which translates to 59.1 m (194 ft) for 14,423 stages. If the theoretical limit projected by the CFD model of 0.1 cm could be reached, the column would further reduce to 14.4 m (47.3 ft). The best available commercial structured packing made by Sulzer can achieve a 2 cm HETP, which would require 289 meters (946 ft) of column. The Supercarb 4D packing has achieved 20 cm HETP, which translates to bogging almost 3000 meters or 10,000 feet. To complete the perspective, the column height is also calculated for the 'Low α ' values in Table 6.2. For those relative volatilities that are much closer, the minimum number of stages is 35,695, the minimum and actual reflux ratios are 2584 and 3618, respectively, and the calculated number of stages is 57,664. For this worst case, the column height grows to 236 m (775 ft) for the best experimental result of 0.41 cm HETP that reduces to 57.7 m (189 ft) for the model prediction.

6.3 Projected System Size

The microchannel distillation technology is scalable by adding layers of wicks, widening the wicks, and operating modules in series and parallel. Figure 6.3 illustrates how MCD devices are cascaded to increase the number of stages of separation. Liquid is siphoned from the MCD #1 device into the MCD #2 device, so there is an overall height required to operate a cascade. Meanwhile, vapor flows counter-current from MCD #2 device to MCD #1 device. Figure 6.4 illustrates a longer cascade of devices, such as would be required for the large number of separation stages needed for isotopic enrichment. Overall height can be reduced by introducing liquid pumps between sections of the cascade. In addition, the cascade in Figure 6.4 would be replicated as needed to increase production capacity.

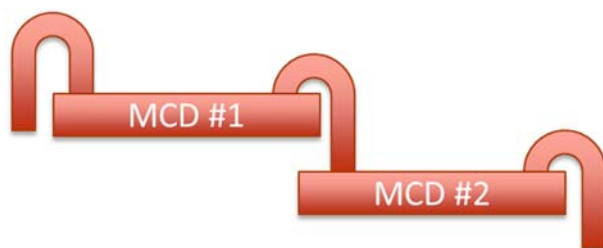


Figure 6.3. Illustration of cascading of MCD devices to increase the number of separation stages.

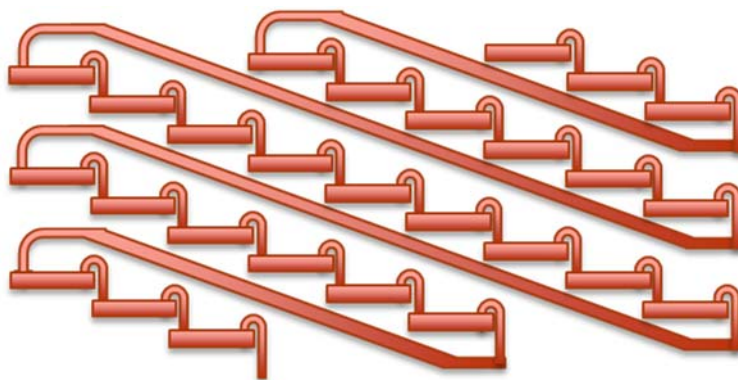


Figure 6.4. Illustration of scaling up a cascade of MCD devices.

The size of a system depends on the design production rate. To produce 1 tonne (1000 kg) of 86% enriched ^{76}Ge for a future neutrinoless double beta decay program in 4 years with a continuous operation requires a production rate of 0.48 g/min of bottoms product. Using a density of 1.53 g/ml for liquid germane and mass balances to calculate flow rates, the bottom product flow of enriched ^{76}Ge is 0.311 ml/min, the natural feed is 14.4 ml/min, and the distillate flow is 14.1 ml/min. The reflux of liquid into the system is 7972 ml/min due to the very high reflux ratio.

The number of 10-inch devices needed for the 4-year production is calculated from the operating point of 0.5 cm HETP at 1.125 ml/min liquid flow rate in Table 4.2 above. At an HETP of 0.5 cm, the total column length is 69 meters which requires 284 10-inch devices operating in series. To attain a total liquid flow of 7972 ml/min, 7,160 parallel trains would be required for a total number of devices of over 2 million. Fortunately, the number of MCD devices can be dramatically reduced by scaling to larger devices, similar to the scaling of the 11-wick, 5-inch to a 20-wick, 10-inch device. In the current architecture, scaling the footprint—wick length and width is limited by fabrication of the wicks and assembly of the devices in a load press. The number of wicks is limited by the hydraulic head between the top and bottom of the wick stack that must be compensated for by the siphons. To illustrate the scaling, scale-up to 2 feet long by 1 foot wide wicks and a stack of 40 wicks are assumed. This reduces the number of devices to 118 devices in series and 470 parallel trains for a total of 55,575 devices, a dramatic reduction from 2 million 10-inch devices.

Additional development of MCD technology to reduce HETP closer to the theoretical 0.1 cm is justified by the potential reduction in the number of devices and system size. A 0.1 cm HETP reduces the number of larger 2-foot by 1-foot devices to 24 for each train and to 11,115 total to produce 1 tonne of 86% ^{76}Ge in 4 years of operation.

One of the advantages of parallel cascades of MCD devices is redundancy and reduced risk associated with equipment failure risks. The 470 parallel cascades could be operated independently or in groups,

such that an equipment failure would cause a minimal loss in production capacity and most of the system could continue to operate while on cascade is being repaired. Furthermore, the capital investment could be spread out over time as production capacity is brought online in stages, thereby reducing the financial risk.

The normal boiling point of germane is -88°C , so operating a cryogenic distillation system for enriching germanium involves considerable capital and operating costs associated with cooling the system, preferably in a vacuum chamber to minimize thermal losses and interactions. Capital and operating costs of cooling the system in a vacuum is related to the system size, so a compact MCD system will be less costly. The internal active volume of wicks and vapor channels is calculated to be 560 liters (20 ft^3) for each of the 470 cascades of 24 larger scaled-up devices. The total volume for all of the cascades is 395 m^3 (14000 ft^3). Instead of packaging the distillation system in 1000-foot tall columns containing Sulzer advanced structured packings, the MCD system can be arranged in more horizontal arrangements as depicted in Figure 6.4. If the entire system were to be arranged in a cubic room, the size would be 7.3 m (24 ft) on a side, which is more tractable than vertical columns.

Projected sizes of a MCD systems capable of producing 1 tonne of 86% ^{76}Ge in 4 years are summarized in Table 6.3 based on using the 10-inch devices with an HETP of 0.5 cm and liquid flow of 1.125 ml/min, assuming HETP can be decreased to 0.1 cm, and assuming a device can be scaled up to 1-foot by 2-foot footprint containing 40 wicks.

Table 6.3. Size of MCD systems for producing 1 tonne of 86% ^{76}Ge in 4 years.

	10-inch devices, 0.5 cm HETP	10-inch devices, 0.1 cm HETP	2-ft x 1-ft devices, 0.5 cm HETP	2-ft x 1-ft devices, 0.1 cm HETP
Total length	72.1 m	14.4 m	72.1 m	14.4 m
Devices per cascade	284	58	118	24
Parallel cascades	7160	7160	470	470
Total devices	2,032,714	413,048	55,575	11,115
Volume of devices per cascade	55.2 L	11.0 L	841 L	168 L
Total volume of devices	385 m^3	79 m^3	385 m^3	79 m^3
Cubic room size	7.3 m	4 m	7.3 m	4 m

7.0 Conclusions

A microchannel distillation technology has been successfully demonstrated for isotopic enrichment of methane. A record number of separation stages, 60 at the lowest HETP, was achieved in a device operating at the normal boiling point of methane, -162°C . Scalability of the technology was demonstrated by increasing the length by a factor of 2.5 and doubling the number of channels with an improvement in performance. The minimum length of a separation stage, HETP, was 0.41 cm and was relatively constant over a range of flow rates.

The minimum HETP achieved is a factor of 5 lower than the best commercial structured packing, 8-cm diameter Sulzer laboratory packing, albeit at a lower flow capacity. Lower mass fluxes in MCD devices are enabled by operating in a horizontal configuration using capillary forces and siphons to control hydrodynamics. Horizontal operation facilitates a lower equipment profile and compact system that is more amenable to insulating for operating temperatures far from ambient. Low profile and compactness are also important for distributed manufacturing applications.

Dimensional analysis and computational fluid dynamics (CFD) modeling indicate the potential for additional significant improvements. CFD models of the smaller test device show the potential for reducing HETP to 0.1 cm. Dimensional analysis shows that vapor phase dispersion is detrimental to performance except at the highest flow rates tested, and performance would be enhanced by reducing the height of the vapor channel. Dimensional analysis indicates there is the potential for an additional 5-10X improvement in HETP beyond the effects of vapor dispersion.

Isotopic enrichment by distillation requires many more separation stages than chemical separations, as well as large reflux ratios, due to low relative volatilities that are available in the literature for many compounds, but are unavailable for germane isotopes, the target application to supply 86% enriched ^{76}Ge for future physics experiments. Attempts to measure relative volatilities of germane using GC/MS methods were not attempted due to limited success with methane. Instead, relative volatilities used for design calculations were surmised from similar compounds silane and methane. Using the assumed relative volatilities, the Fenske-Underwood-Gilliland method was used to obtain 14,423 and 904 as the number of stages and reflux ratio, respectively, needed to enrich $^{76}\text{GeH}_4$ to 86%. Using the best HETP measured in an MCD device, an HETP of 0.41 cm would require a total active length of 59.1 meters for 14,423 stages, compared to 289 meters with the Sulzer laboratory structured packing. If performance improvements were to approach the theoretical potential of 0.1 cm HETP, the total active length would shrink to 14.4 m. This illustrates the power of process intensification with MCD technology.

In order to produce 1 tonne of 86% $^{76}\text{GeH}_4$ in 4 years, multiple parallel cascades of MCD devices are projected. The number of cascades is projected to be 470, if the MCD device can be scaled up to 1-ft wide by 2-ft long footprint. Each cascade would have 118 devices in series for a total of 55,575 MCD devices needed to meet the production target. If the potential of 0.1 cm HETP were to be realized, the number of devices per cascade would shrink to 24 and the total number of devices to 11,115. The total active volume within the devices is 385 m^3 and 79 m^3 for the 0.41 cm and 0.1 cm HETP, respectively. Configuring the cascades into a compact arrangement would allow the system to fit within a two-story structure.

Overall, the MCD technology holds promise for reducing the size of equipment needed for isotopic enrichment of compounds below about 100 amu. Further investment in improving performance will pay important dividends in further size reduction. Next steps in technology development are further scale-up of the devices and demonstration of cascades to demonstrate greater separation factors.

8.0 References

1. *Meeting Isotope Needs and Capturing Opportunities for the Future: The 2015 Long Range Plan for the DOE-NP Isotope Program*. 2015, The DOE/NSF Nuclear Science Advisory Committee Isotopes Subcommittee.
2. Aalseth, C. and e. al. *The MAJORANA DEMONSTRATOR: An R&D project towards a tonne-scale germanium neutrinoless double-beta decay search*. in (*MAJORANA collaboration*). 2009. The American Institute of Physics, Conf. Proc. 1182.
3. Ackermann, K.-H. and e. al., *The GERDA experiment for the search of $0\nu\beta\beta$ decay in $Ge-76$* , in (*GERDA Collaboration*). 2013, European Physical Journal C 73.
4. TeGrotenhuis, W.E. and V.S. Stenkamp, *Methods of Contacting Substances and Microsystem Contactors*. 2005: U.S. Patent 6,869,462.
5. TeGrotenhuis, W.E. and V.S. Stenkamp, *Improved Conditions for Fluid Separations in Microchannels, Capillary-Driven Fluid Separations, and Laminated Devices Capable of Separating Fluids*. 2005: U.S. Patent 6,875,247.
6. TeGrotenhuis, W.E. and V.S. Stenkamp, *Methods for Fluid Separations, and Devices Capable of Separating Fluids*. 2006: U.S. Patent 7,051,540.
7. TeGrotenhuis, W.E. and V.S. Stenkamp, *Method for Fluid Separation, and Devices Capable of Separating Fluids*. 2007: U.S. Patent 7,272,941.
8. TeGrotenhuis, W.E. and V.S. Stenkamp, *Conditions for fluid separations in microchannels, capillary-driven fluid separations, and laminated devices capable of separating fluids*. 2008: U.S. Patent 7,344,576.
9. TeGrotenhuis, W.E., et al., *Microsystem Capillary Separations*. 2003: U.S. Patent 6,666,909.
10. ASTM, *Standard Test Method for Boiling Point Range Distribution of Petroleum Fractions by Gas Chromatography*, in *Annual Book of Standards*. Vol. 05.02, ASTM: 100 Barr Harbor Dr., W Conshohocken, PA 19428 USA.
11. Frisch, O.R., *Progress in Nuclear Physics*. Vol. 6. 2013, New York: Peramon Press
12. Matwiyoff, N.A., B.B. McInteer, and T.R. Mills, Los Alamos Science Summer 1983, 1983.
13. Fukada, S., *Tritium Isotope Separation by Water Distillation Column Packed with Silica-gel Beads*. Journal of Nuclear Science and Technology, 2004. **41**(5): p. 619-632.
14. Zuzel, G., et al., *The DarkSide Experiment: Present Status and Future*. International Conference on Particle Physics and Astrophysics, 2017. **798**.
15. Back, H.O., et al., *^{136}Xe enrichment through cryogenic distillation*. Journal of Instrumentation, 2017. **12**(09): p. P09033.
16. Jancso, G. and W.A. Van Hook, *Condensed phase isotope effects*. Chemical Reviews, 1974. **74**(6): p. 689-750.
17. Jones, W.M., *Vapor Pressures of Tritium Oxide and Deuterium Oxide. Interpretation of the Isotope Effects*. The Journal of Chemical Physics, 1968. **48**(1): p. 207-214.
18. Li, H.-L., et al., *Separation of isotope ^{13}C using high-performance structured packing*. Chemical Engineering and Processing: Process Intensification, 2010. **49**(3): p. 255-261.
19. Hickey, T., *Advanced Distillation Final Report*. 2009, Velocys, Inc.

20. *Structured Packings: Energy-efficient, innovative and profitable*, Sulzer, Editor.
21. Bessou, V., et al., *Performance characteristics of a new structured packing*. Chemical Engineering Science, 2010. **65**(16): p. 4855-4865.
22. Sundberg, A.T., P. Uusi-Kyyny, and V. Alopaeus, *Microscale distillation*. Russian Journal of General Chemistry, 2012. **82**(12): p. 2079-2087.
23. Tonkovich, A.L., et al., *Distillation process using microchannel technology*. 2006, Velocys, Inc., USA. p. 32 pp.
24. MacInnes, J.M., et al., *Experimental demonstration of rotating spiral microchannel distillation*. Chemical Engineering Journal, 2010. **159**(1-3): p. 159-169.
25. Zhang, Y., S. Kato, and T. Anazawa, *Vacuum membrane distillation by microchip with temperature gradient*. Lab on a Chip, 2010. **10**(7): p. 899-908.
26. Sundberg, A., P. Uusi-Kyyny, and V. Alopaeus, *Novel micro-distillation column for process development*. Chemical Engineering Research & Design, 2009. **87**(5a): p. 705-710.
27. Huang, X.W., et al., *Hydrodesulfurization of JP-8 fuel and its microchannel distillate using steam reformate*. Catalysis Today, 2008. **136**(3-4): p. 291-300.
28. TeGrotenhuis, W.E. and M.R. Powell. *Packing Structure Capable of Sub-Centimeter HETP for High Purity Distillation of Low Relative Volatility Compounds*. in *American Institute of Chemical Engineers Conference Proceedings*. 2012. Houston, TX.
29. Rohsenow, W.M., J.P. Hartnett, and Y.I. Cho, *Handbook of heat transfer*. 1998: McGraw-Hill.
30. Perry, R.H. and D.W. Green, *Perry's chemical engineers' handbook*. 7th ed. 1997: New York: McGraw-Hill.
31. Johns, T.F., *Vapour Pressures of Some Isotopic Substances*. Angewandte Chemie-International Edition, 1957. **69**(17): p. 564-564.
32. Miller, C. and G. Kaibel, *Packings for fixed bed reactors and reactive distillation*. Chemical Engineering Science, 2004. **59**(22): p. 5373-5379.
33. Zheng, F., et al. *Microchannel Distillation of JP-8 Jet Fuel for Sulfur Content Reduction*. in *AiChE*. 2006. San Francisco, CA.
34. Tyn, M.T. and W.F. Calus, *Diffusion coefficients in dilute binary liquid mixtures*. Journal of Chemical & Engineering Data, 1975. **20**(1): p. 106-109.
35. Bird, R.B., W.E. Stewart, and E.N. Lightfoot, *Transport Phenomena*. 2nd ed. 2001: Wiley.
36. Dymond, J.H., *Corrected Enskog theory and the transport coefficients of liquids*. The Journal of Chemical Physics, 1974. **60**(3): p. 969-973.
37. Lee, H. and G. Thodos, *Generalized treatment of self-diffusivity for the gaseous and liquid states of fluids*. Industrial & Engineering Chemistry Fundamentals, 1983. **22**(1): p. 17-26.
38. Jancso, G. and W.A. Van Hook, *Condensed Phase Isotope Effects (Especially Vapor Pressure Isotope Effects)*. Chemical Reviews, 1974. **74**(6): p. 689-750.
39. Baker, D.B. and B.K. Christmas, *A Thermodynamic Analysis to Explain the Boiling-Point Isotope Effect for Molecular Hydrogen*. Journal of Chemical Education, 2000. **77**(6): p. 732.
40. Meza-Montes, L. and P. Hoffmann-Pinther, *A Note on "A Thermodynamic Analysis to Explain the Boiling-Point Isotope Effect for Molecular Hydrogen"*. Journal of Chemical Education, 2001. **78**(3): p. 416.

41. Van Hook, W.A., L.P.N. Rebelo, and M. Wolfsberg, *Isotope effects on VLE properties of fluids and corresponding states: Critical point shifts on isotopic substitution*. Fluid Phase Equilibria, 2007. **257**(1): p. 35-52.
42. Bradley, D.C., *Fractionation of Isotopes by Distillation of some Organic Substances*. Nature, 1954. **173**(4397): p. 260-261.
43. Karki, S.S. and S.K. Sinha, *Phase equilibria of polar Lennard-Jones fluids*. Indian J. Phys., 2001. **75A**(1): p. 91-2.
44. Dey, T.K. and S.K. Sinha, *Semiclassical theory for thermodynamics of molecular fluids*. Indian J. Phys., 1998. **72A**(5): p. 397-401.
45. Pitzer, K.S., *Corresponding States for Perfect Liquids*. The Journal of Chemical Physics, 1939. **7**(8): p. 583-590.
46. Pitzer, K.S., *The Volumetric and Thermodynamic Properties of Fluids. I. Theoretical Basis and Virial Coefficients I*. Journal of the American Chemical Society, 1955. **77**(13): p. 3427-3433.
47. Pitzer, K.S. and R.F. Curl, *The Volumetric and Thermodynamic Properties of Fluids. III. Empirical Equation for the Second Virial Coefficient I*. Journal of the American Chemical Society, 1957. **79**(10): p. 2369-2370.
48. Mills, T.R., *Silicon Isotope Separation by Distillation of Silicon Tetrafluoride*. Separation Science and Technology, 1990. **25**(3): p. 335-345.
49. Humphrey, J.L. and G.I. Keller, *Separation Process Technology*. 1997, New York: McGraw-Hill.



Pacific Northwest
NATIONAL LABORATORY

*Proudly Operated by **Battelle** Since 1965*

902 Battelle Boulevard
P.O. Box 999
Richland, WA 99352
1-888-375-PNNL (7665)

U.S. DEPARTMENT OF
ENERGY

www.pnnl.gov